

THESIS

PENETRATIVE OSSEOINTEGRATIVE P HOSPHOLIPID COATINGS ON 3D  
TITANIUM LATTICE STRUCTURES

Submitted by

Hannah Katherine Hudson

Department of Mechanical Engineering

In partial fulfillment of the requirements

For the Degree of Master of Science

Colorado State University

Fort Collins, Colorado

Spring 2012

Master's Committee:

Advisor: Susan James

David Prawel  
Nicole Ehrhart

## ABSTRACT

### PENETRATIVE OSSEOINTEGRATIVE PHOSPHOLIPID COATINGS ON 3D TITANIUM LATTICE STRUCTURES

Titanium is a commonly used material for implantable metallic devices though these devices still have many issues. The cost of implant surgery and the likely revision surgery that will follow is high. Cementless implants frequently fail due to aseptic loosening of the device, typically as a result of poor osseointegration.

Phospholipids are naturally occurring substances that have been used to enhance new bone growth and integration of this bone with the implants.

Electrospraying (e-spraying) is a method that uses electrical forces to drive source material to a target conductor. It typically has very high efficiency because it uses electrical charge to carry the material. This process also provides good control of coating morphology as this can be effected by the parameters used to e-spray.

In our work the E-spraying technique was used to apply coatings of 1,2-dioleoyl-*sn*-glycero-3-phospho-L-serine (DOPS) to Ti-6V-4Al porous lattice structures. These lattice structures are created using Electron Beam Melting (EBM). This manufacturing process is an additive process, part of the solid free form fabrication group, a subset of rapid prototyping. EBM enables precise control of complex geometries. When e-spraying these lattice structures can become Faraday cages when an electric field is applied to them. A Faraday cage is a conductor that becomes an equipotential surface when an electric field is applied and thus in its interior lacks an electric field. The

exclusion of an internal electric field can inhibit to the e-spray process which relies on field lines to carry material to the target.

In our work the Faraday cage effect was observed in two conditions, one in which the lattice structures were externally, circumferentially insulated and one in which the lattices were not insulated. Three different porosity lattices, with different pore sizes, were tested and all became Faraday cages when insulated and only the lowest porosity lattice became a strong Faraday cage when not insulated. The lattices that did coat did not exhibit conformal and uniform coatings when the Faraday cage effect was present. E-spray parameter variation was not able to mitigate the Faraday cage effect nor was it able to affect the morphology of the coatings. The surface topography of the structures is important for preferential cell adhesion and can be controlled using acid etching to modify the surface.

In attempt to coat titanium lattice structures with a phospholipid coating this work discovered the Faraday cage effect as it relates to the electro spraying of phospholipids. It currently defines the limitations of the e-spray process as well as outlines what has been tried to mitigate the Faraday cage effect and discover how the Faraday cage effect changes coating morphology. In the future continuing work on mitigating the Faraday cage effect will be done as well as combining the e-spray process with one that uses a mechanical force to accelerate particles

## ACKNOWLEDGEMENTS

I would like to thank the people that supported me and helped me with my work on this thesis. First and foremost I would like to thank my advisor, Dr. Sue James for all of her help in traveling down this path of research. She kept me focused and calm when I was at my worst and provided extremely useful insight into my work. I am also very grateful to Dr. David Prawel whose research was the starting point for mine. Having someone so versed in the basics of my research made it possible for me to explore new ideas while still maintaining the basics of the process.

I would also like to thank everyone in the James Research Group for their support and help along the way. I am indebted to Mike Finch for all of his help with the experiments I set up. He offered me his time in running experiments allowing me to focus on the results. I am also grateful to have a lab mate as fun and supportive as Casey Dean. I hope that now he's finished his thesis he'll be able to wean himself from the Rockstar.

I am glad to have been able to work with the people at Medical Modeling who manufactured the parts I used to do my research, without them I wouldn't have had a project. Their continued support has been highly appreciated throughout my work. I would like to thank Pat McCurdy for his expertise on SEM and Jack Clark for his time spent helping me gather data and understanding SWLI.

Finally I would like to say thanks to my parents, Nancy Elder and Bobby Hudson, and my brother Scott Hudson. They have been available at all levels, as backboards for crazy ideas, and people to talk out my thoughts with. My brother was a good source of

never ending encouragement. My dad was always willing to listen to my thoughts on my research and offer his opinions as an engineer with experience both in doing research and working in industry. My mom has been really been there for me during this trying time, offering her official services as a librarian as well as her unofficial services as emotional support.

TABLE OF CONTENTS

**ABSTRACT** ..... ii

**ACKNOWLEDGEMENTS** ..... iv

**1 Background**..... **1**

    1.1 Phospholipids..... 1

    1.2 Biomineralization ..... 2

    1.3 Implant Materials..... 4

        1.3.1 Titanium Implants..... 4

        1.3.2 Bone Cements and Fillers ..... 8

    1.4 Implant Design ..... 9

        1.4.1 Porous Implant Structures ..... 10

        1.4.2 Electron Beam Melting ..... 11

    1.5 Implant Coatings ..... 13

        1.5.1 Coatings and Methods ..... 13

        1.5.2 Phospholipid Coatings ..... 14

        1.5.3 Electro Spray ..... 16

        1.5.4 The Faraday Cage Effect ..... 17

**2 Motivation and Long Term Goal** ..... **20**

    2.1 Implant Rates ..... 20

    2.2 Implant Infection Rates..... 20

    2.3 Other Implant Failures ..... 21

    2.4 Research Goals..... 22

**3 Proposed Research, Specific Aims, and Hypotheses**..... **23**

    3.1 Specific Aims and Hypotheses ..... 24

        3.1.1 Specific Aim 1: Titanium Lattices and the Faraday Cage Effect ..... 24

        3.1.2 Specific Aim 2: DOPS Coatings and the Faraday Cage Effect..... 25

        3.1.3 Specific Aim 3: Process Parameters and their Effects on DOPS Coatings Characteristics..... 25

**4 Materials and Methods**..... **27**

    4.1 Experimental Approach ..... 27

        4.1.1 Sample Prep ..... 28

        4.1.2 Electro Spray ..... 29

        4.1.3 EBM Manufacture..... 32

4.1.4	SEM, EDS, and SWLI Characterization .....	35
4.3	Experiments Done.....	38
4.2.1	Externally Insulated Lattices .....	38
4.2.2	No Insulation, Parameter Variation.....	39
4.2.3	Parameterization .....	39
4.2.4	Time Based.....	40
4.2.4	Surface Area and Coating Morphology.....	40
4.2.4	Acid Etching Effects.....	40
4.2	Statistics.....	41
<b>5</b>	<b>Results and Discussion .....</b>	<b>42</b>
5.1	Titanium Lattices and the Faraday Cage Effect .....	43
5.1.1	External Insulation and Faraday Cages .....	44
5.1.1.1	Discussion .....	46
5.1.2	Lattice Porosity and the Faraday Cage Effect .....	49
5.1.1.1	Discussion .....	55
5.2	DOPS Coatings and the Faraday Cage Effect .....	57
5.2.1	Lattice Porosity and Coating Morphology .....	57
5.2.1.1	Discussion .....	60
5.3	Process Parameters and Coatings.....	63
5.3.1	Parameter Variation and DOPS Coatings.....	63
5.3.1.1	Discussion .....	75
5.3.2	Surface Roughness and Area .....	78
5.3.2.1	Discussion .....	89
<b>6</b>	<b>Conclusions and Future Work.....</b>	<b>93</b>
6.1	Conclusions from Current Work .....	93
6.2	Future Work.....	97
	<b>References .....</b>	<b>99</b>
	<b>Appendices .....</b>	<b>105</b>

# 1 Background

## 1.1 Phospholipids

Phospholipids are a part of the broad category of molecules called lipids. Lipid molecules include fats, oils, waxes, steroids, and some other related compounds. Lipids are generally considered insoluble in water[1]. Phospholipids are comprised of a hydrophilic polar head group containing 1 or more phosphate groups and a hydrophobic tail made up of two fatty acyl chains. Most phospholipid head groups belong to phosphoglycerides which contain glycerol joining the head and tail, including phosphatidylserine[2]. Lipids are found in small amounts in mineralized cartilage, ranging from about 0.2% to 2%, varying based on the type of tissue. Approximately half of these lipids are non-polar[3].

Phospholipids are found in every animal cell, serving primarily as the cellular membrane. They occur in high quantities in muscle tissue as well as in bone marrow and brain cells[4]. It has been found that more active tissues have larger amounts of phospholipids. Phospholipids in bone and cartilage tissue account for up to 30% of the total quantity of lipids with the majority of the phospholipids being lipids such as phosphatidylcholine, phosphatidylethanolamine and 7 sphingomyelin [3].

Phosphatidylserine is found widely among plants, animals and microorganisms, it usually accounts for only 10% of the total phospholipids with the heaviest concentration in myelin in brain tissue. It can however comprise 10 – 20 mol% of the phospholipid in the plasma membrane and endoplasmic reticulum. It functions not only as a cellular



regulation of this process relies primarily on inorganic phosphate[10]. New bone mineralization occurs primarily extracellularly within a matrix supersaturated with calcium and phosphate. The extracellular matrix of the normally calcifying tissue is comprised predominantly of collagen along with proteoglycans and other non-collagenous proteins. Mineralization generally follows two principal patterns of mineral deposition. The first of these patterns is one characterized by a generally radial-shaped spherulitic deposit composed of individual mineral crystals about a central nucleation point. The organization is generally irregular but conforming to a roughly circular region, this pattern is most often observed in calcifying cartilage of the epiphyseal growth plate. The second pattern is much more regular and organized in nature with crystals appearing extracellularly with a periodic distribution. This pattern is most commonly found during intramembranous and appositional bone development[11]. The bone mineralization occurs at the nucleation center where cell mesenchymal cells proliferate and a network of collagen fibrils form in an amorphous matrix of organic matrix-crystal nucleation within membrane bound vesicles[12].

These membrane bound vesicles contain matrix processing enzymes, calcium phosphate nucleating sites and phosphatases[13]. The lipids of the matrix vesicles have been shown to be involved in the primary mineralization process and have shown that phosphatidylcholine and phosphatidylserine provide the primary binding sites for amorphous calcium phosphate[6-8]. The concentration of complex acidic phospholipids has been shown to increase in mineralizing tissues prior to detectable mineral deposition. This suggests that these lipids are formed to promote calcification [14]. The

calcium binding properties of phospholipids in conjunction with the saturating concentrations of calcium and phosphate in the vesicle interior lead to the formation of crystals which aggregate, disrupt the vesicle, and merge with other nucleation centers [15]. It is only after the vesicles have detached and coalesced into larger deposits that there is mineral crystal appearance and proliferation [9]. Osteoblasts secrete an extracellular matrix with the potential to support calcium phosphate deposition as well as producing the necessary membrane bound vesicles [16]. Osteoblasts regulate the production of these vesicles and are thus responsible for controlling the rate of bone mineralization.

### **1.3 Implant Materials**

Metallic orthopedic implants have long been used in skeletal repair throughout the body. The strength of the implant-bone interface, and the stress-shielding effects are important things to consider in the choice of an implant material [17]. An implant material designed for bone integration will ideally encourage new bone mineralization as well as reducing inflammation to levels necessary for tissue regeneration [12]. Poorly designed biomaterials will typically have nonintegration of the implant with the surrounding tissue or infection [18]. The balance between strength of implant and bone integration must be carefully considered when choosing and designing an implant material.

#### ***1.3.1 Titanium Implants***

Titanium is widely used in orthopedic, cranio-facial and dental implants. The bio and cyto-compatibility of titanium based alloys such as Ti-6Al-4V and Ti-6Al-7Nb have

been studied in detail and determined to be very suitable for biomedical applications [19]. Titanium and titanium alloys are successful in biomedical applications due to its excellent properties, including low corrosion, low modulus, high strength, light weight and excellent bio-compatibility [20, 21]. Titanium is also very receptive to surface modifications [22-24]. Ti alloys generally have higher fatigue strength than commercially pure Ti (CP Ti) despite CP Ti having better corrosion resistance and bio-compatibility [25-27]. Ti alloy implants are more common in orthopedic applications than CP Ti implants due to the generally increased strength requirements in orthopedics [24].

The morphology of an implant surface has been shown to influence the success of bone fixation to the implant. Implants with higher surface roughness show higher levels of direct bone apposition whereas smoother implants surfaces show more fibrous encasement [28]. This fibrous encasement prevents the bone from attaching to the implant and causes loosening and failure.

Surface modification for roughening and smoothing are done through many processes including chemical etching, grit blasting or abrading, plasma and electropolishing [26].

Macroscopic characteristics of the surface have been shown to influence cellular activity at the biomaterial-bone interface as well as critical influence on long term use of the implant [29-31]. Cells cultured on a rough titanium surface produce more of the chemicals considered critical for bone growth and apposition than those cultured on a smooth titanium surface, such as alkaline phosphatase, osteocalcin, and collagen [32].

Osteoblasts show an initial attachment to rough Ti surfaces [29, 30] and as roughness increases osteoblasts show increased differentiation and decreasing proliferation [32] [30]. Titanium surfaces with an average surface roughness ranging from 22 to 28  $\mu\text{m}$  exhibited significantly higher bone/implant index than smooth surfaces [33]. The specific surface roughness can influence the hydrophilicity of a surface which effects the configuration and conformation of the proteins that are important in cell adhesion deposited on the implant surface [34]. On various polymers as well as titanium the adhesion strength of both osteoblasts and fibroblasts increases with increasing surface roughness [18, 32, 35, 36].

A particular benefit of titanium is its natural inclination to form a surface oxide layer when exposed to air [25, 26]. This oxide layer is important in bone remodeling on titanium surfaces. The oxide layer formed typically consists of primarily titanium dioxide with smaller amounts of other oxides present as well as a layer of primarily hydrocarbons [25]. Different cleaning procedures produce varying oxide thicknesses on machined CP Ti. A solvent-cleaned surface typically has an oxide layer of 2-3 nm with no appreciable oxide growth during storage in room temperature air or under irradiation sterilization. A surface autoclaved and dry heat sterilized however typically has an oxide thickness of 5-10nm due to increased temperatures [26]. Oxide layers on retrieved titanium implants are shown to increase with implantation time and also to incorporate ions from the physiological environment [37].

The surface morphologies of CP Ti and Ti alloys also affect the thickness and morphology of the oxide layer that forms. The oxide layers change due to variations in

the crystallinity of the Ti as the segregation of the alloy components [37]. In different alloys of Ti the grain structure will be different due to different chemical composition of the material. These modifications can result in differing cell response to the varying titanium compositions. Osteocalcin and alkaline phosphate production is reported higher on CP Ti while osteoblast proliferation is higher on Ti-6Al-4V [32]. Despite some advantages of Ti-6Al-4V there are known cyto-toxicity issues with Vanadium as well a possible link between aluminum and an Alzheimer-type dementia [38].

Osseointegration is defined as direct contact between bone and an implant surface. It is shown that when direct contact exists the bond is much stronger and longer lasting than one in which there is a thin fibrous tissue layer between bone and implant [39]. Implant design impacts osseointegration, in one study it was found that threaded implants showed full osseointegration while non-threaded (smooth) ones showed less osseointegration as it was interrupted by patches of fibrous tissue [40]. Bone integrating around a titanium implant is characterized by a slow mineralization process as directed from the surrounding tissue towards the metallic implant. Integration of the bone with an implant takes place primarily at the implant-tissue interface [39]. New bone formation begins almost immediately after implantation as the osteoblasts begin to adhere to the Ti surface. Initial bone growth occurs around 4 days and mature bone forms approximately 4 weeks post-surgery with maximum bone ingrowth seen at about 6 weeks [41]. Maximum levels of osseointegration are typically reached between 8 and 12 weeks following surgery [16]. The bone ingrowth process is characterized by two mechanisms, first the response of the host to the implant and

second the behavior of the biomaterial in the host [42]. The chemical properties, surface characteristics and viscoelastic properties of the implant surface have a direct influence on the fast and permanent ingrowth of bone into the implant [43]. Human-like osteoblast cells undergo 4 phases when attaching to titanium. In the first week they undergo proliferation and migration as the first undifferentiated preosteoblasts adhere to the metal, in the following weeks up to the first 4-6 weeks the cells are secreting extracellular matrix proteins and beginning to anchor to the implant. Beginning at week 4 the matrix begins to mineralize and become denser, from week 6-8 the matrix begins to reorganize and become more osteon like. This is when the bone has reached maturity [44].

### **1.3.2 Bone Cements and Fillers**

Many implants use a bone cement (frequently poly(methyl methacrylate) PMMA) to fill the voids and spaces that occur due to the impact match of the implant and tissue. This bone cement can fail and cause the implant to fail via aseptic loosening [45]. PMMA does not display the ideal characteristics for its role *in vivo*. In cyclic bending and tensile stresses PMMA becomes brittle and fracture occurs much lower than expected based on ultimate strength values. This combined with the potential of bone necrosis due to the toxic nature of PMMA is what allows for a fibrous tissue layer to form at the implant interface allowing for micromotion and providing a space for wear particles to accumulate. This causes pain to the patient and is the root cause for the loosening and eventual implant failure [46]. It is these factors that lead surgeons to

prefer a cementless, press-fit type implant for many patients, especially those under the age of 65 where it becomes likely that the patient will outlive his or her implant.

Cementless arthroplasty is common in young patients who place higher demand on their prostheses and will tend to have them for longer periods of time than elderly patients. Longer survival rates of cementless implants hinge on the biological fixation of the implant, requiring high apposition of bone to the actual implant surface as well as good initial mechanical stability [47].

Long-term success of cementless or press-fit implant devices depends on [48]:

1. a highly adherent, mechanically stable, biological fixation at the device-bone interface;
2. close apposition between the implant device and the implantation site;
3. a low foreign body/immune response;
4. material properties of the biomaterials, such as viscoelastic properties of an implant surface, as discussed in the following sections.

#### **1.4 Implant Design**

The design of orthopedic implants is a complicated and challenging process. While metallic implants have long been used for skeletal repair in the body there are still many issues. The bone-implant interface and stress-shielding effects are very important in choice of implant material and design [17]. Bone regeneration and repair are promoted by mechanical loading [49] thus making the particular design of the titanium critical. Solid Ti implants are sometimes found to carry a disproportionate

amount of the biological load, creating the stress-shielding of the surrounding tissue, leading to eventual loosening of the implant by causing resorption of the bone [50]. Porous coatings have been developed to promote long lasting interface strength not found in smooth implants [17].

#### **1.4.1 Porous Implant Structures**

Cementless implants are now common among orthopedic implants. They depend on osseointegration as the means of attachment to the surrounding bone. Implants are fabricated as porous structures to capitalize on osseointegration. The use of scaffolds is important in orthopedic tissue engineering as they provide a source of biological anchoring to the surrounding bone tissue through the ingrowth of mineralized tissue into the porous structure [51]. Some ceramics and polymers are biodegradable and bioresorbable and have been considered as scaffolds though they have been found inadequate to support the loading conditions *in vivo* to allow for bone growth. This makes metallic implants ideal because they have the necessary strength and fatigue resistance and their elastic moduli can be adjusted to match that of the natural bone in order to limit stress shielding [52].

The effect of pore size, morphology and spatial distribution must be considered in terms of the stiffness, strength, and fatigue resistance of a metallic material. Studies have shown that predictive modeling and analysis can accurately predict the results of changing pore size, morphology and distribution on the properties of CP Ti and Ti-6V-4Al [17]. Though optimal range of pore size for bone ingrowth is frequently reported as 50-400um, pore sizes larger than 150um are preferred as they provide a more suitable

environment for bone reorganization and vascularization [53]. Pre-osteoblastic cells cultured on Ti scaffolds showed higher levels of differentiation, proliferation and mineralization compared to those cultured on mirror polished titanium [52].

There are many methods of developing porous titanium scaffolds including compression and sintering of beads and fibers, combustion synthesis, solid state foaming by expansion of gas filled pores, polymeric sponge replication and electron beam melting [54].

#### ***1.4.2 Electron Beam Melting***

Electron beam melting (EBM) creates non-random, open cell geometry, one that has a repeating lattice structure. Reports have found that non-stochastic open cell structures can lead to better mechanical properties when compared to stochastic foams or geometries that lack a repeating unit and have random variations in cell size and structure [55]. Rapid prototyping or solid free form fabrication, a quick fabrication method using 3D CAD data, has a distinct advantage for producing orthopedic scaffold implants because there is very tight control over internal architecture and potential for complex shape pores [56]. EBM is a direct metal fabrication method of solid free form fabrication.

The EBM process is a direct metal layered fabrication technique. It starts with a CAD file of the desired 3D part. The software that controls the EBM machine converts the file into 2D sliced data for the process. There is a bed of Ti powder in a vacuum chamber of the machine used to create each layer of the part. The electron beam selectively heats the powder to create a weld pool that will become the component.

Each layer of powder is first preheated by scanning the beam at low power and high velocity to lightly sinter the particles, and then the electron beam is scanned over the part at higher power. This process is repeated until the full part has been formed [57]. EBM can be used to create virtually any geometry desired based on the given repeating unit cell. Dodecahedrons have been used to accurately model the orthotropic properties of bone making it an ideal unit cell for a titanium lattice implant [58].

In a study comparing turned Ti-6V-4Al samples to EBM samples both showed similar levels of % bone implant contact, BIC, (30-40%) though due to the much larger surface area of the EBM samples the absolute level of BIC is much higher for the EBM samples. This increase could potentially create increased biomechanical stability of an implant [59]. In an *in vivo* study in pigs it was found that after 60 days porous EBM implants had ~40% bone ingrowth. The bone growth was steady throughout the period of 60 days and at the end of the study the bone was very similar to the pristine bone around the implant [60]. In a long term (26 week) study on sheep porous implants had 60% BIC. It was also found that solid implants showed significantly thicker fibrous encapsulation than the porous implants [61]. In many cases porous EBM Ti structures showed much thicker oxide layers than traditional machined structures with oxide layers up to 4x as thick on the EBM Ti compared with machined Ti. The thicker oxide layer is a result of the high temperature of EBM and the oxygen in the Ti powder is situated at the surface. This thicker oxide layer provides protection against leeching of Ti ions into the body [59-61].

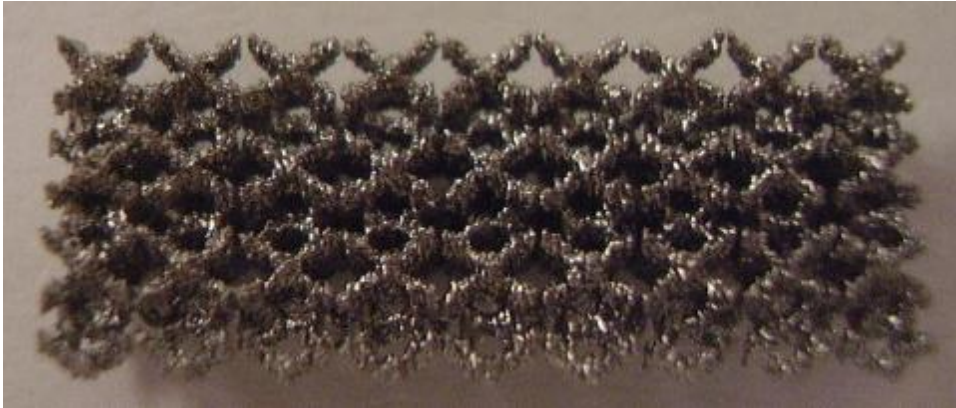


**Figure 2.2.** Dodecahedron unit cell Ti-6V-4Al lattice structure

## **1.5 Implant Coatings**

Implants with mechanically stable, adherent coatings can help to improve bone fixation and apposition between bone and implant as well as improve the osseointegration of implant. This will lead to a longer implant life and improved quality of life for patients receiving an implant. Various porous coating have been shown to improve osseointegration and BIC while reducing infection leading to prolonged implant life time [62, 63].

### ***1.5.1 Coatings and Methods***

Hydroxyapatite ( $\text{Ca}_5(\text{PO}_4)_3\text{OH}$ ), a mineral constituent in bone, has been widely acknowledged to encourage osseointegration [64-66]. Hydroxyapatite coatings have been shown to encourage osseointegration by preventing fibrous encasement of implant, increasing bone apposition rates, providing a strong and continuous BIC that can transmit compressive, tensile and shear loads, and accelerated healing [64]. Multiple studies have shown promise for hydroxyapatite coating in total joint replacements [65, 66]. Despite the promise, hydroxyapatite coatings have their issues,

they have been shown to have weak adherence to Ti [64]. The relatively high crystallinity of hydroxyapatite coatings can make them brittle and prone to degradation under biomechanical stresses [67]. Hydroxyapatite coatings can be applied many ways including electrochemically deposited [65], aerosol sprayed [66] and plasma sprayed [64, 67]. Plasma sprayed hydroxyapatite have to mismatch between the crystallinity of the coating and the bone mineral phase causing a mismatch in mechanical properties that leads to delamination of the coating [67].

Dip coating and drip coatings are two common techniques used in applying phospholipids to Ti. Dip coating is simple and easy, and is done by dipping the titanium sample into a bath of phospholipids dissolved in a solvent [68]. However with dip coating it is difficult to control or quantify the amount of phospholipid deposited on the surface. Drip coating consists of dripping the phospholipid solution onto the sample and is advantageous as it allows for direct control of the quantity of phospholipids deposited and is easy to do [69]. The resulting coating is not well adhered to the Ti and is uneven in thickness and continuity. This process also does not work well on 3D surfaces [15, 68].

### ***1.5.2 Phospholipid Coatings***

Phospholipid coatings have been shown to produce bioactive chemicals that are capable of encouraging and accelerating matrix mineralization as well as osseointegration in addition to helping fight inflammation [7, 8, 12, 14] which leads to faster patient recovery. Studies have shown that a negatively charged phospholipid coating can induce hydroxyapatite crystal nucleation [3, 12]. The compound formed by

the interaction of phospholipid, calcium and inorganic phosphate may be essential for inducing calcium phosphate deposition [8]. There is evidence that phospholipid-calcium-phosphate complexes are involved in initiating the mineralization process, playing a role in encouraging matrix mineralization and osseointegration especially in calcium rich environments [14].

The specific phospholipid, phosphatidylserine, DOPS, has been shown in various studies to be most effective for encouraging osseointegration and matrix mineralization [6-8]. Relatively DOPS has a high negative charge of -1 when at pH 7, this could account for the high effectiveness of DOPS as calcium binding capacity correlates to the negative charge of the lipid head group [70]. DOPS coatings have also been shown to increase the apposition of new bone on a titanium surface when compared to uncoated titanium as well as to enhance bone ingrowth. Phosphatidylserine coatings have not been shown to encourage the formation of a fibrous tissue layer [15]. These coatings have been shown to stimulate deposition of bone precursor minerals as well as afford good surface properties for adhesion of osteoblasts [71, 72].

Almost immediately after implantation monocyte derived macrophages begin to adhere at the implant surface and frequently fuse to form foreign body cytokines, and growth factors. These monocyte derived molecules contribute to cell activation involved in inflammation, wound healing including neutrophils and fibroblasts. This cell activation is what leads to fibrous encapsulation of the implant and an inflammatory reaction [70]. The negatively charged phospholipid coatings have the potential to reduce the effects of the macrophage adhesion and help to reduce the inflammatory

response. It has been shown that phosphatidylserine has some pro-inflammatory effects [73].

### **1.5.3 Electro Spray**

Electrohydrodynamic atomization (electrospray or e-spray) refers to the atomization of a liquid through the coulombic interaction of charges on the liquid and an applied electric field. The electric field accelerates the liquid resulting in disruption into particles as well as a buildup of charge [74]. Despite a long history e-spray has only recently been used in biomedical applications and is capable of creating thin, uniform, adherent coatings. It has been used to apply many types of coatings, including living organisms to many different materials [75-77].

E-spray creates a high efficiency coating due to the charged source material being carried directly to the destination material by the field lines [76]. In e-spray a pump slowly pushes the fluid through a capillary where the electric field is applied. The electric field is the primary atomization and acceleration force, dissimilar to mechanical atomization in which case pressure is primary atomization and accelerating force [74]. Pressure-based spray systems tend to be less efficient because there is no direct control of where the material is going [76]. E-spraying facilitates good control of spray in creating uniform and conformal coating morphologies on many surfaces including rough and complex shaped surfaces [78]. The process can create a coating with extremely precise, uniform thickness [76].

The applied electric field induces mutually opposite forces (surface tension and viscoelastic forces) on the fluid that help to retain the hemispherical shape of the

droplet formed while the charge induced through the electric field wants to deform the droplet into a conical shape called a Taylor cone. Once the voltage breaches a threshold value the electric forces are overwhelmed and a charged jet emerges from the Taylor cone. Electro spraying occurs when this jet breaks into small, charged droplets [76, 79, 80].

When this process is applied to high viscosity fluids it results in a protrusion of fine threads called electrospinning. Low viscosity fluids are those that break up into particles when an electric field is applied and leave the capillary as very fine mist in electro spraying [80]. There are many different forms of electro spray modes all based on differing fluid properties, primarily conductivity, and the resulting spray cone and meniscus [79]. Many parameters in the e-spray process affect the particular morphology created at the target including, voltage potential, source fluid conductivity, viscosity, density and surface tension, source fluid concentration, pump rate through capillary, working spray distance, capillary diameter, time and surface area of target material [76, 79, 81, 82]. It is also important to consider other parameters that might affect a particular application such as in the case of biological applications the chemical composition of the source material (cyto and bio- toxicity) are important considerations.

#### ***1.5.4 The Faraday Cage Effect***

A Faraday cage is a volume of space that is totally enclosed by an electric conductor. When an external electric field is applied the charges in the conductor move and reflect causing the electric field inside the cage to cancel. When Faraday cages are intentionally created to provide a shield against external charges, frequently to protect

sensitive electronics they are usually made of a metal mesh. These shields are not perfect as with a mesh small amount of charge are able to enter the cage [83]. The Faraday cage is an equipotential surface. On an equipotential surface there is no flow of charge. By Gauss' Law, a law relating the distribution of electric charge to the resulting electric field, if there is no electrical charge inside the conductor there will be no electric field. An applied electric field produces the forces on the charge carriers, electrons, within the conductor. As soon as this field is applied to the surface of an ideal conductor it generates a current that causes displacement of charge inside the conductor which cancels out the applied field within [84].

It is often difficult to penetrate a Faraday cage when trying to apply charged powder particles to recessed areas or hidden corners in a part [85]. Powder coating is similar to electro spraying in that both use charged particles and electric field lines to move the source material to the target, though e-spray uses a liquid working fluid while powder coating uses a gaseous (air) working fluid. The Faraday cage effect is a very serious problem in the powder coating industry. Part geometries are frequently complex and have features that induce local Faraday cages when electric fields are applied, thus preventing coating of these areas. Electric field lines also tend to concentrate on recessed edges, primarily because those edges are closer to the spray apparatus than interior surfaces [86].

Another problem prevalent in the powder coating industry is back ionization, which can compound the Faraday cage effect. When an electron passes through a strong electric field, like the field induced for coating with a voltage potential, it will

begin to move along the field lines and be accelerated by the field force. If it has enough kinetic energy it will split to form ions. Then more electrons will split and form ions and electrons and so on, in a self-sustaining process. At high enough voltages this rapidly creates excess free ions; and an effect called corona discharge [87]. The excess free ions will move rapidly towards the target and saturate it with extra charge, leading to back ionization or rejection of charged material at the target [88]. While corona discharge is not as well addressed in the literature of e-spray with relationship to the Faraday cage effect, it has shown in up some studies regarding electrospray, where it has been demonstrated to have an effect on the spray pattern [89, 90].

There is ongoing debate in powder coating as to what parameters can be adjusted to mitigate the Faraday cage effect. One highly considered parameter is the voltage of the particles. Some believe that particle velocity should be reduced while others feel it should be increased [88]. It is clearly an important parameter - the most important one in terms of Faraday cage effect. If the particle charge to mass ratio could be reduced to nearly zero and used in a system that does not induce a high strength field the Faraday cage effect would be completely mitigated [85]. A free ion collector can also be used to collect excess ions formed in the corona discharge [88].

## **2 Motivation and Long Term Goal**

### **2.1 Implant Rates**

Medical device implantations in humans are increasingly popular, with millions of new implantation and revision surgeries occurring each year. In the last decade the number of implants and internal fixation devices needed worldwide has grown rapidly, by 2010 more than 4.4 million people had at least 1 internal fixation device and 1.3 million people had a joint replacement[91]. Approximately 600,000 total joint replacements are carried out each year in the United States[92]. The rate of hip fractures is expected to triple from 1.66 million in 1990 to 6.26 million worldwide by 2050[93]. In the European Union an increase from 414,000 to 972,000 cases of hip fracture is expected to occur in the next 50 years. Osteoarthritis contributes an estimated 50,000 total hip replacements in the United Kingdom and 193,000 in the United States[94]. The expected lifespan of total knee replacements is generally about 12-15 years[95]. The average age of patients who undergo a total knee replacement is approximately 50 years of age[93]. With the average age of the population increasing the number of joint replacement and revision surgeries is expected to increase. Primary total knee arthroplasty and total hip arthroplasty cost on average \$2.249 million and \$1.136 respectively each year[96].

### **2.2 Implant Infection Rates**

Infection is one of the leading causes of implant failure. The rate of infection during major surgery is 0.5-6% despite the use of prophylactic antibiotics. In trauma cases with contamination, vascular injury or exposed bone there is a rise of infection

from 2.5% to 12% and in cases with fungal or bacterial bone infection the rate is reported to be from 10-50%[93]. The rate of prosthetic joint infection is 1% to 3% even with surgeons adhering to strict use of correct surgical techniques, aseptic measures, and antibiotic prophylaxis[97]. Infective complications for prosthetic hip replacement and knee replacement due to osteoarthritis are 2% - 6% and 0.7% - 9% respectively[93]. Infection in craniofacial restorative surgery is especially common. In one study

Kummoona found that there was restorative failure in 10% to 24% of patients due to infection of the underlying tissue or an allergic reaction to the osteomesh [98]. Osteomyelitis is a common result of the introduction of pathogens from skin into bony tissue. It occurs in 1% to 13% of cases during orthopedic surgeries repairing fracture or in joint replacements. Osteomyelitis can occur in up to 33% of cases of oncological orthopedic surgeries [99]. In 5% - 33% of cases of open fractures chronic osteomyelitis or acute infection occurred[100]. In 2001 there were an estimated 100,000 to 200,000 cases of fracture fixation-associated device infections[93].

Infection is also a common cause for revision surgeries. In a study by Grimer of 34 patients experiencing infected endoprosthesis it was found that 26% of people experienced reinfection, and then 17% required amputation of the infected limb[99].

### **2.3 Other Implant Failures**

Implant loosening due to particulate wear debris and poor osseointegration is a common cause of implant failure, accounting for about one third of total joint replacement failure. In a UK study of 331 patients with total hip replacements 10% of patients required revision surgery and 60% of those cases were caused by device

aseptic loosening[101]. Aseptic loosening is often caused by poor binding of the bone to the metallic surface of the implant [102] and non-mineralized tissue that impedes direct contact of the bone with the implant. The non-mineralized tissue that forms is rich in collagen and proteoglycans and despite its thinness impairs the mechanical stability of the prosthesis leading to failure. In some circumstances this tissue can even trigger a protracted inflammatory response which leads to the formation of a relatively thick fibrotic capsule interposed between the bone and the implant[15].

## **2.4 Research Goal**

The ultimate goal of this research is to extend the e-spray process into coating Ti lattice implants with phospholipids. Phospholipid coatings are known to enhance the growth and proliferation of osteoblasts as well as the mineralization of bone precursor minerals. They are also non-cytotoxic, and enable delivery of antibiotics that can fight and prevent infection at the site of the implant. In the long term this research could provide a customizable coating designed specifically for each patient's needs. This work has the potential to provide a platform for future osseogenic and therapeutic coatings with varying drugs or bioactive agents to enable controlled elution profiles.

### 3 Proposed Research, Specific Aims and Hypotheses

In this work electrospray was investigated for efficacy of spraying 1,2-dioleoyl-*sn*-glycero-3-phospho-L-serine (DOPS) onto 3D Ti 6V-4Al lattice structures. The structures used in testing were designed to show the capability of the process on clinically relevant porosities and depths. Tests were done to determine the effect of parameter variation on the coating morphology and depth as well as whether they could impact the Faraday cage effect of the induced electric field. The surface morphology of the raw parts was also considered and acid etching was done to determine if it could be changed.

In the initial work the titanium lattices were discovered to be Faraday cages when externally, circumferentially insulated. This insulation was originally done to allow for smaller part sizes and still demonstrate depth of coating. After the discovery of the Faraday Cage Effect, parameter variation was done to determine if electrospray process parameter variation could mitigate the Faraday cage effects and achieve deep, uniform coatings. There were no parameters with any noticeable effect on the Faraday cage effect. The external insulation increased the Faraday cage effect so much that we decided to consider lattices without external insulation.

Lattices were tested without any external insulation to determine if the Faraday cage effect was still present. Three different lattice porosities were tested. We discovered that 71% and 61% porosity lattices could be coated. The 54% porosity lattice did demonstrate the Faraday cage effect. The coatings on 71% and 61% porosity lattices were not uniform and consistent from area to area despite that DOPS was present

everywhere. The 54% porosity lattice had overspray at the edges of the lattice where the DOPS was unable to penetrate.

The 71% and 61% (capable of being coated) were used to determine if parameter variation had any effect on the morphology of the coating, including its uniformity and conformity. Increasing time did increase the coverage of the lattice, and variation of the other parameters caused some small morphology changes though all lattices showed overspray at the edges and some showed inconsistent morphologies throughout the inner faces of the part. When all parameters are held constant and time is adjusted with surface area the coating morphology is consistent, uniform and conformal. When the parts are chemically etched it affects the morphology of the surface though it does not affect the roughness of the part on a macro scale. Any chemical etching creates the same nano scale morphology that is consistent with Ti-6V-4Al.

### **3.1 Specific Aims and Hypotheses**

#### ***3.1.1 Specific Aim 1: Titanium Lattices and the Faraday Cage Effect***

**Specific Aim 1:** Determine whether titanium lattices exhibit Faraday Cage Effect under differing DOPS electro spray coating conditions

**Hypothesis 1a:** Titanium lattice cylinders when externally circumferentially insulated will demonstrate the Faraday Cage Effect.

**Hypothesis 1b:** When unmasked titanium lattice cylinders reach certain low enough percent porosity they will begin to exhibit the Faraday Cage effect

### ***3.1.2 Specific Aim 2: DOPS Coatings and the Faraday Cage Effect***

**Specific Aim 2:** Characterize the relationship between the Faraday Cage Effect and e-sprayed phospholipid coatings

**Hypothesis 2a:** Lattice percent porosity relates to coating coverage and conformity, when the lattice has a high enough percent porosity the DOPS will coat fully in a uniform and conformal fashion

**Hypothesis 2b:** Lattices demonstrating the Faraday Cage effect will have spotty, uneven coating with overspray at the outside of the lattice.

### ***3.1.3 Specific Aim 3: Process Parameters and Their Effects on DOPS***

#### ***Coating Characteristics***

**Specific Aim 3:** Evaluate the effects of e-sprayed parameters on DOPS coatings on 3-dimensional titanium lattice structures by comparing the effects of e-spray process variables (distance, voltage, concentration) on phospholipid coating uniformity, conformity, and penetration depth into the titanium lattice structure.

**Hypothesis 3a:** Decreasing voltage will increase coating uniformity and conformity

Increasing e-spray time will increase coating coverage (depth) of penetration of coating

Decreasing surface roughness (changing surface area) will not affect coating uniformity, conformity or penetration depth if the spray time is constant with surface area

**Hypothesis 3b:** Surface roughness of titanium lattice can be controlled with chemical etching – with roughness decreasing as etching time increases until an asymptote is reached.

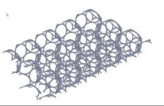
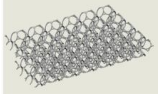
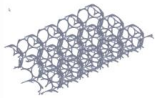
## 4 Materials and Methods

### 4.1 Experimental Approach

This chapter focuses on the overall experimental design and materials and methods used in this work. The e-spray process has much potential for being used to create osseointegrative coatings on orthopedic implants. It is important to find out what the limitations of the process are as it is applied to more complex geometries. This work builds upon work recently done using e-spray to coat flat Ti squares with DOPS, following the same protocols and using similar parameters [48]. Coatings were examined using SEM and EDS to verify their presence as well as categorize the particular morphologies created.

Table 4.1 presents all sample used in this work and the corresponding sections of methods and results.

**Table 4.1.** All samples used in this work

Sample Name	Percent Porosity	Pore Size (mm)	Etched	Hypo	Methods	Results	Picture
61% Insulated	61%	2.2	No	1a	4.2.1	5.1.1	
54% Porosity	54%	1.6	No	1b, 2b	4.2.2	5.1.2, 5.2.1	
61% Porosity	61%	2.2	No	1b, 2a, 3a	4.2.2, 4.2.4	5.1.2, 5.2.1, 5.3.1	
71% Porosity	71%	3.2	No	1b, 2a, 3a	4.2.2, 4.2.3	5.1.2, 5.2.1, 5.3.1	
Flat Ti	N/A	N/A	No	3a	4.2.5	5.3.2	
Strut	N/A	N/A	Yes	3b	4.2.6	5.3.2	

#### **4.1.1. Sample Preparation**

The Ti lattice structures were manufactured using electron beam melting and were provided by Medical Modeling. Three different porosity structures (54%, 61% and 71%) were designed to create relevant pore sizes for bone ingrowth. The parts were also designed to be sized to show that the process could coat at clinically relevant depths.

Ti samples were cleaned according to the *Ti Cleaning and Preparation Protocol*, provided in appendix A. Samples were sonicated for 30 minutes in 100 ml acetone to remove any oil and organic debris that might be present, then rinsed in tap water and sonicated for 15 minutes in 100 ml of 2% Liquinox (stirred every 5 minutes to ensure proper mixing of solution around samples). Samples were then rinsed three times in de-ionized water (DI-water) to remove any remaining Liquinox, sonicated for 15 minutes in 100 ml of DI-water (stirred every 5 minutes), rinsed once in ethanol and once in acetone, then allowed to dry completely in room air before use. Samples were usually cleaned immediately prior to use, when not used immediately samples were stored in well plates at room temperature.

The portion of the work done to determine the effects of acid etching on EBM titanium lattices followed the same cleaning protocol mentioned above as well as the etching and passivation process as detailed in the *Ti Cleaning and Preparation Protocol* in Appendix A, which is adapted from ASTM B600 – *Standard Guide for Descaling and Cleaning*. Samples were bathed in 3.5% HF for a minimum of 30 seconds and a

maximum of 5 minutes. This removed the existing titanium oxide layer as well as modified the surface morphology of the structures. Samples were then soaked in 35% HNO<sub>3</sub> for 30 minutes at 50 C to generate a new oxide layer and then soaked in DI water for 24 hours. Following this the samples were dried and used immediately.

#### **4.1.2. Electrospraying**

The phospholipid molecule used in our work is synthetic 1,2-dioleoyl-*sn*-glycero-3-phospho-L-serine (DOPS) - C<sub>42</sub>H<sub>77</sub>NO<sub>10</sub>PNa. This choice was based on our prior work as well as the research done on DOPS use in osseointegration.

Samples were E-sprayed according to the *Electro-Spraying Titanium* protocol found in Appendix B. Briefly, phospholipids were first dissolved in chloroform. All storage containers were either glass or polytetrafluoroethylene (PTFE), and plastic caps on mixing bottles were lined with PTFE liners. DOPS was E-sprayed at 1.3% with other parameters initially determined from prior work to create thin, conformal, consistent coatings. Figure 4.1 shows a diagram of the e-spray process.

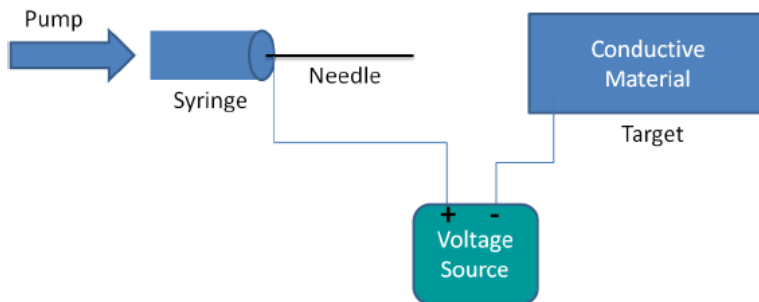


**Figure 4.1.** E-spray process diagram

A syringe pump pushes the liquid source material at a controlled rate onto a target material to which a high voltage potential has been applied. The target material

is mounted at a specified distance from the source and an electric field is formed over this distance. Figure 4.2 shows the e-spray apparatus setup used in this work.

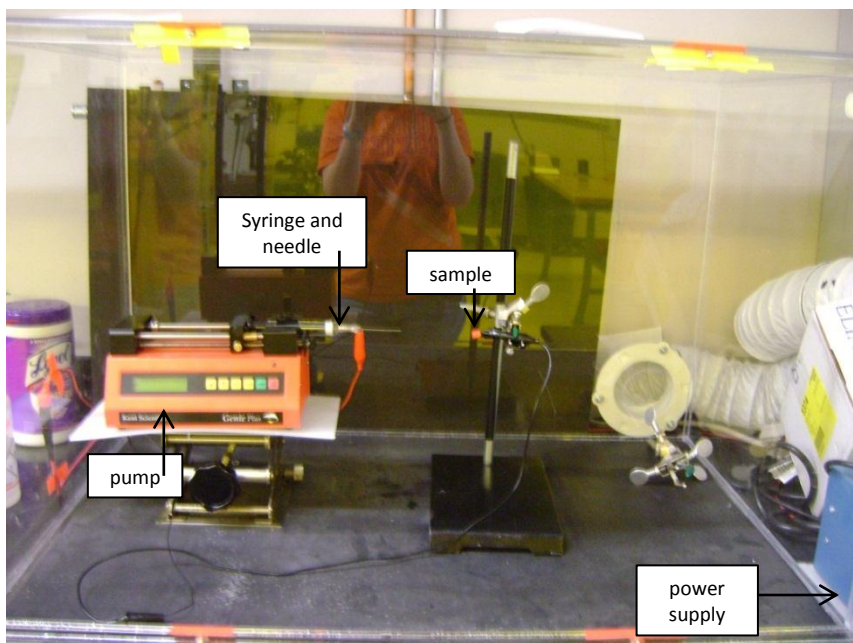


**Figure 4.2.** E-spray apparatus setup

Target samples were held with a small copper alligator clip that was clipped onto both halves of each sample. The target sample was positioned at the specified distance from the needle which was connected to the positive pole of a controlled voltage source. The copper alligator slip was connected to the negative, ground, pole of the voltage supply. The syringe pump (Kent Scientific) was set to specific spray rate to work with the syringe (10cc, glass, air tight, Hamilton) used for this research. The target sample was aligned so its center axis lined up with the needle.

As the syringe pump was activated, source material sprayed from the syringe needle as a very fine, almost indiscernible mist which emerged from the needle in a cone-shaped pattern and became invisible within an inch of the needle, as shown in figure 4.3. In some work the sample had external insulation (tape) around it to direct

the spray only into the front (spray side) of the lattice. Electrical tape was frequently used to mask certain areas from exposure to the E-sprayed solution, such as any exposed area that was grounded in the system.

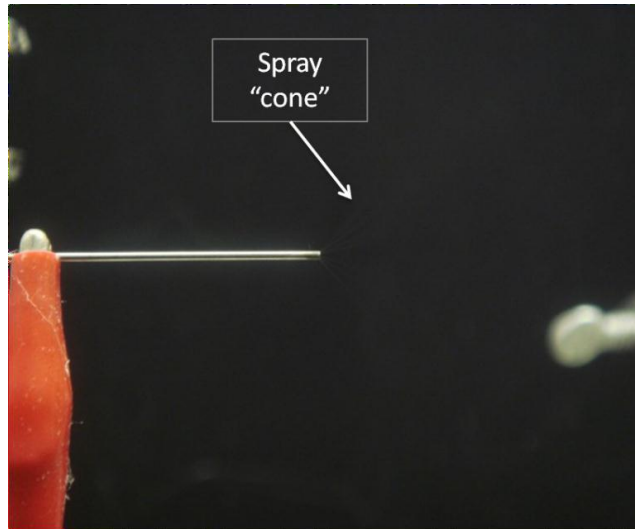


**Figure 4.3.** Nearly invisible e-spray spray cone at needle tip

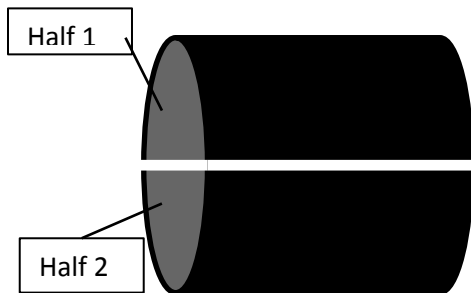
The base parameters used in initial work (developed previously in the James Research Group at Colorado State University by Dr. Prawel) were a spray distance to the back of the sample of 8 cm, 12kV, spray rate of 14 ml/hr and DOPS concentration of 20mM [48]. The spray rate was never varied though the other parameters were. The spray time was based on surface area (previous work suggesting that 1 minutes of spray per 1 cm<sup>2</sup> of surface area) though in this work that was difficult due to the complexities of the parts. The surface area of the part is calculated as following the *Lattice Surface Area Calculation Protocol* in Appendix C. The nominal surface area was calculated by measuring the diameter and length of a strut and using those to generate a volume for 1 strut. The mass was calculated using the previously calculated volume and the density of Ti-6V-4Al. The length and diameter were also used to calculate the surface area of

one strut. The actual mass of the sample was measured and then a factor was generated that was the ratio of the true mass of the sample to the calculated mass of a single strut. This ratio was applied to the surface area as the relationship is the same.

The source material (DOPS dissolved in Chloroform) was prepared according to the *Mixing PL Protocol*. DOPS was kept frozen at -4 C until use.

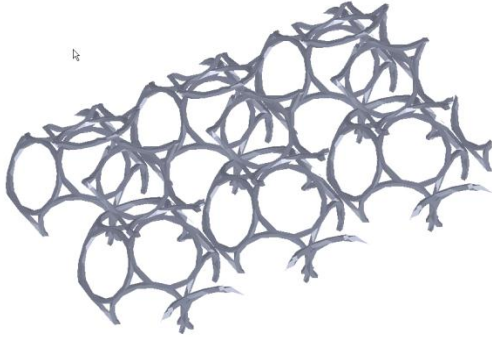
### **4.1.3 EBM Manufacture**

The lattices were manufactured in two matching halves that fit together so that after coating the halves can be separated and the inner face can be viewed under SEM, see figure 4.4. The lattices were created using an Arcam EBM Systems Model S-12, manufactured in Amsterdam under these parameters: 60kV electron beam, 2.4mA current, 0.5 mS spot time, 50um layer thickness.

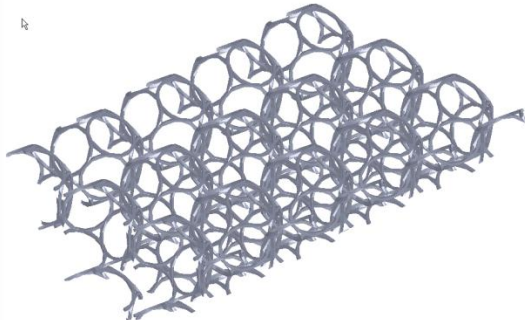


**Figure 4.4.** Cylinder halves in setup

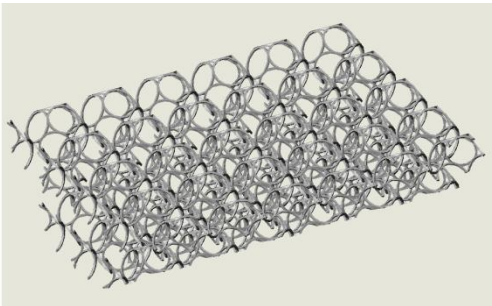
Computer models of each percent porosity lattice are in figures 4.5-4.7. A unit cell is the repeating structure that makes up lattice based on a pore size (figure 4.8). The pore sizes are 1.6mm, 2.2mm, and 3.2mm respective to the porosities 54%, 61%, and 71%. The dodecahedron unit cell was chosen to optimize surface area to free volume of the structure. This is to allow for high surface area for cell adhesion and high void space for good flow of fluids. Figures 4.9-4.11 show the real picture for each lattice porosity.



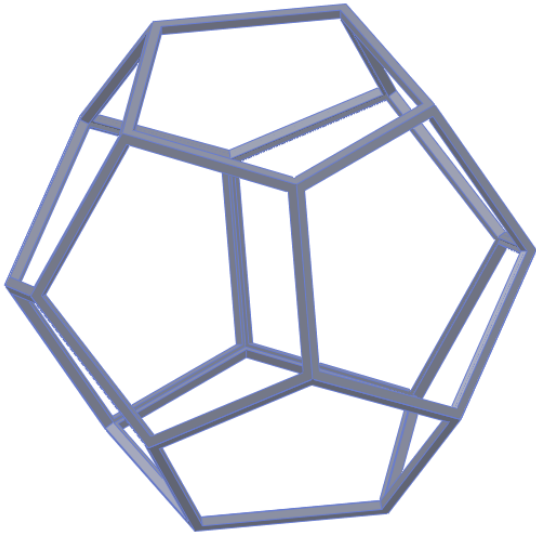
**Figure 4.5.** Computer model of 71% porosity lattice



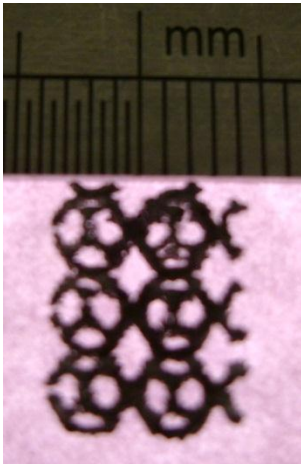
**Figure 4.6.** Computer model of 61% porosity lattice



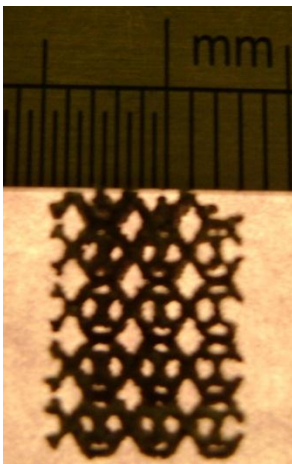
**Figure 4.7.** Computer model of 54% porosity lattice



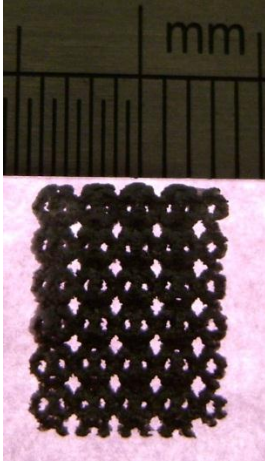
**Figure 4.8.** Dodecahedron unit cell



**Figure 4.9.** Picture of 71% porosity lattice



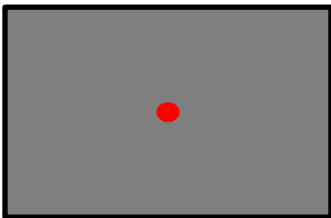
**Figure 4.10.** Picture of 61% porosity lattice



**Figure 4.11.** Picture of 54% porosity lattice

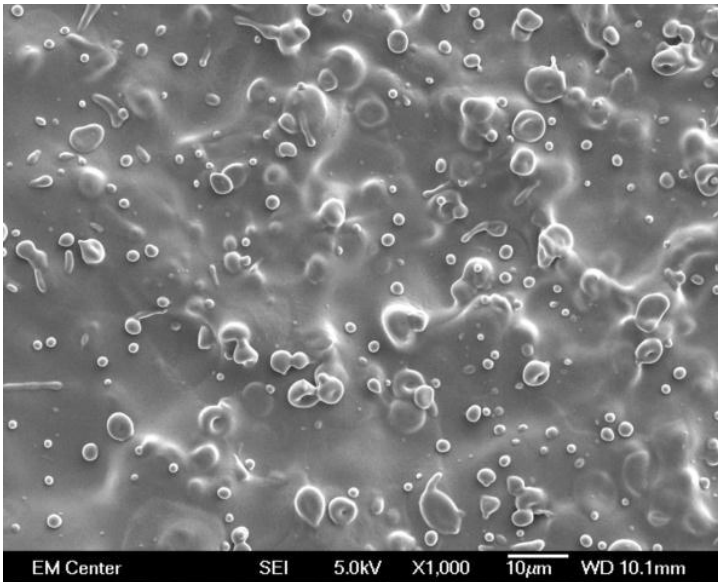
#### ***4.1.4 SEM, EDS, and SWLI Characterization***

The bulk of characterization was performed with SEM. The samples were gold coated (20 nm) and imaged with an accelerating voltage of 15kV (except where figures indicate otherwise). The images captured are representative of the samples (except where figures indicate otherwise) and were used to characterize the surface morphology. All SEM work was done with a JEOL JSM-6500F, manufactured in Japan. The lattices were viewed with SEM on the inner face of the lattice to determine the extent of penetration except in those figures where it is labeled otherwise. We define the term “middle” of the inner face as shown in figure 4.12.



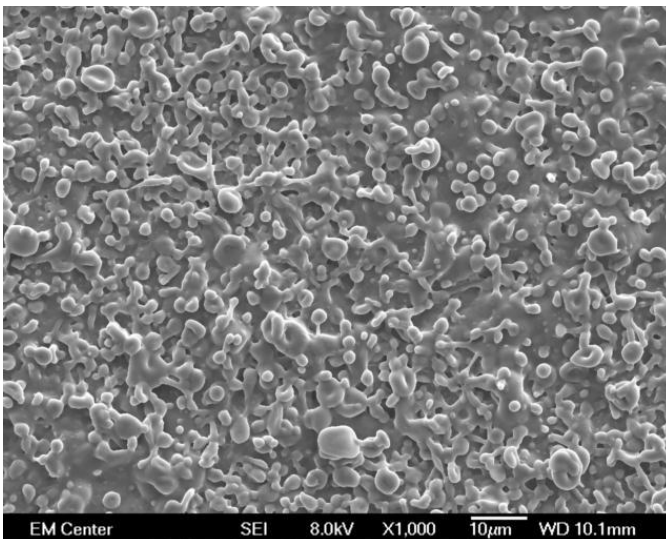
**Figure 4.12.** Inside face of 1 half of lattice, red dot indicates middle; grey indicates space filled with lattice

Figure 4.13 shows a sample of flat Ti e-sprayed with DOPS as the parameters used in this work. This figure shows how DOPS looks on Ti and is used as comparison for the work done on lattice structures.



**Figure 4.13.** DOPS e-sprayed on flat Ti at 8cm, 12kV and 20mM

Figure 4.14 shows an overspray morphology on flat Ti. “Particles” of DOPS can be seen on the surface.



**Figure 4.14.** DOPS e-sprayed on flat Ti – overspray morphology

Electron dispersive spectrometry (EDS) was performed on samples to verify the presence of DOPS. The image was captured with the SEM and EDS performed to determine the different material components present on the surface. The EDS software is made by Thermo Electron Corporation in Illinois.

Scanning white light interferometry (SWLI), a surface metrology tool that uses a white light laser to capture the topology of surfaces, was used to characterize surface roughness and surface area of EBM struts. A New View 5400 series optical profilometer, manufactured by Zygo in Arizona, was used for this work. All parts were scanned between 400nm-800nm depth with a 20x objective. The software has the capability to remove underlying part form as well as allowing for a line profile to be set at the user's discretion. In this work the cylindrical shape of the strut was removed with a 4<sup>th</sup> order remove to allow for an accurate surface topological roughness. The software was used to collect Ra and Rz. Ra is the average of the absolute values and Rz is the average distance between peaks and valleys. These were collected as they provide representative values to numerically describe the surface.

## ***4.2 Experiments Performed***

### ***4.2.1 Externally Insulated Lattices***

To determine that the titanium lattices could be e-sprayed at clinically relevant depth they were externally insulated to provide only one e-spray entry point into the lattice. This was to quantify depth of spray.

In this experiment the 61% porosity lattice was externally, circumferentially insulated using paper tape (Fisherbrand Colored Label Tape, 0.5" thick, red). The setup

is seen in figure 4.8. Table 4.2 lists the parameters varied against those being controlled. The experiment was run with a sample size of 3. Results were gathered with SEM and EDS.

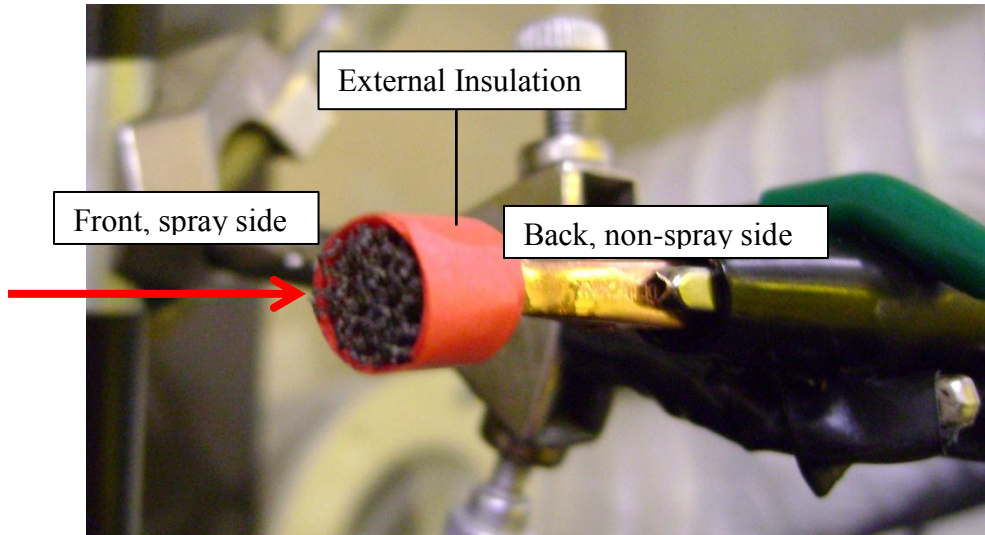


**Figure 4.8.** Insulated cylinder spray set up, red arrow indicates spray direction

**Table 4.2.** Parameter interaction on externally insulated cylinders, X indicates the parameter variations that were tested on 61% porosity lattices

Voltage Constant (12kV)			Distance Constant (8cm)		
	20mM	10mM		20mM	10mM
8cm	X	X	12kV	X	X
4cm	X		18kV	X	
Concentration Constant (20mM)					
	8cm	4cm			
12kv	X	X			
18kV	X				

#### **4.2.2 No Insulation, Porosity Variation**

After discovering that the lattices become Faraday Cages when externally insulated all lattice porosities were e-sprayed without external insulation to determine if the Faraday Effect could be mitigated by porosity. The same setup was used as in figure 4.7 except the lattice did not have the external insulation.

The experiment was run on 54%, 61%, and 71% porosity lattices. The parameters used were 8cm, 12kV and 20mM DOPS, no parameter variation was done in this work. The study was done with n=3. The results were gathered with SEM and EDS.

#### ***4.2.3 Parameterization***

This study investigates the relationship of parameterization on the coating morphology created on the lattices. The 71% porosity lattices were e-sprayed with the same parameter variations in table 4.1 without any external insulation. The study was run with n=3. The results were gathered with SEM and EDS.

#### ***4.2.4 Time Based***

In an experiment using the 61% porosity lattices with the parameters held constant at 8cm working distance, 12kV and 20 mM concentration DOPS the time was varied to determine if increasing the spray time increased the DOPS coverage of the lattice. The study was run with 8 time points, starting at 1 minute of e-spray and increasing in 1 minute intervals to 8 minutes of e-spray. The study was run with n=3 and results collected with SEM and EDS.

#### ***4.2.5 Surface Area and Coating Morphology***

A study was run to determine the effect of surface area on coating morphology. Five different surface areas (0.25cm<sup>2</sup>, 1cm<sup>2</sup>, 2.25cm<sup>2</sup>, 4cm<sup>2</sup>, 6.25cm<sup>2</sup>) were electrospayed with time adjusted to increase proportionally with surface area. The e-spray parameters were constant for all samples, 8cm, 12kV, 20mM. The spray time was determined using the relationship specified above of 1min/cm<sup>2</sup>. This study was run with n=4 and results were collected with SEM and EDS.

#### **4.2.6 Acid Etching Effects**

An experiment was run to determine the effects of acid etching on the raw EBM material, individual struts were placed in hydrofluoric acid for 0, 2, 3, 4 and 5 minutes. The etching was done according to the *Ti Cleaning and Preparation Protocol* as discussed above. SEM and SWLI were used to collect the data.

#### **4.3 Statistics**

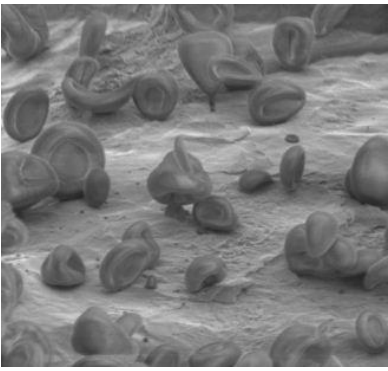
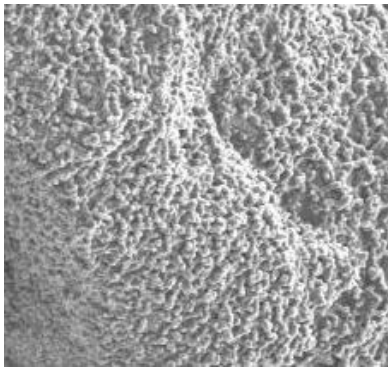
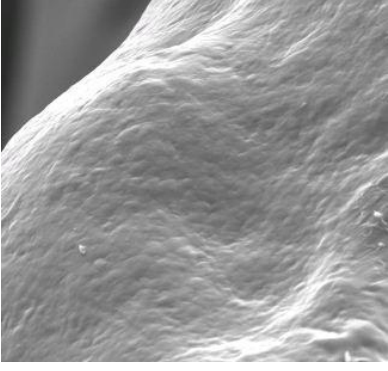
All statistics were performed using Sigmaplot, owned and manufactured by SYSTAT Software. The tests performed were all one way ANOVA to compare sets of data to each other. Data differences were considered statistically significant if the p value was less than 0.05.

## 5 Results and Discussion

In this chapter, the results pertaining to each specific aim and the associated hypothesis is presented and then discussed. The discussion section is labeled with a header to indicate that there is a switch from results to discussion.

Table 5.1 shows the different DOPS coating morphologies found in this work. Table 5.2 presents the results of this work with references to the section it can be found in, samples named consistently with table 4.1.

**Table 5.1.** DOPS coatings morphologies in this work

	
<b>Blood Cell Morphology</b>	<b>Overspray Morphology</b>
	
<b>Smooth 1 Morphology</b>	<b>Smooth 2 Morphology</b>

**Table 5.2.** Compiled results from this work

Section	Sample	Results
5.1.1	61% Insulated	All lattices: 0.5-1 unit cell of spray depth, no full coating, Faraday cage effect induced
5.1.2	54% Porosity, 61% Porosity, 71% Porosity	61% porosity, 71% porosity coat fully, 54% porosity did not coat fully
5.2.1	54% Porosity, 61% Porosity, 71% Porosity	61% porosity, 71% porosity coat fully but coatings are not uniform or conformal, 54% porosity did not coat fully and where it did coat is spotty and uneven
5.3.1	61% Porosity, 71% Porosity	Parameterization (voltage, distance, concentration) on 71% porosity does not cause changes in coating morphology, uniformity or conformity. On 61% porosity increasing spray time does increase coating coverage
5.3.2	Flat Ti, Strut	Increasing surface area (with time increased proportionally) does not cause coating morphology changes. Strut surface morphology can be controlled with acid-etching but surface roughness does not decrease with increased acid-etch time

### **5.1 Specific Aim 1: Titanium Lattices and the Faraday Cage Effect**

Electrospraying can be used to create thin, conformal, uniform coatings on flat plates of titanium. This work focuses on applying the same procedure to titanium lattice structures used to emulate the porous titanium of an orthopedic implant. This work was done to prove that e-spray could be used to apply similar, thin, conformal coatings on different porosity titanium lattice structures. The specific aim addressed in this section is: Determine whether titanium lattices exhibit Faraday Cage Effect under differing conditions. Scanning electron microscopy (SEM) was used to visually inspect

the cylinders for phospholipid coatings that had been deposited on the surface. The coatings can be seen with the naked eye only when extreme overspray is present and appears as a white coating on the affected areas. The results and discussion of these results are presented below in 5.1.1 and 5.1.2.

### **5.1.1 External Insulation and Faraday Cages**

Even when e-sprayed at varying parameters (distance, voltage, DOPS concentration) the lattices demonstrated an inability to coat at any depth. Figures 5.1-5.4 show the externally insulated cylinders with the varied parameters.

In each case the e-spray coating was able to penetrate approximately 0.5 to 1 unit cell in depth into the lattice as seen in the figures below.

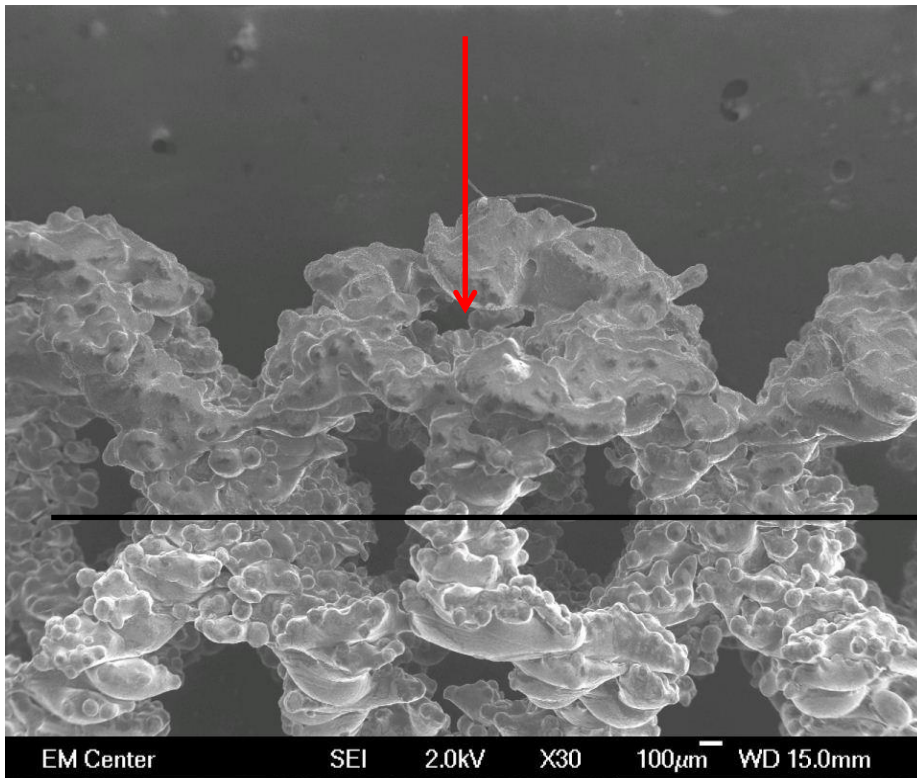


**Figure 5.1.** Insulated 61% porosity lattice sprayed at 8 kV, 8cm, 20mM, black line indicates maximal extent of full coverage coating, red arrow indicates spray direction

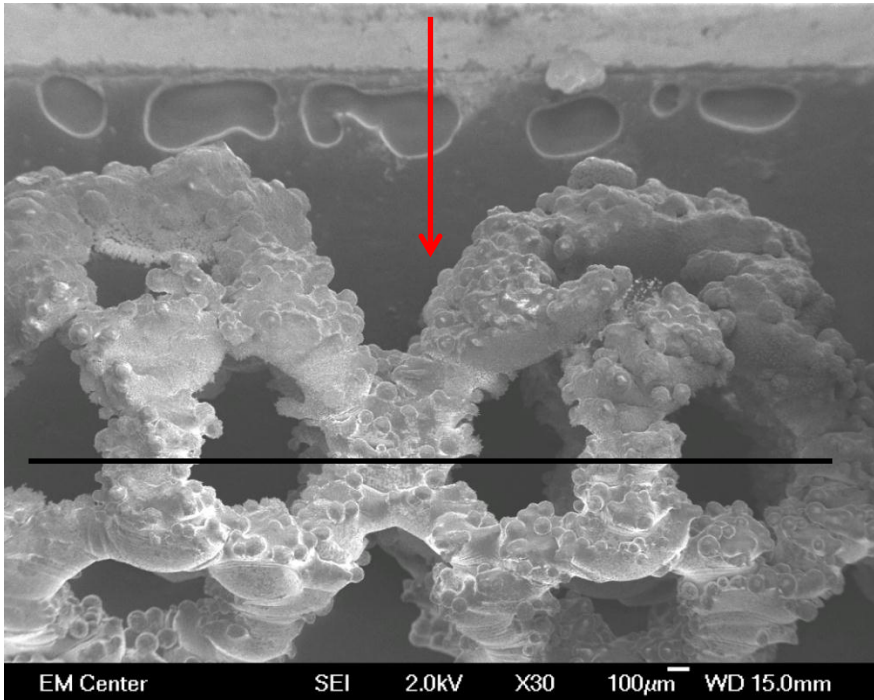


**Figure 5.2.** Insulated 61% porosity lattice sprayed at 12 kV, 4cm, 20mM black line indicates maximal extent of full coverage coating, red arrow indicates spray direction

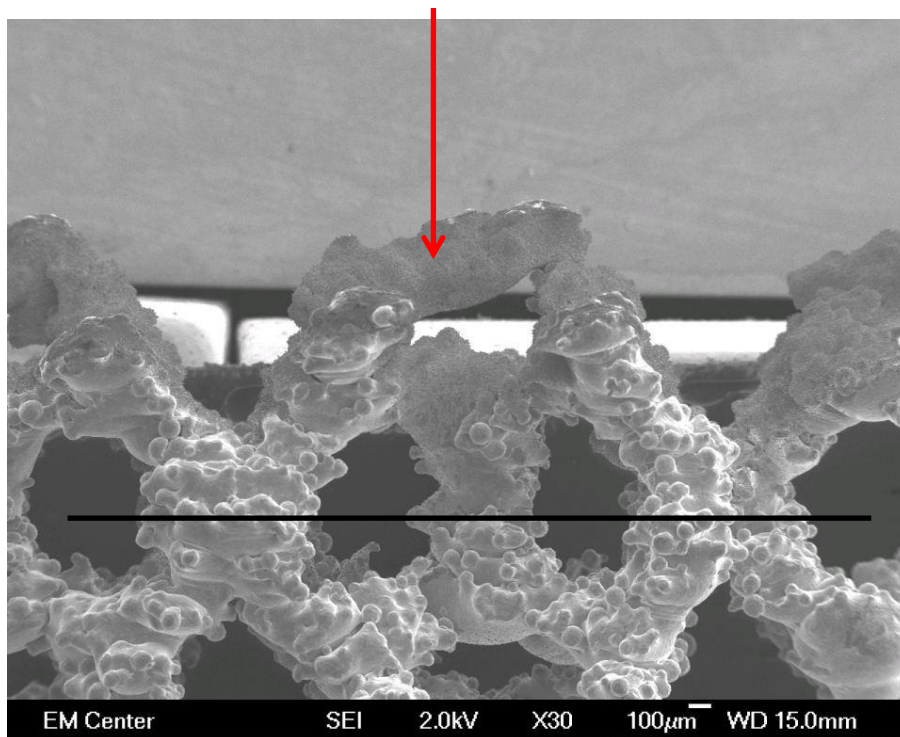


**Figure 5.3.** Insulated 61% porosity lattice sprayed at 18 kV, 8cm, 20mM black line indicates maximal extent of full coverage coating, red arrow indicates spray direction

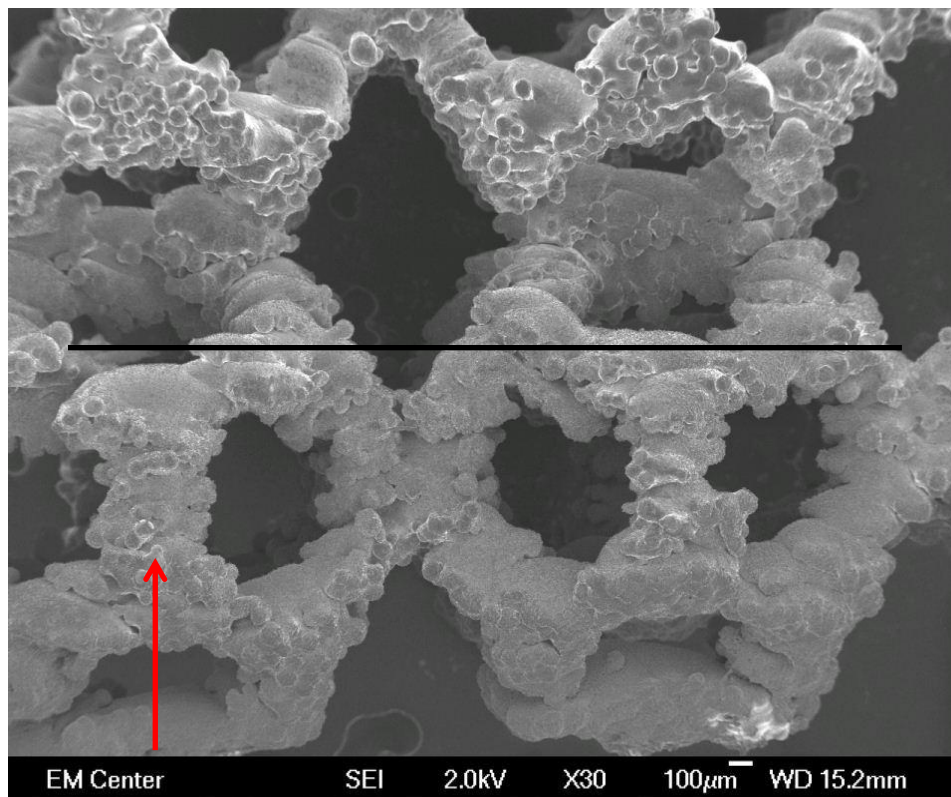


**Figure 5.4.** Insulated 61% porosity lattice sprayed at 12 kV, 8cm, 10mM black line indicates maximal extent of full coverage coating, red arrow indicates spray direction

#### 5.1.1.1 Discussion

When the inside faces of the lattices were imaged with SEM the insulated lattices showed overspray at the spray side or front of the lattice with little penetration of coating into the lattice. During the e-spraying of all samples mentioned above, in addition to the overspray seen on the lattice itself DOPS was seen on other conducting material in the e-spray chamber including the mounting stand, the grounding wire, and the power cord of the syringe pump. Overspray is evidenced by the DOPS morphology – it builds up into a very thick coating, it loses its smooth morphology and takes on one in which the DOPS looks more like individual particles (see figure 4.7). A small amount of material was also deposited on the non-spray side, or back, of the lattice which was not

externally insulated. Coating was deposited at the back of lattice, indicating that field lines were present. As e-spray is a process that hinges on electric field lines to deposit material, the lack of material deposited would indicate that there are not field lines or the material is not conducting. When field lines are canceled out this is known as the Faraday Cage Effect, as explained in section 1.5.3.

To further understand this effect, the parameters were varied to determine if any one parameter had a particularly strong impact on the Faraday Cage effect. In figures 5.1-5.4 the coating coated approximate 0.5-1 unit cell in depth. The intention of parameterization was to see the coating depth increase, this would have indicated that the corresponding parameter change was able to influence or mitigate the Faraday cage effect. From figures 5.1-5.4, no single parameter, when varied against the other controlled parameters, was able to mitigate or show any effect on the ability of the lattices to coat. The Faraday cage effect causes the coating to collect at the front of the lattice and not penetrate in. This overspray forms because the field lines are strongest at the outer edges of the lattice. Each lattice, when externally insulated, and e-sprayed is acting as a Faraday cage and shielding the electric field lines intended to carry the source material to the target. As a result of the external field causing the internal electrical charges to redistribute an equipotential surface is created where no charge flows.

The coating was able to penetrate approximately 1 unit cell in depth into the lattice. In the powder coating industry the Faraday cage effect is a frequently encountered problem. It is especially prevalent in the powder coating of pipes. The

traditional method of powder coating with a corona gun tends to induce the Faraday cage effect [88]. The samples were initially externally insulated to provide a clear indication of e-sprayed coating depth into the lattice. This led to the discovery of the Faraday cage effect and prompted us to try and mitigate it. Through this work we discovered that within the limits of electrospray we were unable to vary any parameter (voltage, spray distance, DOPS concentration) enough to cause a quantifiable change in coating penetration depth if the sample is externally insulated. The parameters can only undergo so much variation before the process of e-spraying breaks down and no coatings are formed because the e-spray parameters are wrong. This has been especially evident in e-spraying on to flat Ti squares. Usually a stronger electric field would act to deliver more of the material to the surface [74, 79] but in the case where a Faraday cage is formed a stronger electric field only intensifies the Faraday cage effect [83].

Spray time is determined based on the given surface area of a part; the relationship for this was developed in previous work [48]. The spray time was long enough that the lattices should have been coated at depth. When this is combined with the excess spray seen in the chamber it indicates that increasing spray time would not impact the ability to spray at depth as a result of the Faraday cage effect. While variation of the parameters would typically cause changes in morphology [48], the overspray was so extreme that all coatings appeared similar. Despite the inability to coat at depth, the areas that did coat for each set of parameters displayed uniform coatings from part to part; visually, they all looked very similar, potentially because of

overspray. This highlights the repeatability of the e-spray process, indicating that all parts were inducing similar Faraday cages and thus being coated the same in each test.

This work is potentially limited by the selection of external insulation material or grounding problems in the system. It is possible that contributing the Faraday cage effect is poor grounding of the sample. If sections of the lattices aren't grounded then field lines would not go to those areas and source material would not reach that target area. Complete grounding of the sample is required for a good circuit and for source material to reach the target, this is what makes e-spray such a high efficiency process [76]. In the future it would be advisable for all lattices to be checked for proper grounding once they are in the e-spray chamber. This will eliminate this as a potential source of error.

In summary it is evident that when the titanium lattice cylinder 1 cm in height and 6mm in diameter is circumferentially, externally insulated a Faraday cage effect is induced in the parts.

### ***5.1.2 Lattice Porosity and the Faraday Cage Effect***

After discovering that the lattices become Faraday cages when externally insulated all lattice porosities (54%, 61%, 71%) were e-sprayed without external insulation to determine if the Faraday cage effect could be mitigated through porosity. When viewed with SEM, all porosities of lattice still showed overspray at the outer edges of the cylinder. The 71% porosity lattice showed DOPS coverage into the middle of the inner face as seen in figure 5.5. EDS verified the presence of DOPS in the middle

of the lattice (figure 5.6). Phosphorous is a key component of 1,2-dioleoyl-*sn*-glycero-3-**phospho**-L-serine, DOPS.

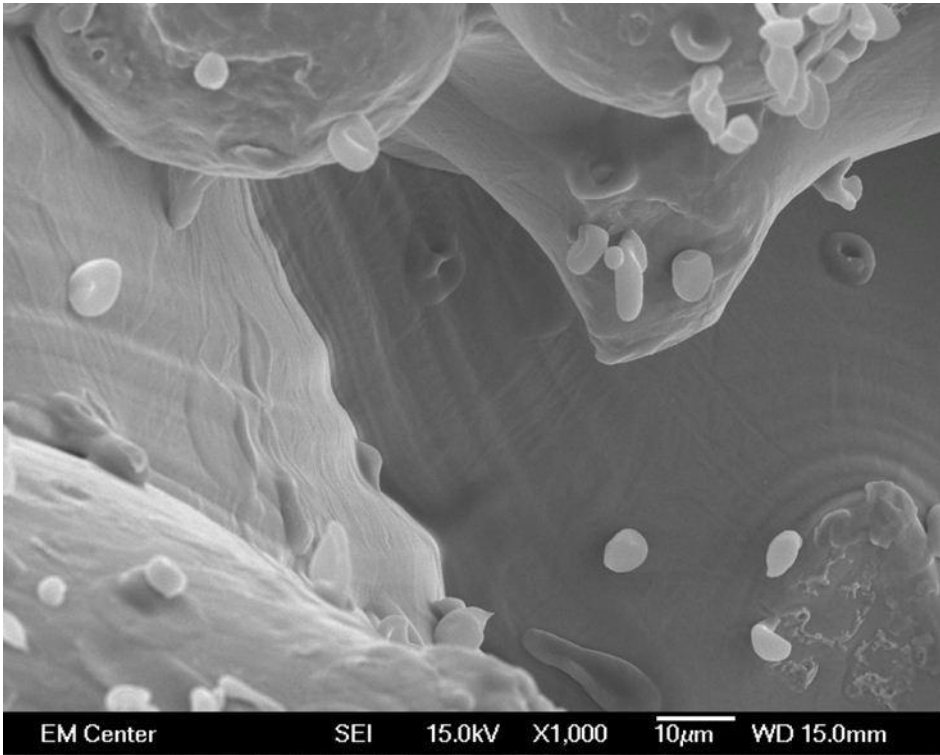


**Figure 5.5.** DOPS coating in the middle of the 71% porosity lattice

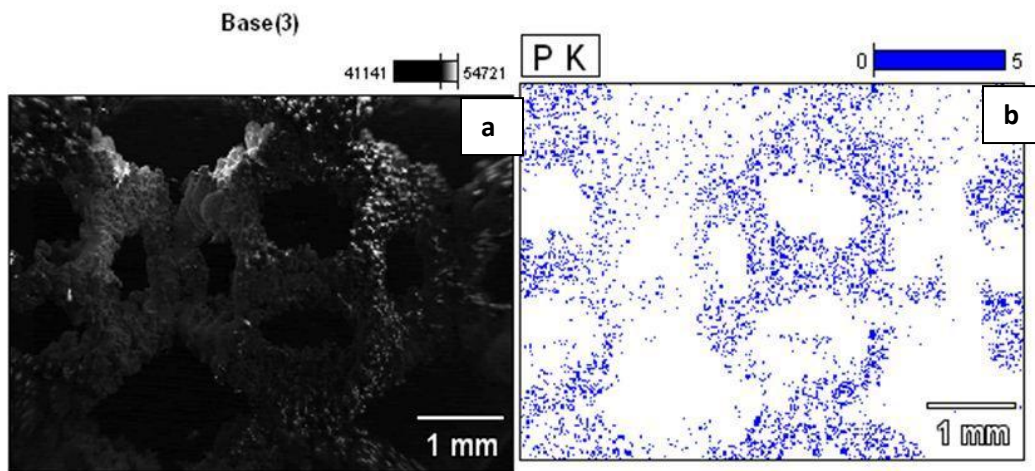


**Figure 5.6. (a)** Base image of middle of 71% porosity lattice under EDS **(b)** Indication of DOPS by phosphorous (blue)

DOPS was visible in the middle of the lattice on the 61% porosity structure when viewed with SEM and EDS (figures 5.7-5.8). The coating could also be seen transitioning from overspray to a morphology commonly seen on Ti as it went deeper into the lattice (figure 5.9).

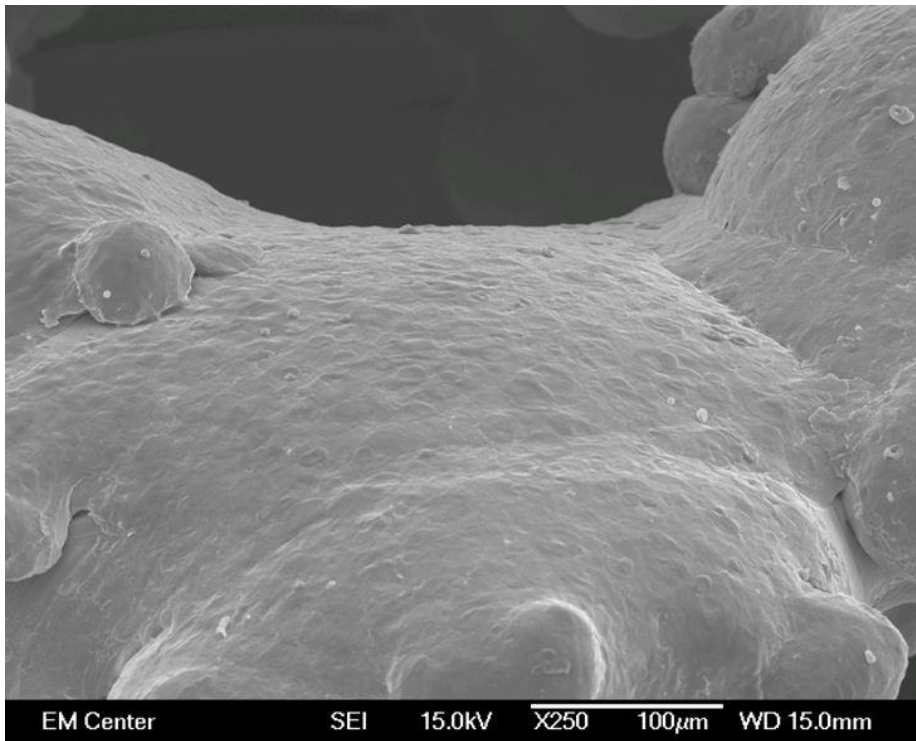


**Figure 5.7.** DOPS coating in the middle of the 61% porosity lattice

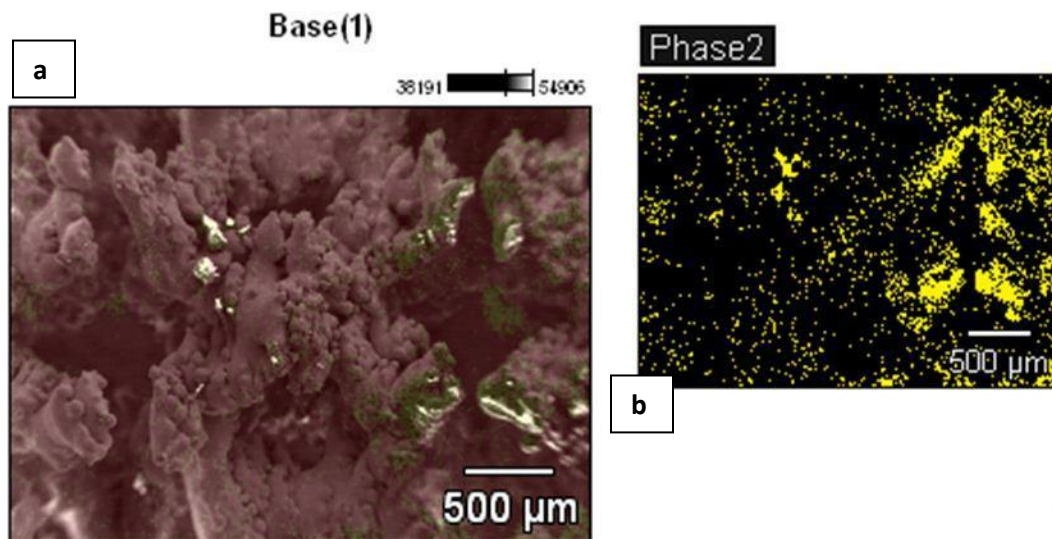


**Figure 5.8. (a)** Base image of middle of 71% porosity lattice under EDS **(b)** Indication of DOPS by phosphorous (yellow, named phase 2)

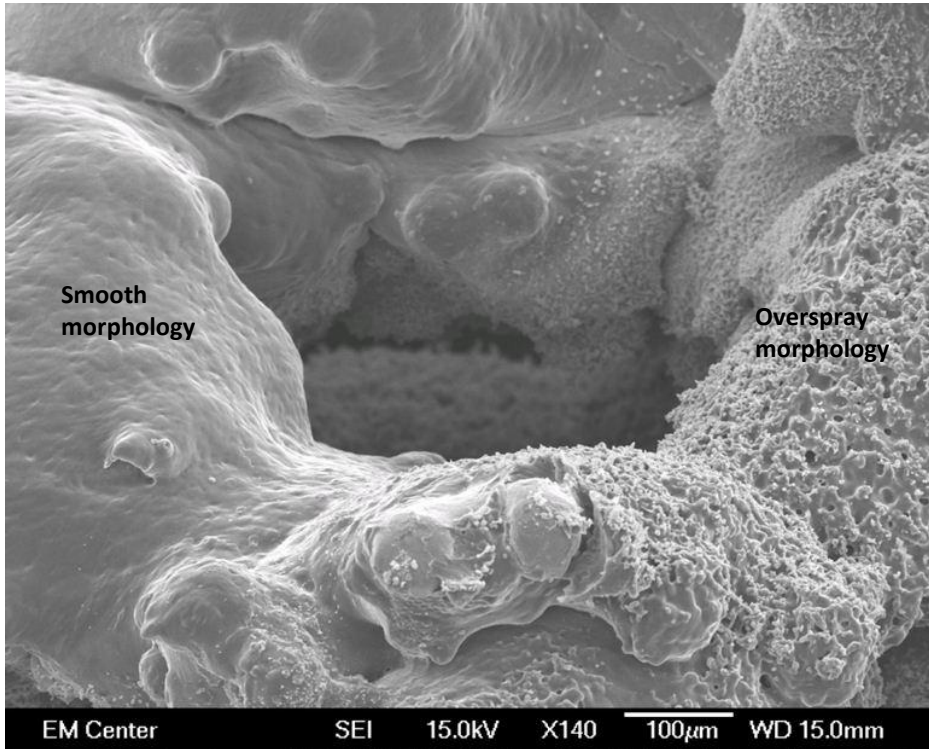


**Figure 5.9.** 61% porosity lattice outer edge transition from overspray morphology

The coating could also be seen transitioning from overspray to a morphology commonly seen on Ti as it went deeper into the lattice as labeled on figure 5.9.

The 54% porosity lattice did not have DOPS in the middle of the lattice as found with SEM and EDS, though DOPS was present at the outer edges where it exhibited the overspray morphology.

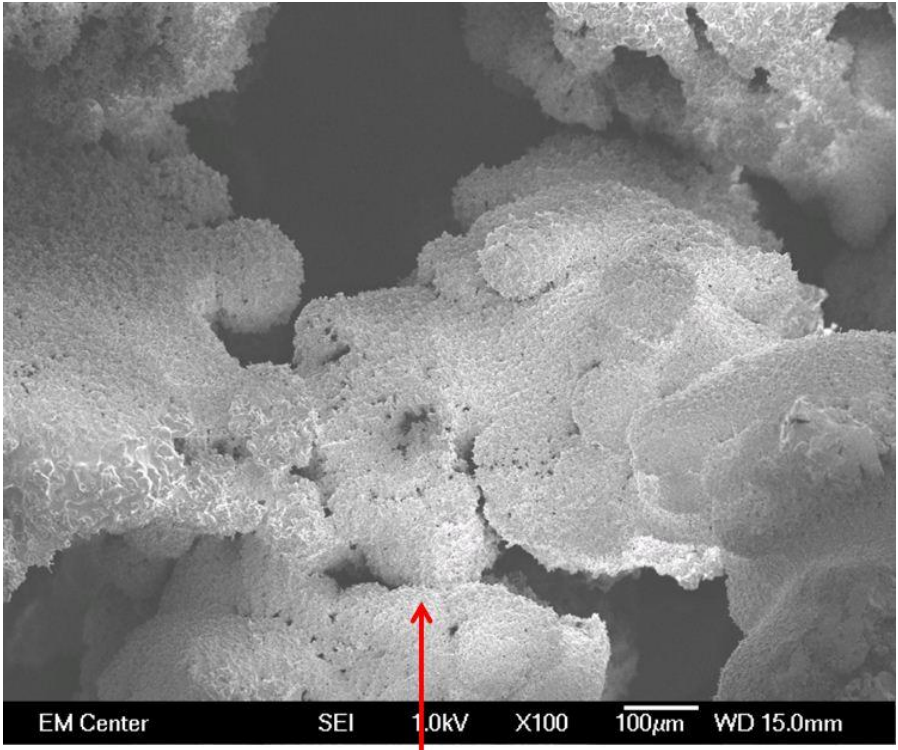


Figure 5.10. 54% porosity lattice, outer edge at “front” of lattice (indicated by red arrow)

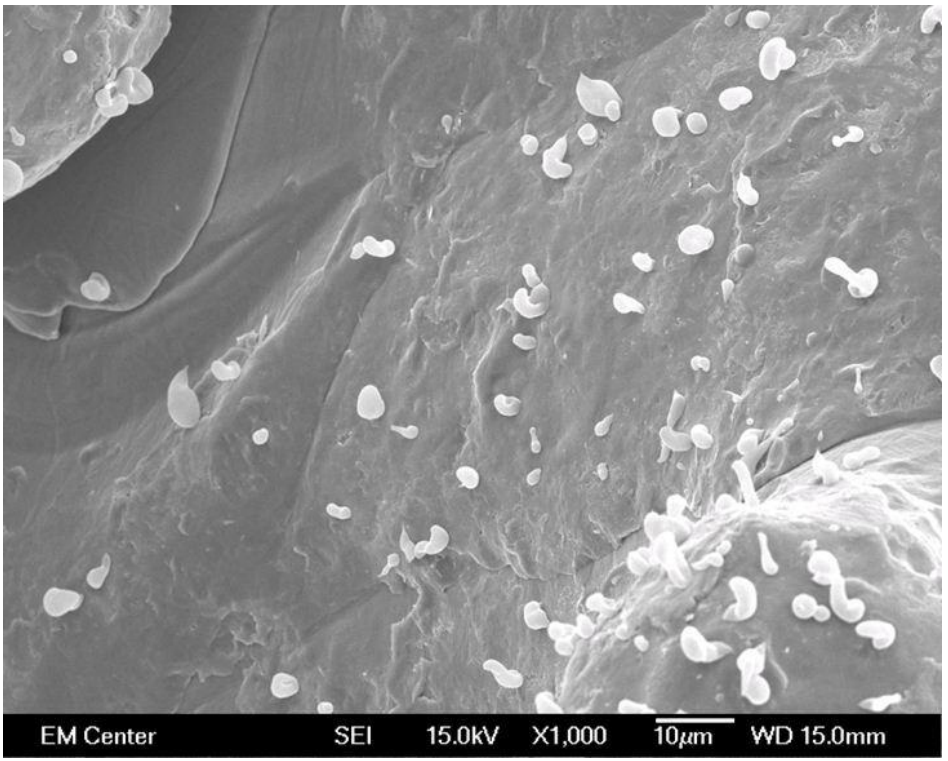
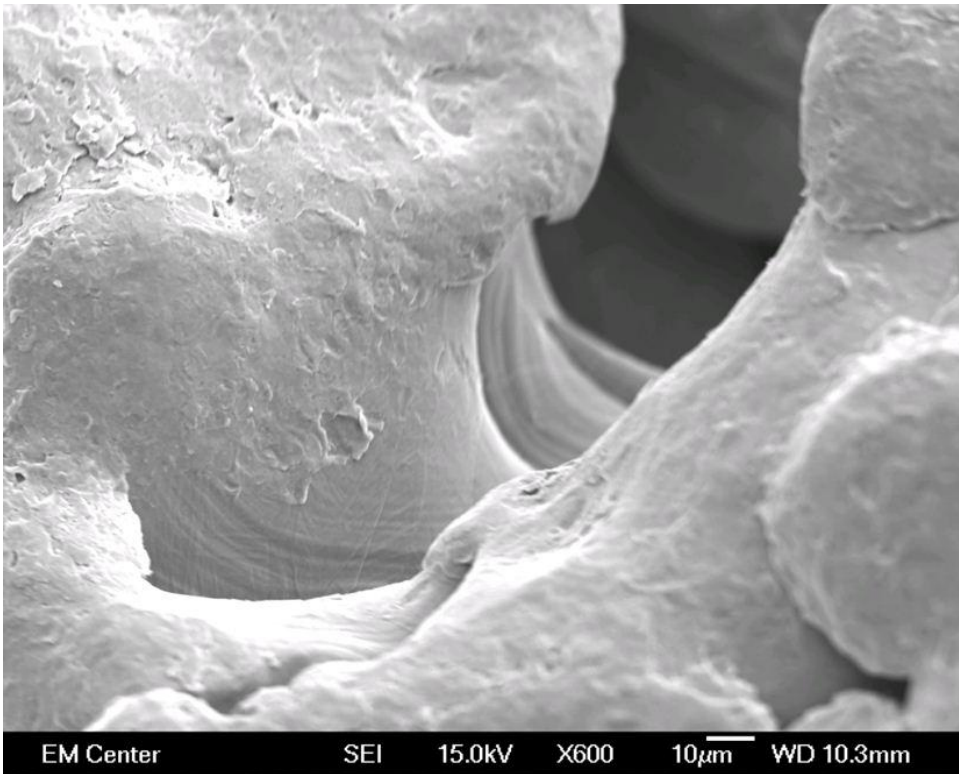


Figure 5.11. Middle of 54% porosity lattice, showing incomplete coating of DOPS

The 54% porosity lattice did not have a full coating of DOPS in the middle of the lattice (figure 5.11) despite having overspray at the outer edges (figure 5.10). This is identifiable from the SEM images, by comparing figure 5.11 with figure 5.6. In figure 5.6 the surface appears smooth and soft, which is a common morphology of DOPS while the surface in figure 5.11 appears rough and flaky, which is consistent with the as received, un-etched EBM titanium morphology as seen in figure 5.12. This is confirmed with the EDS, as it did not detect phosphorous, the primary indicator for DOPS.



**Figure 5.12.** Unpassivated, uncoated EBM titanium

Though it appeared as though there were complete coatings on the 61% and 71% lattices, DOPS was found on conducting items in the e-spray chamber. Pre- and post-spray weights for each sample were recorded to determine how much DOPS was actually going to each sample. Figure 5.13 shows the sample weight differences. Each

part was sprayed for a length of time corresponding to nominal surface area of the lattice. Based on previous work [48], in order to apply a full coating, all DOPS sprayed would have needed to adhere to the lattice. The average percent loss for the lattice structures of all sizes was approximately 80%. In work done on flat Ti there was negligible loss in the system.

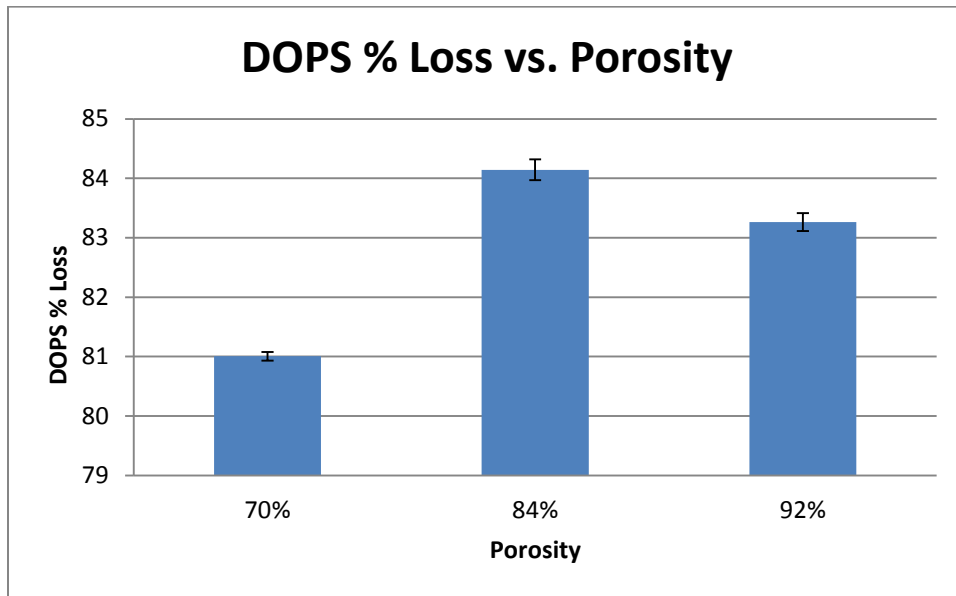


**Figure 5.13.** Graph showing the quantity of DOPS that reached the sample vs the porosity of the sample

#### 5.1.2.1 Discussion

The percent porosity of the lattice was calculated and provided by Medical Modeling using the theoretical surface area and volume generated by the software used to manufacture the parts. There is a positive trend for increasing coverage as porosity increases. As the porosity increases, the Faraday cage effect declines thus allowing more electric field lines within the part to carry the source material to the lattice. This is consistent with work seen in the powder coating industry where they find that as the

radius of a corner is increased there is increased coating of the area [87]. Based on relationships found in this work e-spray will function best when the porosity is higher than 61%. E-spray fails to coat somewhere between 54%-61% porosity and the associated pore sizes listed in section 4.1.2. While there is clear loss in the system it would be better quantified if the lost DOPS could be reliably recovered to verify the loss found from the lattices. This high quantity of loss was unexpected from previous work using DOPS to e-spray on Ti [48]. The loss in the system while also achieving a full DOPS coating on the Ti lattice structures could indicate that the original work done created coatings that were thicker than necessary to just be considered full coatings.

It might be expected that when porosity is high enough for the lattice to fully coat, there would be minimal overspray onto the items in the chamber that are not in the electrical circuit. This expectation is based on the premise that if a conductor can coat in its entirety then there is no reason the charge should be drawn to conductors not in the circuit. In this work this was not true; there was still overspray present in the chamber, not just the parts. This is likely demonstrative that the Faraday cage effect is still present even when the part is fully coated. The Faraday cage effect is reduced in the case of the higher porosities but not totally absent. We hypothesize it is weakening field lines in the lattice, and the DOPS is finding other stronger field lines in the chamber to follow. The source material is carried to the surface of highest current density and in this case that may not be the internal parts of the lattice until a coating deposited on other conducting material in the chamber lowers the charge density below that of the lattice. The overspray on other conducting material in the e-spray chamber is visible

after around 45 seconds, indicative of the Faraday cage effect. The time before which the conducting material in the chamber begins to coat may be explained by the charge density of the lattice being strongest until this point. It also possible that the conducting material in the chamber begins to coat immediately and it takes 45 seconds to become visible to the naked eye.

## **5.2 Specific Aim 2: DOPS Coatings and the Faraday Cage Effect**

It is important in this work to consider the different DOPS coating morphologies present on the lattices as this could impact the preference of osteoblasts to adhere and begin producing new bone. The morphology of a surface is important for osteoblast adhesion *in vivo* as cells appear preferentially adhere depending on surface morphology [28]. Morphology, uniformity and conformity of a coating are of interest in the lattices with a high enough percent porosity (61% and 71% in this work) for full coverage coatings in this study. The specific aim addressed here is: Characterize the relationship between the Faraday Cage Effect and e-sprayed phospholipid coatings

### ***5.2.1 Lattice Porosity and Coating Morphology***

Lattices with 71% porosity were coated completely; all parts were coated, with DOPS penetrating the entire lattice as seen in figure 5.14. However, the coating created was not uniform or conformal as seen in figure 5.15. Overspray was observed at lattice edges.

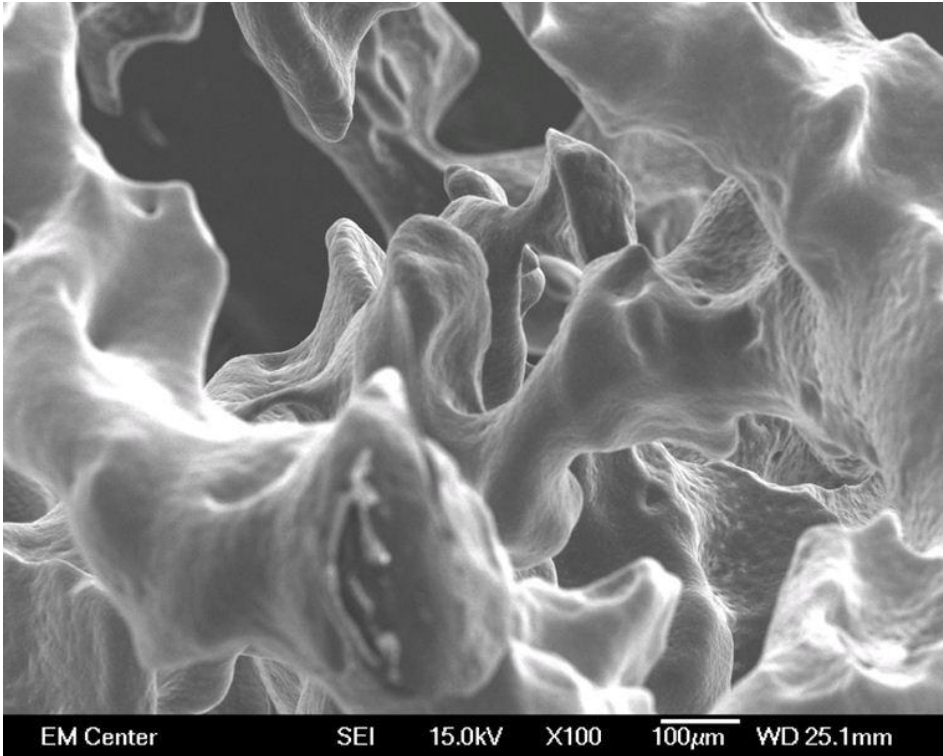


**Figure 5.14.** Fully coated, 71% porosity lattice

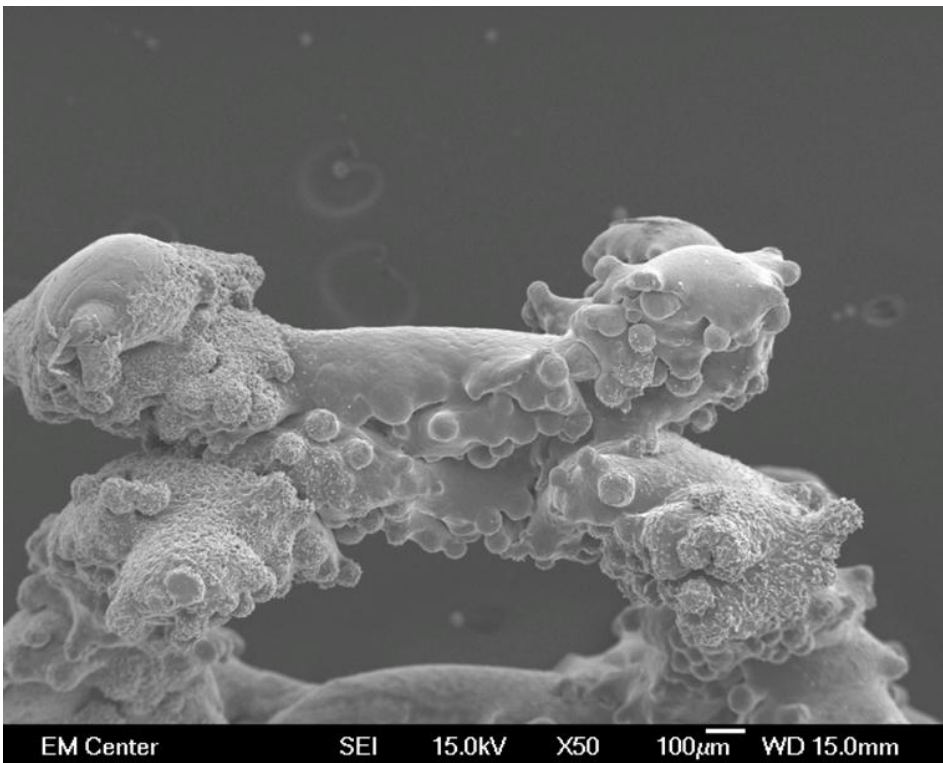


**Figure 5.15.** Fully coated, 71% porosity lattice demonstrating non uniform and non-conformal coating

The 61% porosity lattice also demonstrated similar characteristics to the 71% porosity lattice. All parts of the lattice are coated with DOPS but the coating is not uniform or conformal, with overspray at the edges (figure 5.16).

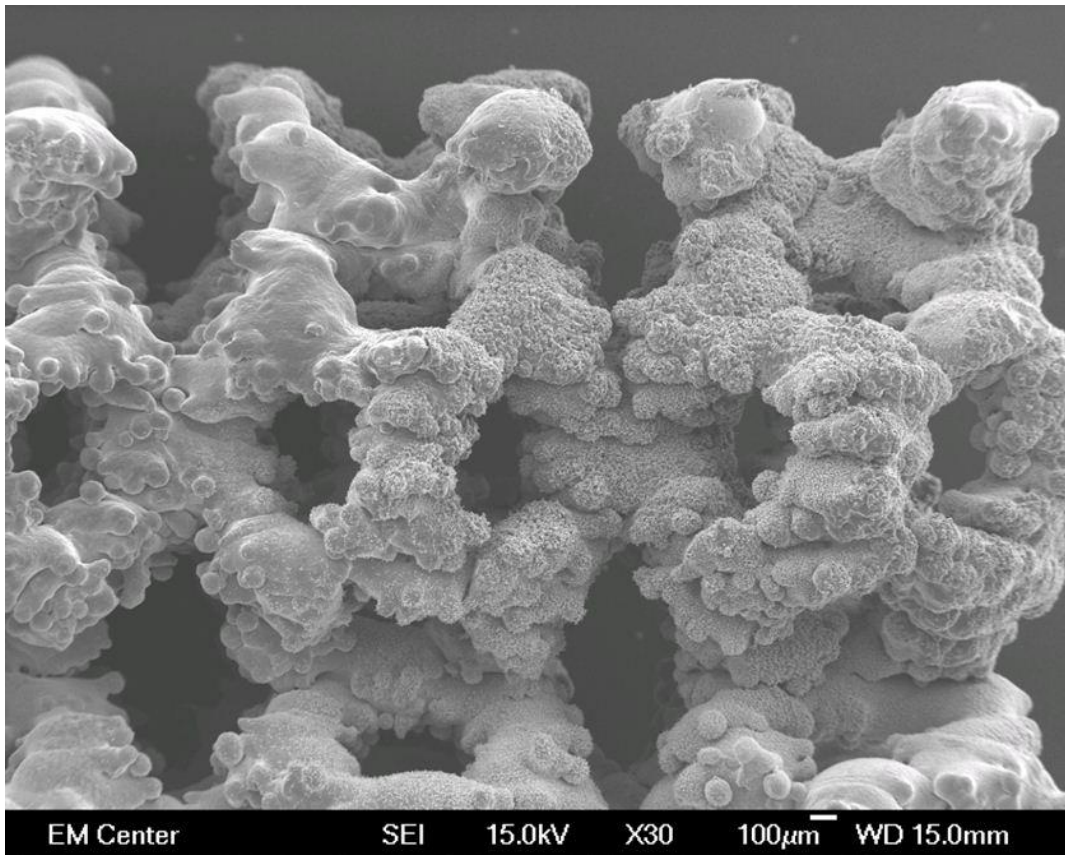


**Figure 5.16.** Fully coated, 61% porosity lattice demonstrating non uniform and non-conformal coating

The 54% porosity lattice was not able to be coated fully, thus demonstrating the Faraday Cage Effect. Coating was found at the outer edges of the lattice with morphology consistent with overspray seen earlier (figure 5.13). Figure 5.17 shows the spotty and uneven coating where the DOPS inconsistently penetrated and coated the

lattice. The DOPS in the image can be seen as dark spots against the lighter colored titanium, confirmed with EDS.

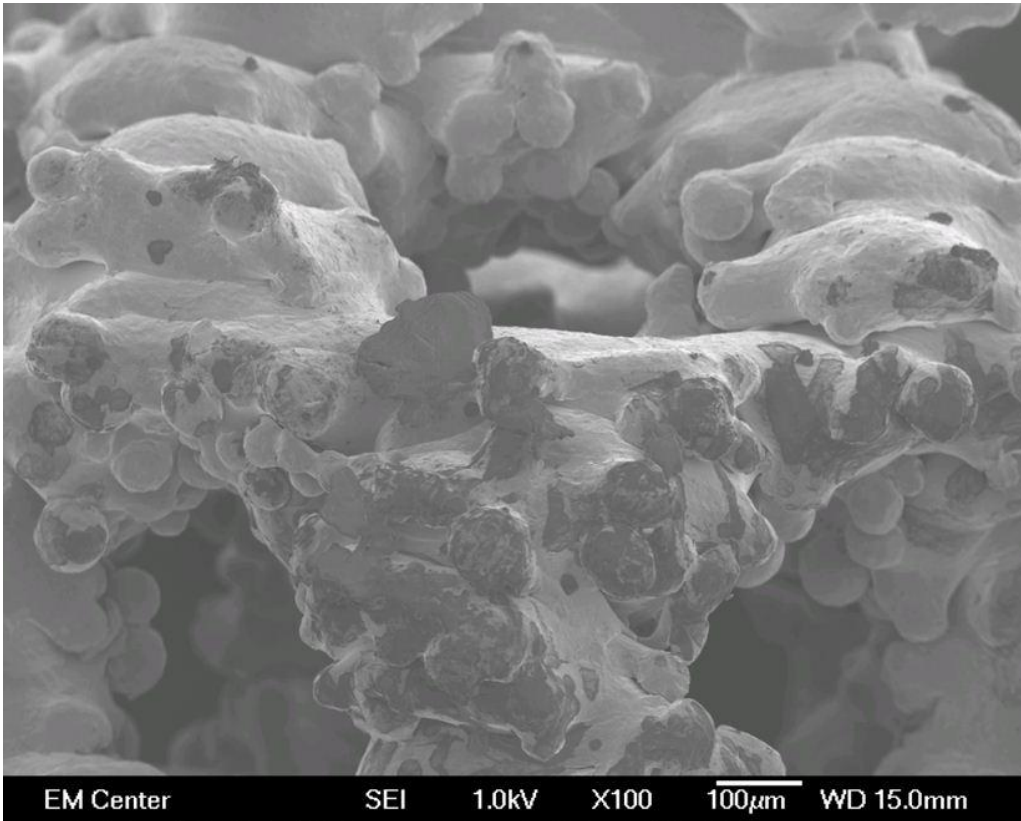


**Figure 5.17.** Spotty, uneven coating of 54% porosity lattice

#### **5.2.1.1 Discussion**

This work helps to further clarify that the Faraday cage effect is also preventing the coating from fully penetrating into the 54% porosity lattice. In our initial work it was hypothesized that the physical barrier (external, circumferential insulation) was the primary reason for the lack of penetration. This has now been shown not to be the case. In this work we showed that the medium and high porosity lattices can be coated when not externally insulated and the lowest porosity lattice still cannot be coated. This

indicates that the physical barrier was not the only reason for poor e-spray performance.

The coating morphology was found to be neither uniform, nor conformal from part to part or from area to area within each part. The lattices tended to display the “overspray” morphology at the outer edges of the part and in some cases showed a smoother morphology in the interior though sometimes the other morphologies were seen. Four different morphologies can be seen in figures 5.8, 5.10, and 5.19. The difference in electric field in each case likely explains the variation in morphology. In each of these cases the spray parameters were the same so it seems evident that the Faraday cage effect acting on the field would be affecting the electric field, and thereby the morphology. Each part, despite being manufactured the same way has its own unique variations due to the manufacturing process; these unique variations will impact the electric field.

It is clear that while electro spraying can be used to coat these complex lattice structures the process is limited by the Faraday cage effect. The relationship between porosity, Faraday cage effect and e-spray is difficult to quantify as both involve many parameters which interact. While the coating was unable to penetrate fully into the 54% porosity lattice there were some inconsistent, random patches of the interior target that did get some coating. Though some coating was found it was never in the center of the lattice but penetrated further in than the typical overspray found at all outer edges. This could possibly be explained by the few field lines that happened to penetrate into the lattice as the lattice is not a perfect Faraday cage. The literature

regarding the Faraday cage effect frequently discusses meshes that are used to intentionally provide a shielding effect even though they do not generate perfect protection [83]. This likely explains how some random areas in the interior of the 54% porosity lattice are able to coat. Despite 61% and 71% porosity lattice being able to coat fully, the coatings were never uniform or conformal.

Percent porosity is the appropriate descriptor for these lattices (as opposed to pore size). Porosity is the ratio of void space volume to total volume. Changing the pore size would change the change the porosity of a structure of the same total volume. Though if the pore size is changed and the total volume of the structure is changed this will create a different porosity. The unit cell used in this work is a dodecahedron (figure 4.8) designed by Medical Modeling to have high void space as well as high surface area. Different unit cells have different quantities of void space. If a unit cell with a lower void space were put into the same total volume as the dodecahedron unit cell it would have a lower porosity even if the two different unit cells had the same pore size. This is why it is important to consider percent porosity. Though percent porosity is the most important descriptor of the lattices it also important to consider the particular geometry of the lattice. Creating two structures with the same percent porosity but one structure has pore sizes double that of the other with likely cause differing levels of Faraday cage effect. The relationship seen in powder coating of pipes is that the coating is able to penetrate approximately 1 diameter in depth into the pipe [103]. In the case of many porous Ti structures the Faraday cage effect will look similar to that of the one in pipes.

Not having a full comprehension of what exactly the field lines look like at the surface of the lattice and the penetrating ones inhibits the best analysis of the resulting coatings. There are parameters that affect the Faraday cage effect that are not fully realized in this work. The powder coating industry has investigated the relationships and found that exact field generated and the charge to mass ratio of the particles are key parameters [85].

In summary the lattice porosity does not show a direct relationship to the uniformity and conformity of coating morphology. However, porosity is related to the efficacy of the e-spray process. Because a part coats does not mean it will coat consistently on the entirety of a single part or consistently between parts. Lattices in which the coating was unable to fully penetrate the lattice did demonstrate spotty and uneven coatings.

### **5.3 Specific Aim 3: Process Parameters and Coatings**

The electrospray process involves a large number of variable parameters that impact the efficacy of coating as well as the morphology of the coating created. Certain parameters are more controllable (e.g. voltage, distance, concentration) and it is necessary to relate these parameters to the phospholipid coating uniformity, conformity and penetration depth. It is also important to consider the effects of the underlying titanium morphology, particularly surface roughness and surface area. The specific aim addressed with this work is: Evaluate the capacity of e-sprayed phospholipid coatings on 3-dimensional titanium lattice structure by relating the effects of e-spray process

variables (distance, voltage, concentration) on phospholipid coating uniformity, conformity, and penetration depth into the titanium lattice structure.

### **5.3.1 Parameter Variation and DOPS Coatings**

Externally insulated 71% porosity lattices were used to test the effects of e-spray parameters on coating morphology. When the voltage was both increased (18kV) and decreased (8kV) from the standard e-spray voltage (12kV) the coatings were not uniform or conformal under any of the conditions. SEM images for 8kV and 18kV can be seen in figures 5.18-5.22.

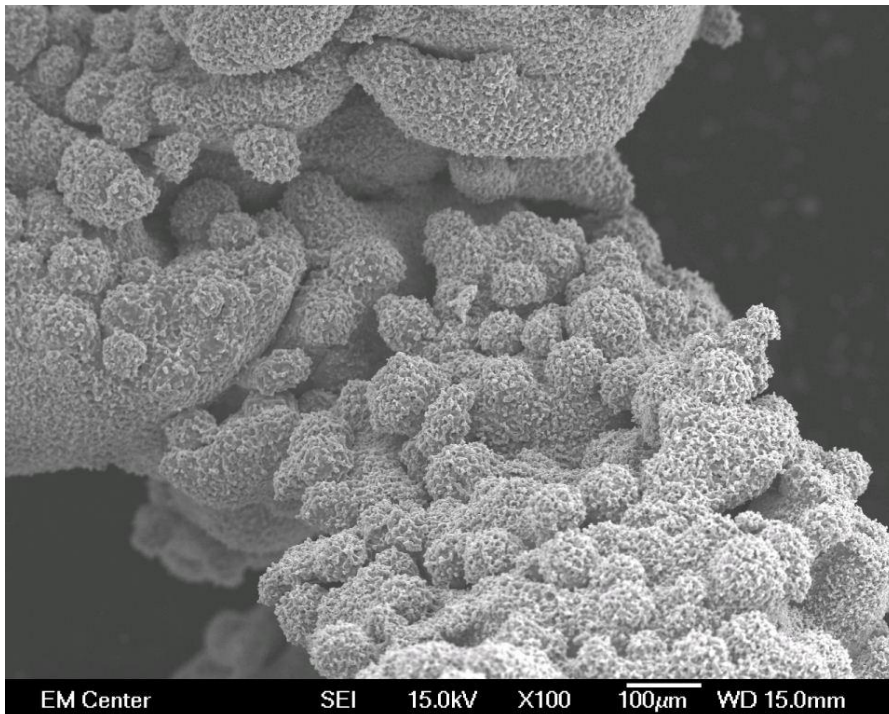


**Figure 5.18.** Morphology of 18kV, 8cm, 20mM DOPS surface

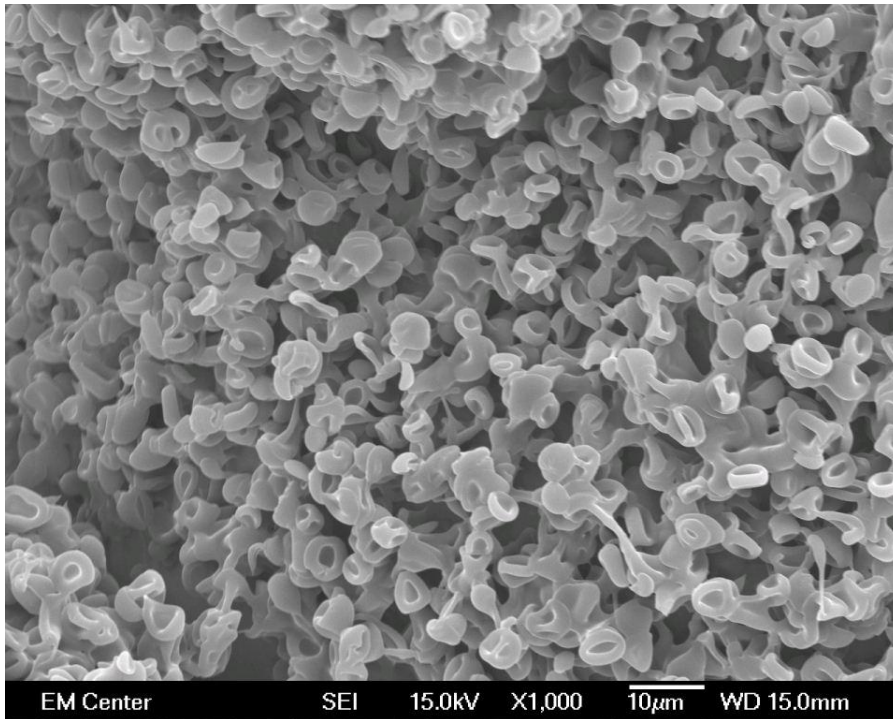


**Figure 5.19.** Characteristic morphology of 18kV, 8cm, 20mM DOPS surface

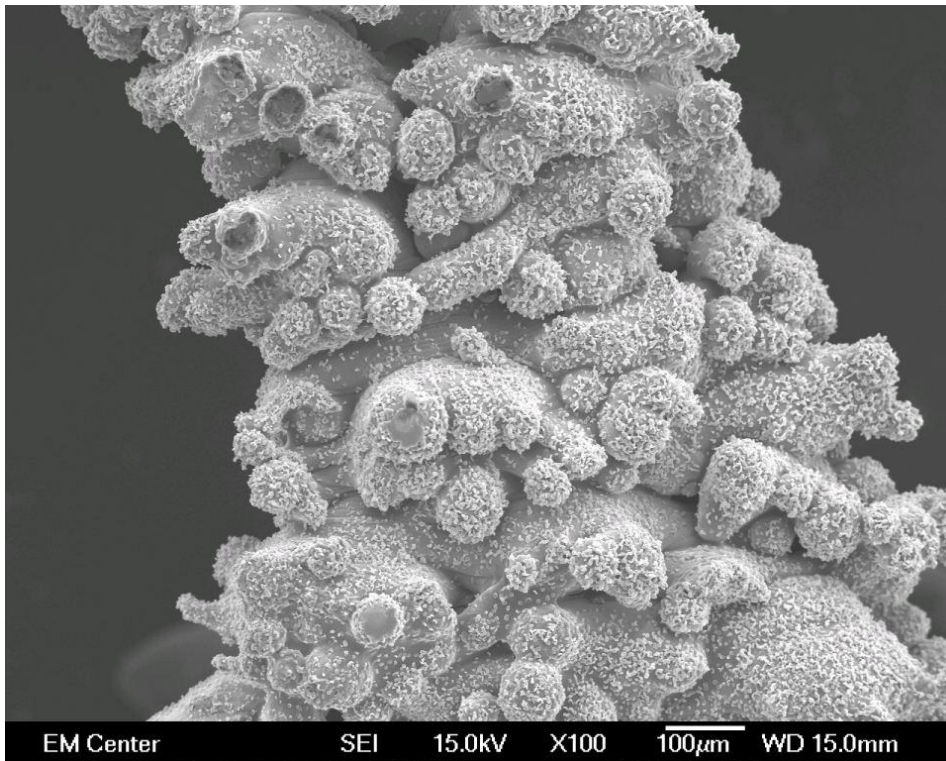


**Figure 5.20.** Morphology of 8kV, 8cm, 20mM DOPS surface



**Figure 5.21.** Smooth morphology found on 8kV, 8cm, 20 mM surface

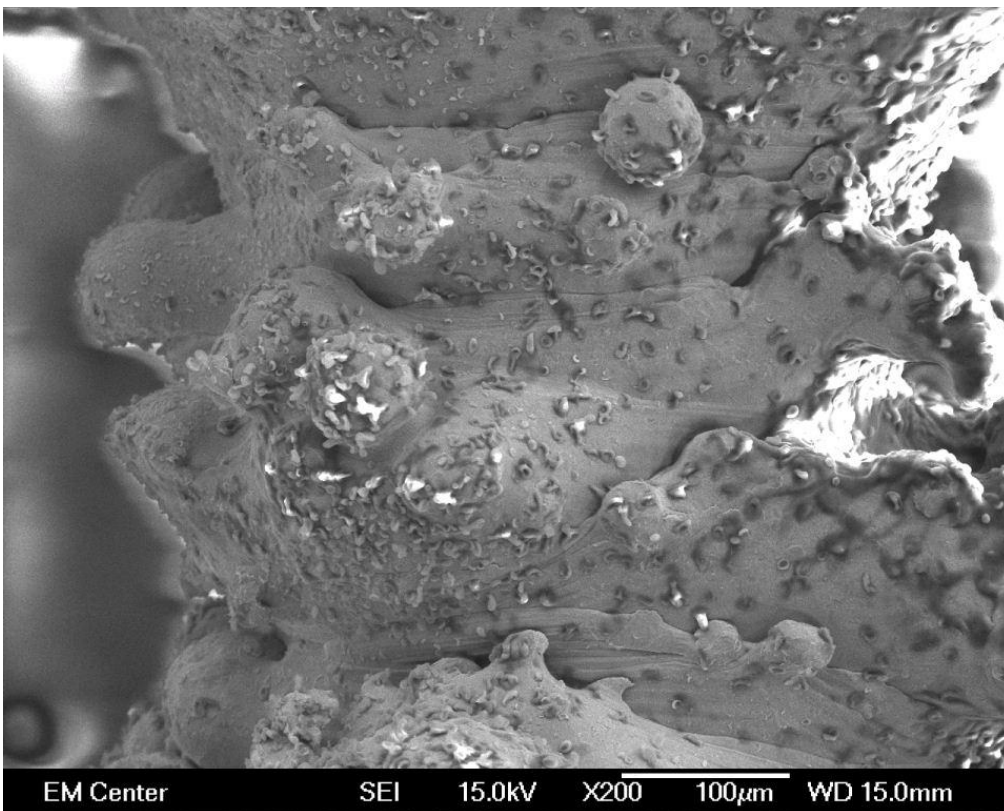


**Figure 5.22.** Blood cell morphology seen on an 8kV, 8cm, 20mM surface

The 71% porosity lattices were used to determine the effects of changing spray distance and source material (DOPS) concentration on the morphology of the DOPS coatings deposited on the lattices because they demonstrated the highest ability to coat fully. The morphologies for different DOPS concentrations can be seen in figures 5.23-5.26. The images are from varying points in the interior of the lattice. EDS was also performed on each lattice to verify that there was full penetration of DOPS coatings. EDS was used in multiple places throughout the lattice though the results reported in figures 5.27-5.30 are those from the middle of the lattice.

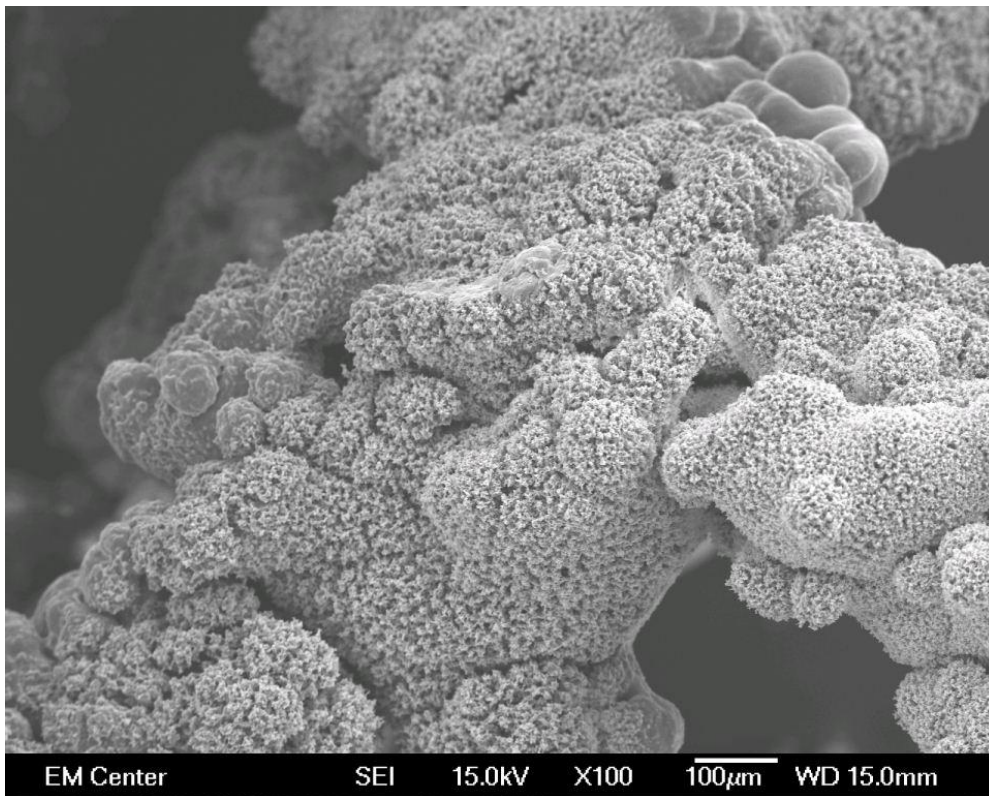


**Figure 5.23.** Morphology of 12kV, 4 cm, 20mM sample

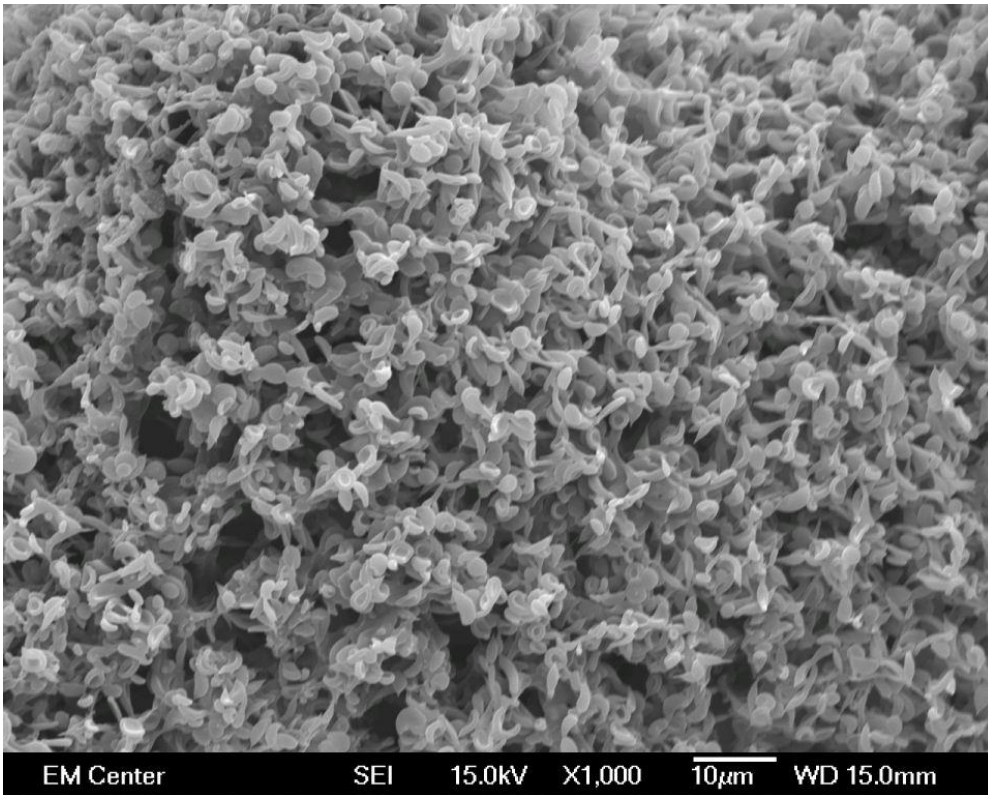


**Figure 5.24.** DOPS morphology of 12kV, 4cm, 20mM sample

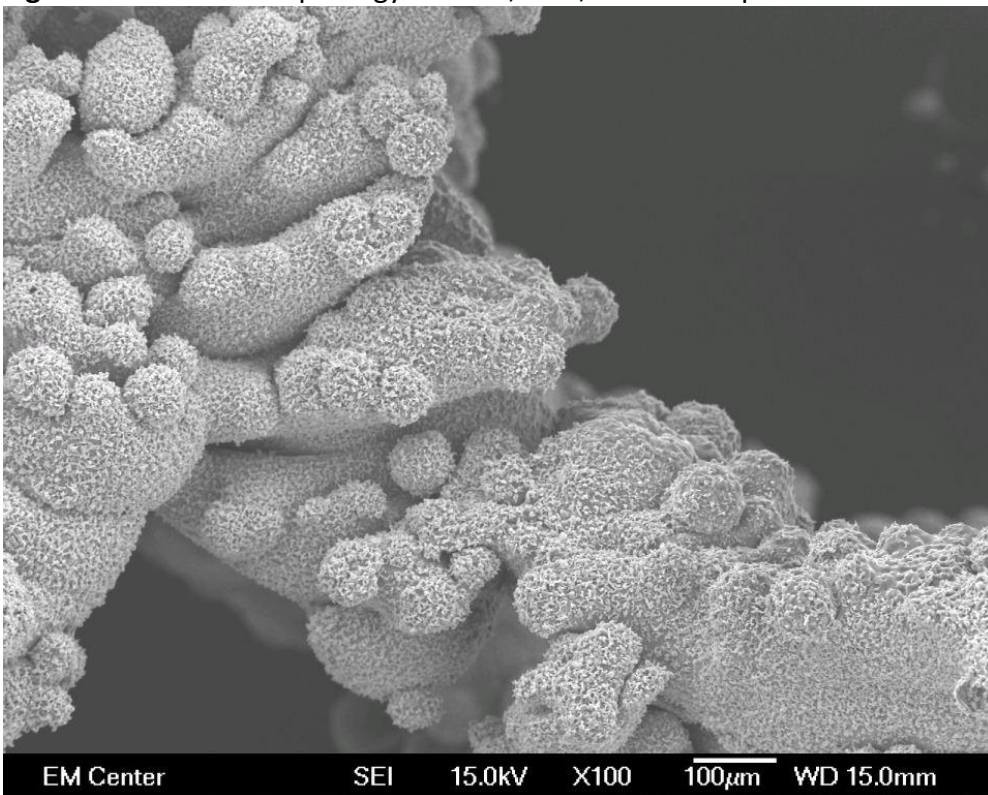


**Figure 5.25.** Morphology of 12kV, 8cm, 10mM sample

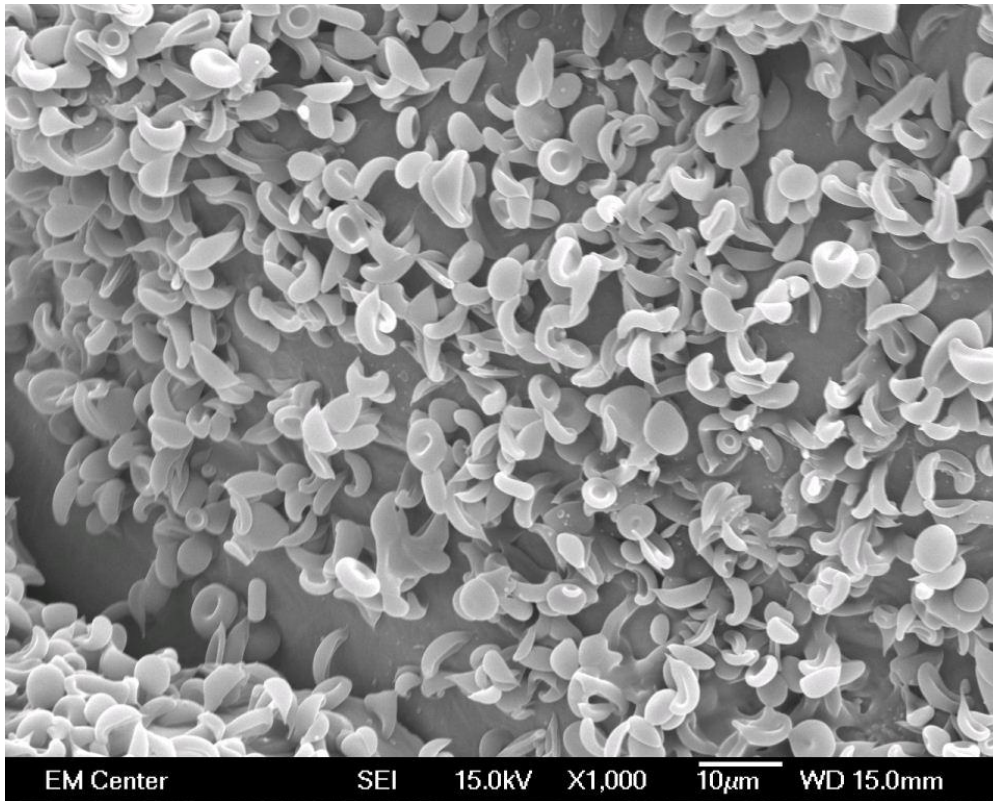


**Figure 5.26.** Morphology of DOPS on 12kV, 8cm, 10mM sample

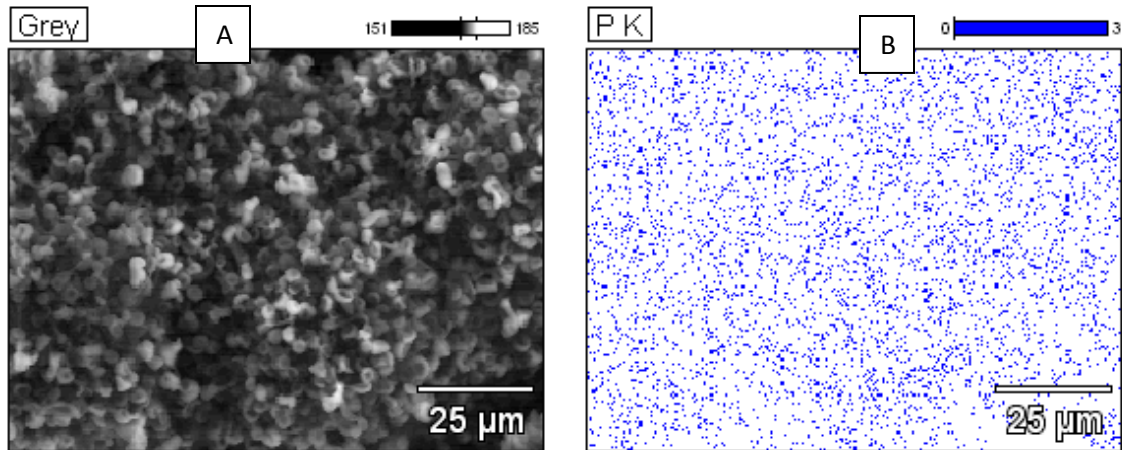


**Figure 5.27.** EDS of 18kV, 8cm, 20 mM surface. A) base image of collection site B) Blue shows phosphorous on surface – indicator of DOPS

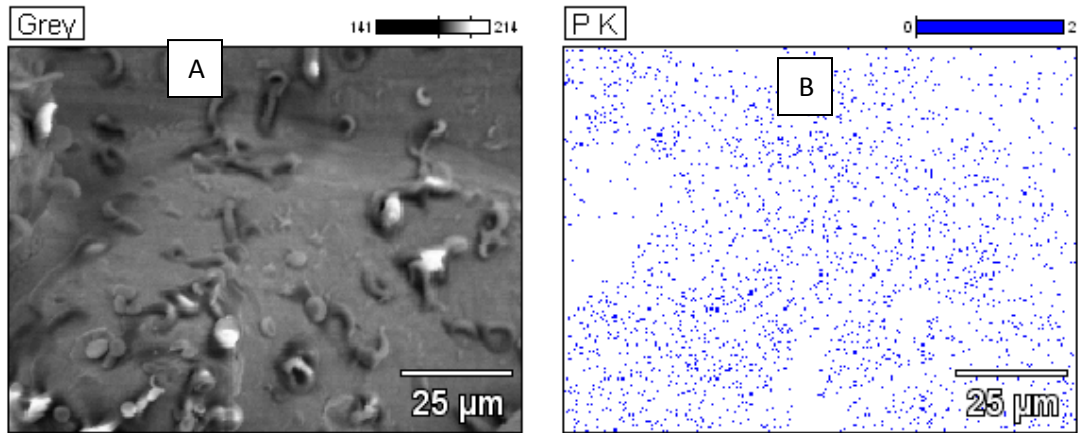


**Figure 5.28.** EDS of 8kV, 8cm, 20 mM surface. A) base image of collection site B) Blue shows phosphorous on surface – indicator of DOPS

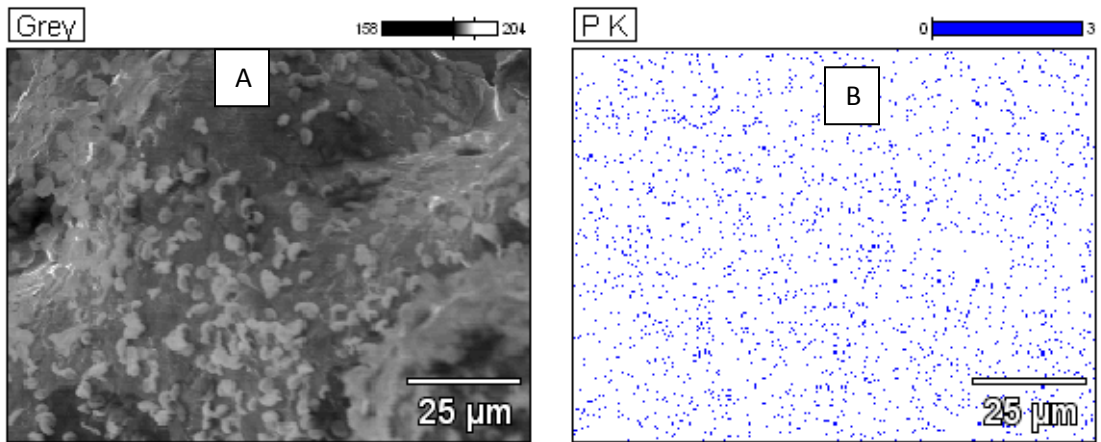


**Figure 5.29.** EDS of 12kV, 4cm, 20 mM surface. A) base image of collection site B) Blue shows phosphorous on surface – indicator of DOPS

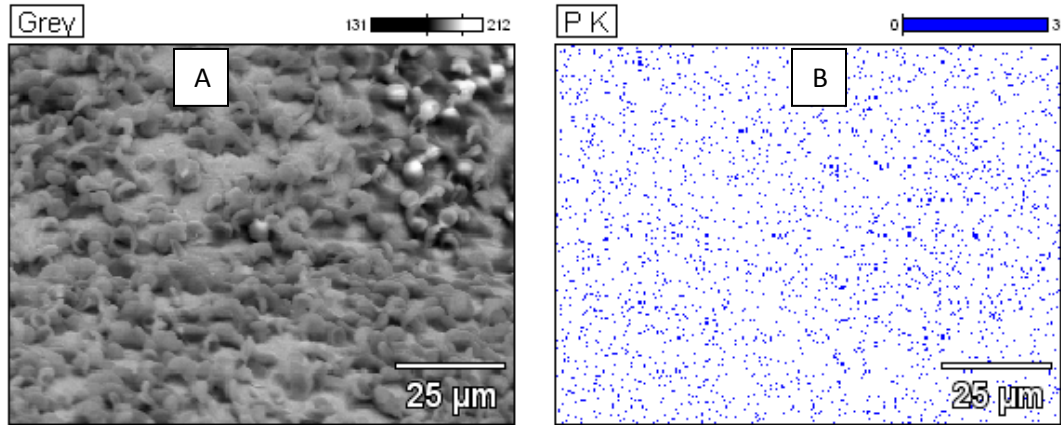


**Figure 5.30.** EDS of 12kV, 8cm, 10 mM surface. A) base image of collection site B) Blue shows phosphorous on surface – indicator of DOPS

In an experiment using the 61% porosity lattices with the parameters held constant at 8cm working distance, 12kV and 20 mM concentration DOPS the time was varied to determine if increasing the spray time increased the DOPS coverage of the lattice. Figures 5.31-5.34 show different segments of a medium porosity lattice that was sprayed for 2 minutes.

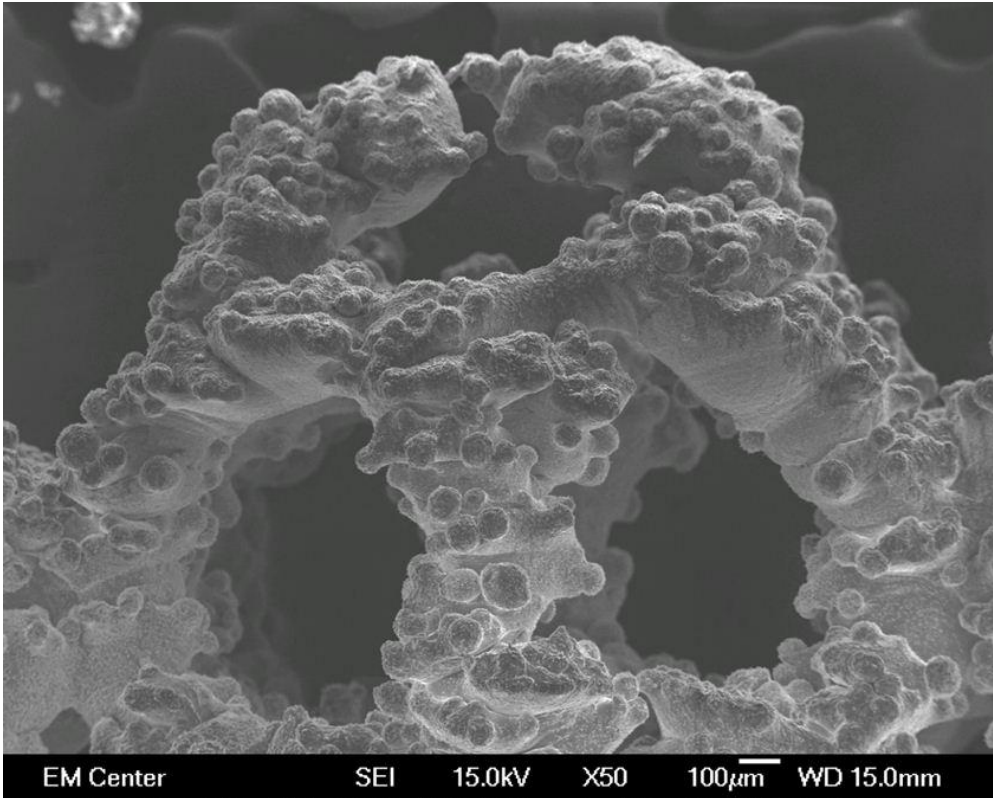


**Figure 5.31.** Top (spray side) segment of 61% porosity lattice sprayed for 2 minutes

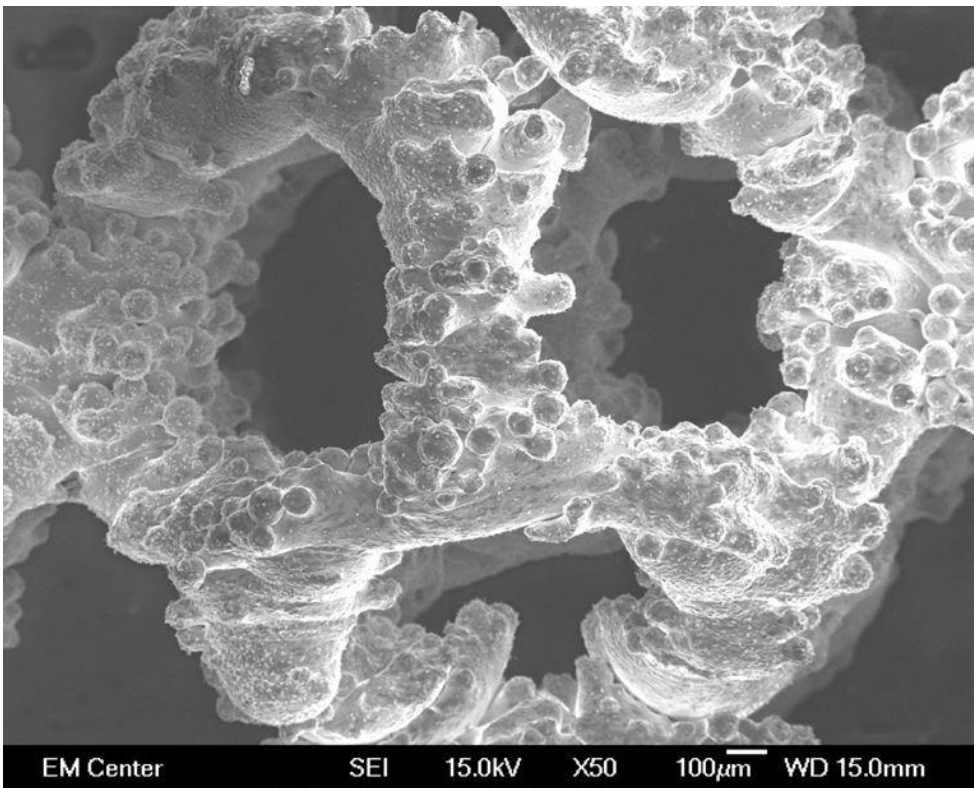


**Figure 5.32.** Middle segment of 61% porosity lattice sprayed for 2 minutes

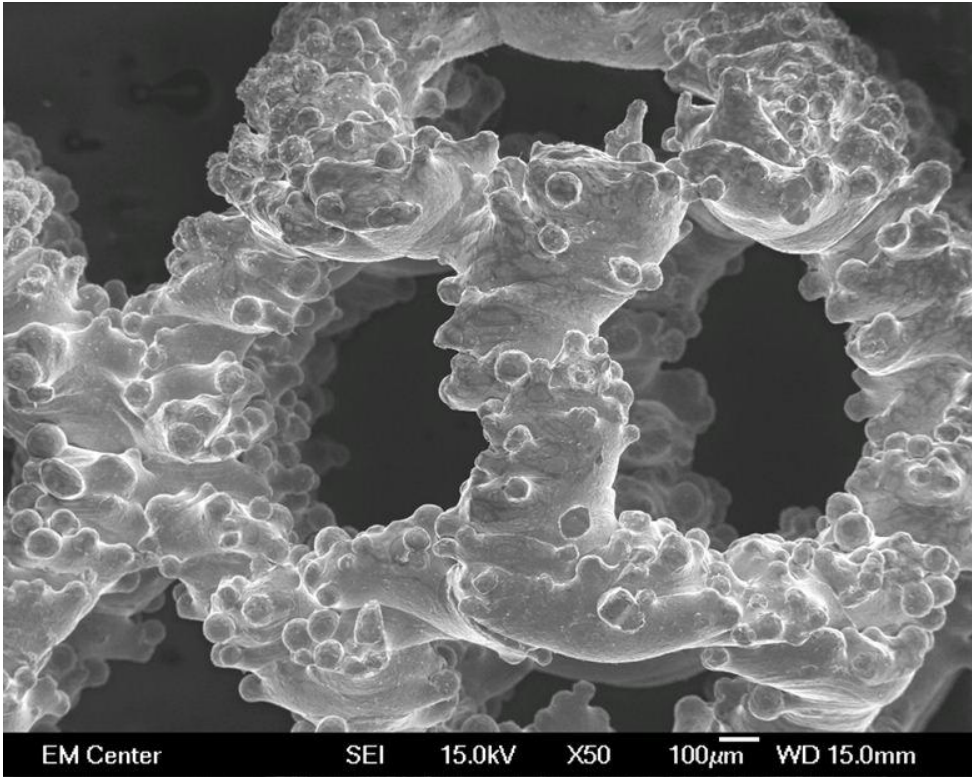


**Figure 5.33.** Middle segment of 61% porosity lattice sprayed for 2 minutes

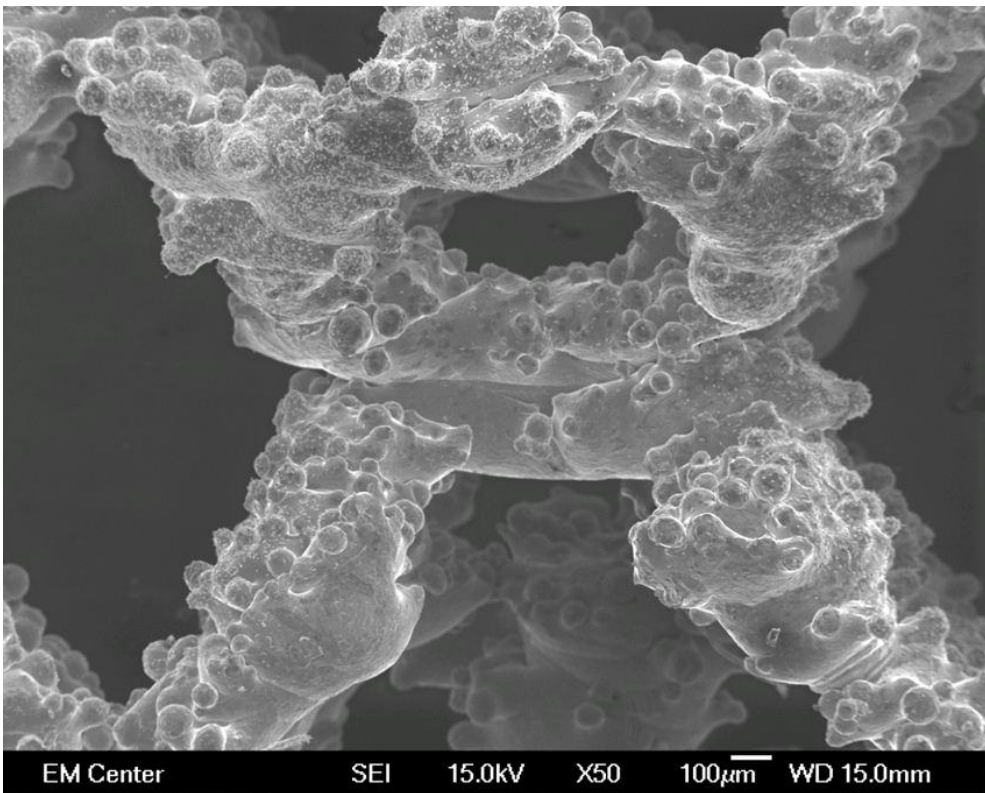


**Figure 5.34.** Bottom (non-spray end) segment of 61% porosity lattice sprayed for 2 minutes

The DOPS can be seen as the “dots” that appear against the lattice, verified with EDS. In figure 5.33, one of the middle segments there is very little DOPS present which is different from the end segment in figure 5.31 where lots of DOPS is present.

Figures 5.35-5.38 show different segments of a 61% porosity lattice that was sprayed for 6 minutes. The 6 minute spray time resulted in much more DOPS than the 1 minute spray time. DOPS was present all the way into the middle of the lattice at 6 minutes and not at 1 minute.

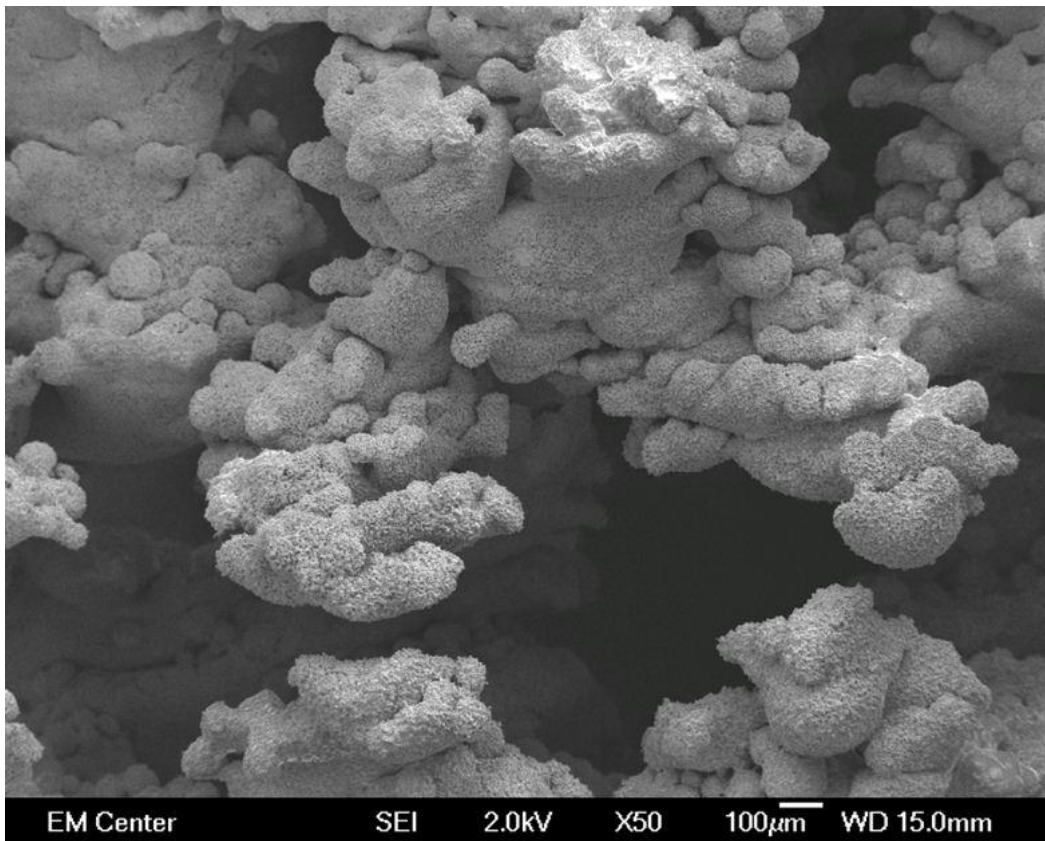


**Figure 5.35.** Top segment of 61% porosity lattice sprayed for 6 minutes

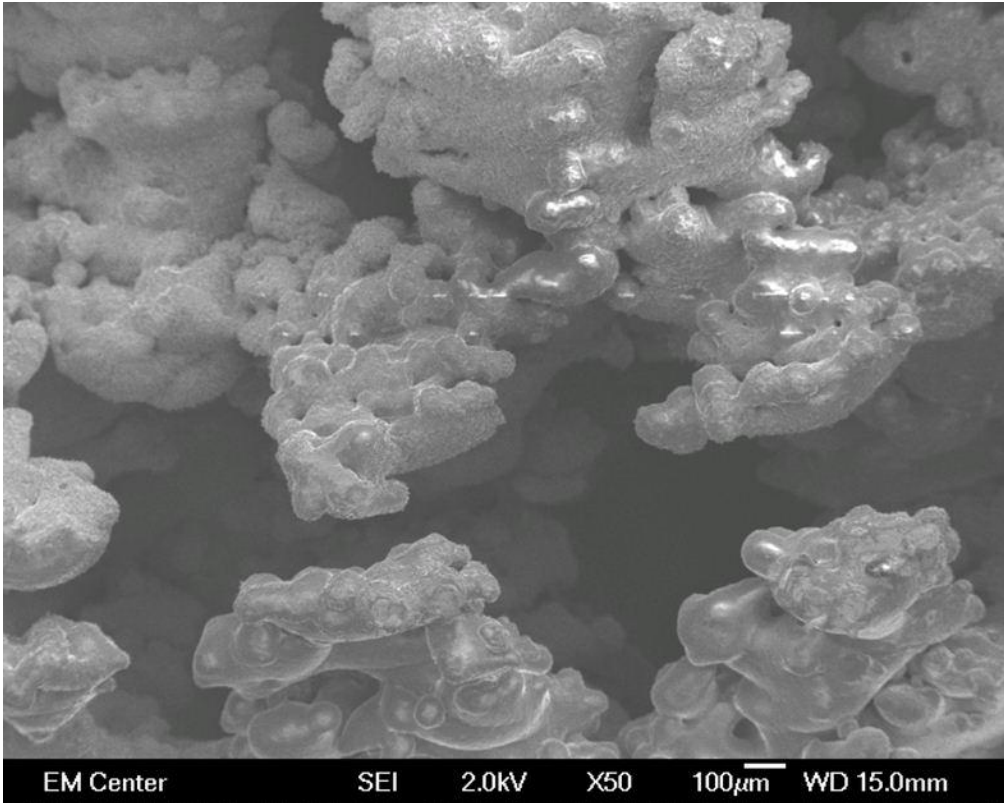


**Figure 5.36.** Middle segment of 61% porosity lattice sprayed for 6 minutes

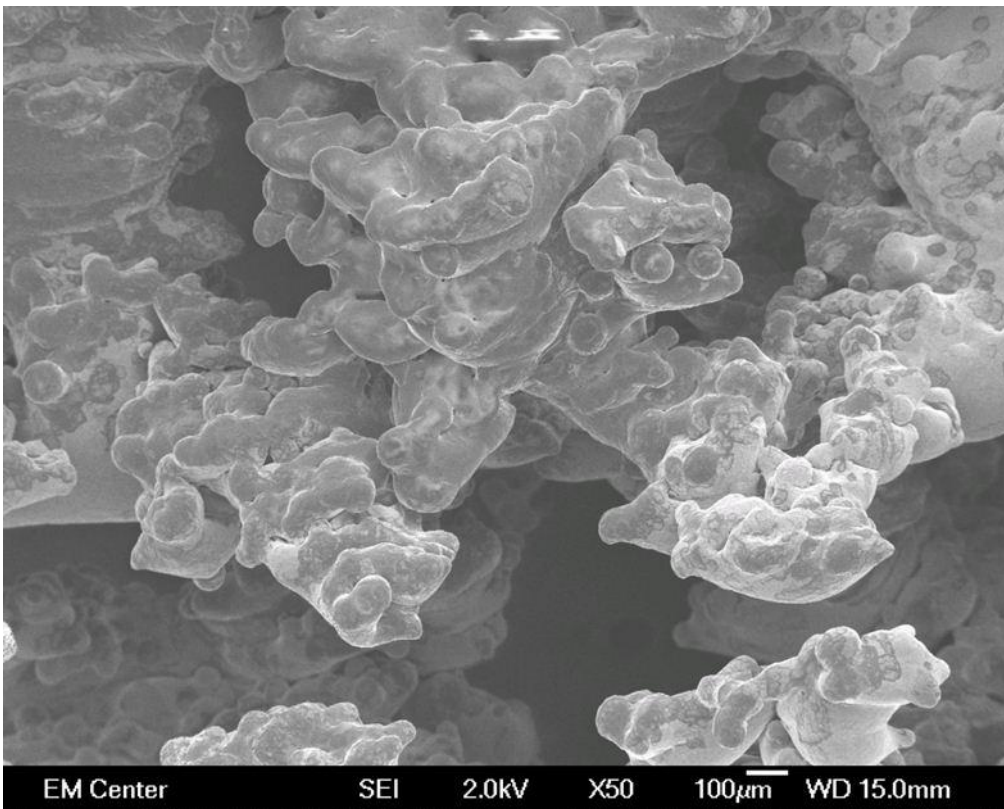


**Figure 5.37.** Middle segment of 61% porosity lattice sprayed for 6 minutes

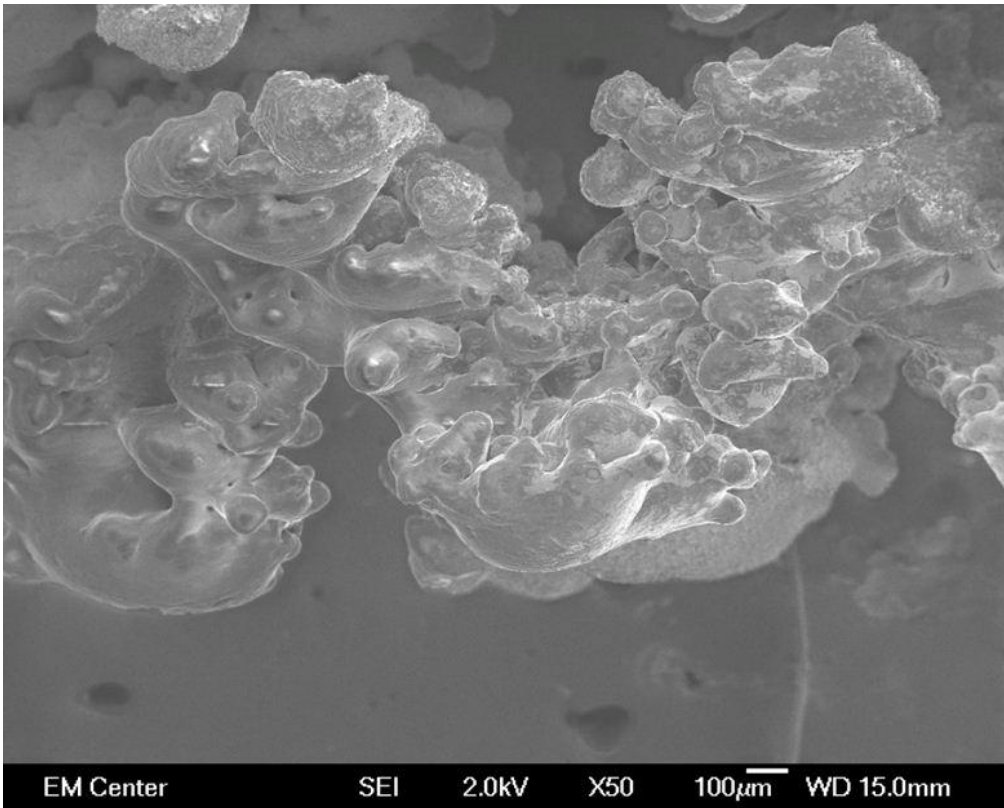


**Figure 5.38.** Bottom segment of 61% porosity lattice sprayed for 6 minutes

### 5.3.1.1 Discussion

The DOPS can be seen in figures 5.35-5.38 as both “dots” and as dark spots on the lattice. In the 6 minute sample in the middle segments (figures 5.36 and 5.37) more DOPS is present on the lattice than in the 2 minute sample.

It was hypothesized that decreasing the spray voltage would help to create more consistent coatings. This was initially proposed because the higher the voltage potential the stronger the current in the system. Higher current exacerbates the Faraday cage effect, thus lowering the voltage would dispel some effects of the Faraday cage. This work was done on the 71% porosity lattices because we hoped that the highest porosity lattice would show the least Faraday cage effect. We hoped that to view the coating

morphology changes without simultaneously seeing the Faraday cage effect on the DOPS coatings. The results of decreasing the voltage actual seem to have introduced more variation in morphology instead of less. However it is possible that the change in voltage was simply insufficient to cause any change given the impact of the Faraday cage effect of the coating morphology. Despite the non-uniform, non-conformal coating created, DOPS was present on the entire lattice as seen in figure 5.28, the EDS of that set of parameters.

The results of this parameterization test showed that the individual parameters control the morphology of the coating deposited on the lattice. There does not seem to be any indication that any particular set of parameters were able to create uniform or conformal coating morphology. No set of parameters was able to create a uniform coating. Many of the parameter sets showed at least two morphologies, one at the outer edges of the lattice and one on the interior faces of the lattice. Though these lattices were fully coated there is likely some Faraday cage effect acting on them. The porosity is sufficiently high to allow enough field lines to penetrate thus creating a full coating. Given the particular geometries of the lattice parts (many edges and sharp points) there are many field line concentrations. Field lines concentrate at part edges and points and this results in a concentration of coating at these areas [84]. The concentration of coating at the edges results in the “overspray” morphology seen in most parts. This is where the DOPS appears more as ball structures, not as a smooth coating and it appears to be very thick.

Some of the different parameter sets create similar looking morphologies though intuitively it seems that they should look different. There are two possible explanations to this. First, it is possible that the effect of field lines (Faraday cage effect) is large enough to overshadow the effect any single e-spray parameter variation might have. As coating is deposited on the target surface the field strength at that point becomes weaker. In flat Ti work, when a thick enough coating has developed the discoid morphology can be seen. The same discoid morphology has been seen in this work with Ti lattice structures in different cases. It is seen in outer edges, most likely the case of overspray where enough DOPS has been deposited to weaken the field there but the discoid morphology is also seen in places without a complete underlying coating. This might be as a result of the Faraday cage effect creating weakened field lines inside the structure resulting in the discoid morphology. This work has discovered that the morphology of the DOPS coating is related to the field strength. Or that an unlimited number of combination of e-spray parameters are possible, many of which could create coatings with similar morphologies. For example, comparing figures 5.19, 5.24 and 5.26 the individual DOPS particles create a very similar looking morphology on a larger scale but when investigated more closely are all slightly different sizes and shapes. The DOPS in figure 5.24 are much smaller and more ellipsoid shaped when compared to the other two. This would seem to be similar to a form of self-assembly common in phospholipids, for example forming liposomes, taking different shapes when under different e-spray parameters. It is also possible that we did not vary any parameter enough to see a change in morphology.

We showed in a time based study that as time increases coating coverage and depth also increase. This was expected because the highest porosity lattice exhibited the lowest Faraday cage effect and would therefore be able to coat more fully. In this way, lattices would act the same as flat Ti squares. With flat Ti the level of coverage is based on the relationship of spray time to surface area. The relationship discovered in prior work was 1 minute of spray time per  $\text{cm}^2$  of surface area [48]. The results of our experiment support the premise that increased time allows for increased coating, to a limit. It is important to consider that an asymptotic level will be reached at which the coating is simply becoming thicker and no longer increasing coverage. This can be seen in the results in which 54% porosity lattices were sprayed. The calculated spray time was based on the surface area of the entire part and when the Faraday cage effect was strong enough, and other e-spray parameters insufficient to overcome, to prevent coating of the inner faces of the lattice the coating built up on the outer edges. If a lattice that was capable of fully coating were e-sprayed for long enough it is likely that this same effect of overspray would be seen in the entire lattice.

This study is limited by the inexact calculation of surface area and thus inexact spray time. The spray time influences the coating morphology and if the e-spray time is very far off the morphology can be changed just by e-spraying too long, creating overspray [48]. It is hard to really quantify this relationship as the Faraday cage effect is also influencing the morphology of the coating.

### ***5.3.2 Surface Roughness and Surface Area***

Increasing surface roughness of a material increases the surface area of a part. The lattice structures exhibit two scales of roughness, the microscale surface roughness typically considered by surface metrologists, and a macro scale, the topographical roughness. This macro scale is particularly important in EBM manufactured parts because as the weld pool is cooling it picks up excess titanium particles. The particles add a considerable amount of surface area to the part.

A study was performed to investigate the effect of surface area on the coating morphology. Figures 5.39-5.40 demonstrate that the effect of changing surface area when spray time corresponds to surface area. Five different surface areas were electrospayed with time adjusted to increase proportionally with surface area. With the time adjusted appropriately for the surface area all surface areas presented the same morphology.

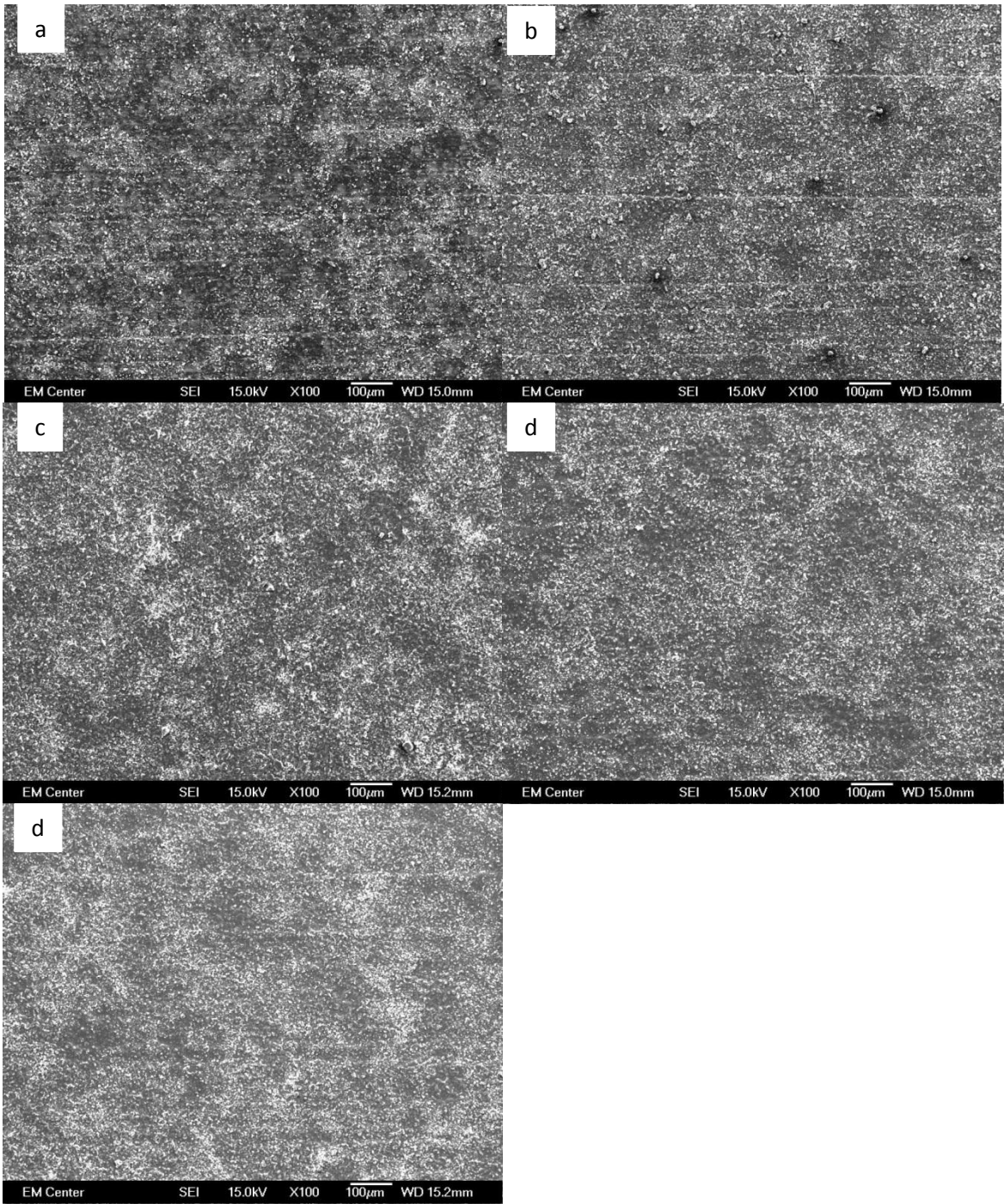


**Figure 5.39.** All five samples showing same DOPS morphologies at 100x

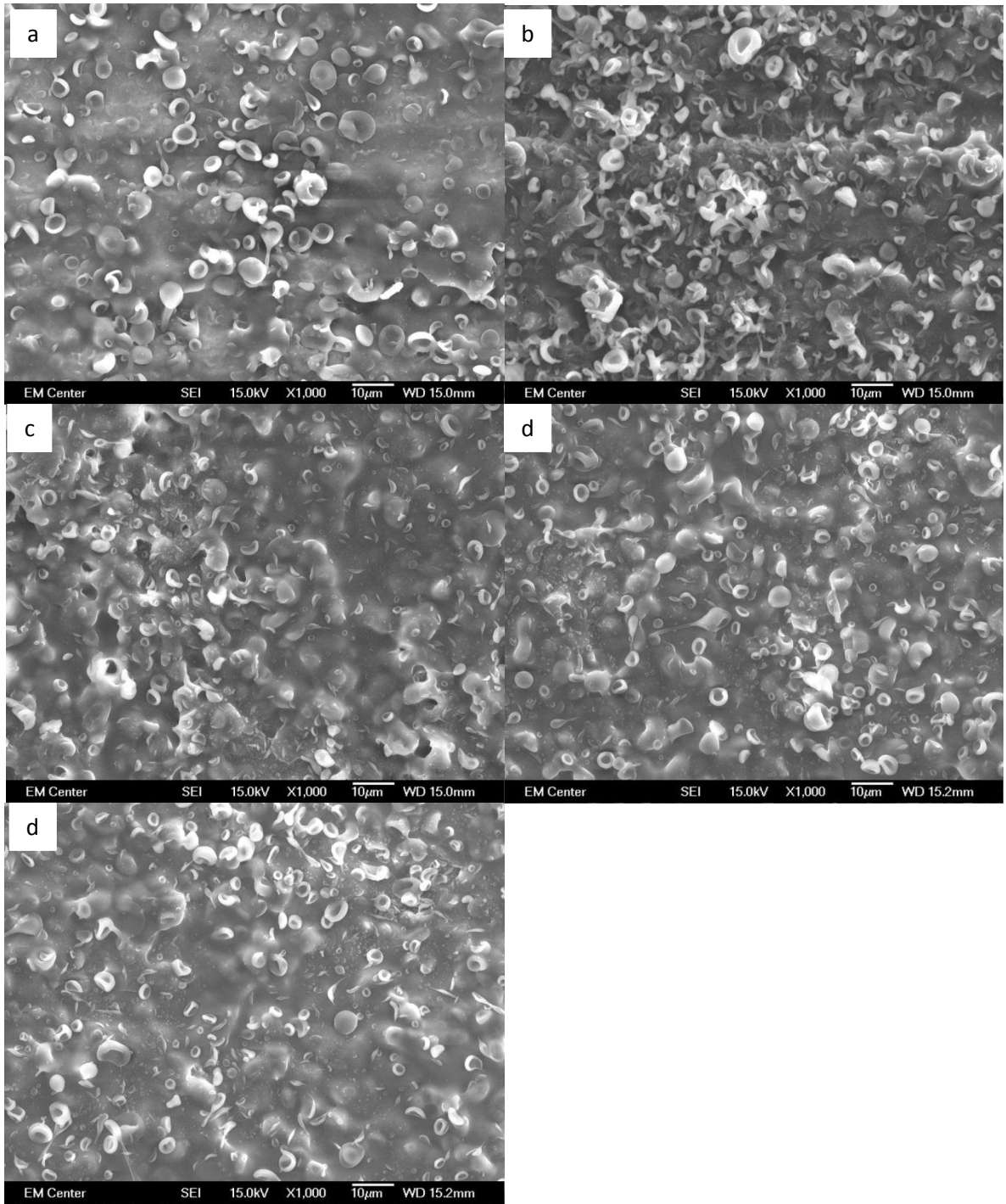


**Figure 5.40.** All five samples showing same DOPS morphologies at 1000x

In another study to determine the effects of acid etching on the raw EBM material, individual struts were placed in hydrofluoric acid for 0, 2, 3, 4 and 5 minutes.

SEM and scanning white light interferometry (SWLI) were then used to characterize the parts. Figures 5.41-5.45 show the results of this study.

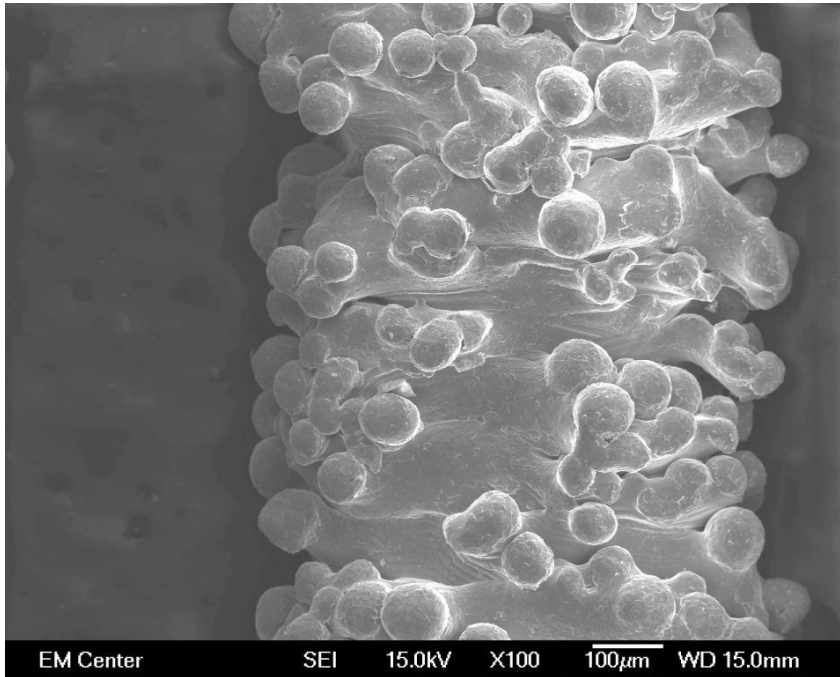


**Figure 5.41.** As received, un-etched EBM strut, 0 minutes in HF

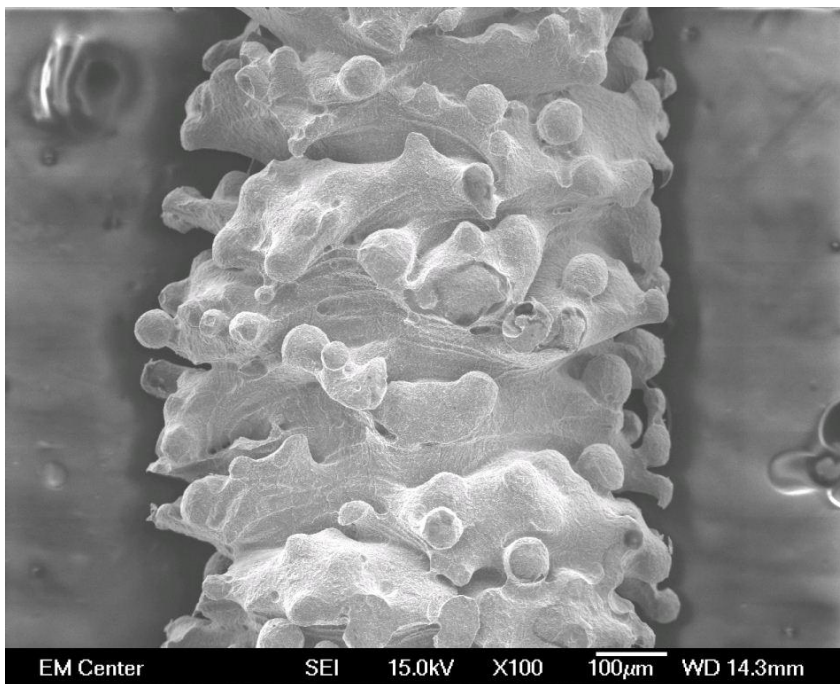


**Figure 5.42.** EBM strut after 2 minutes in HF

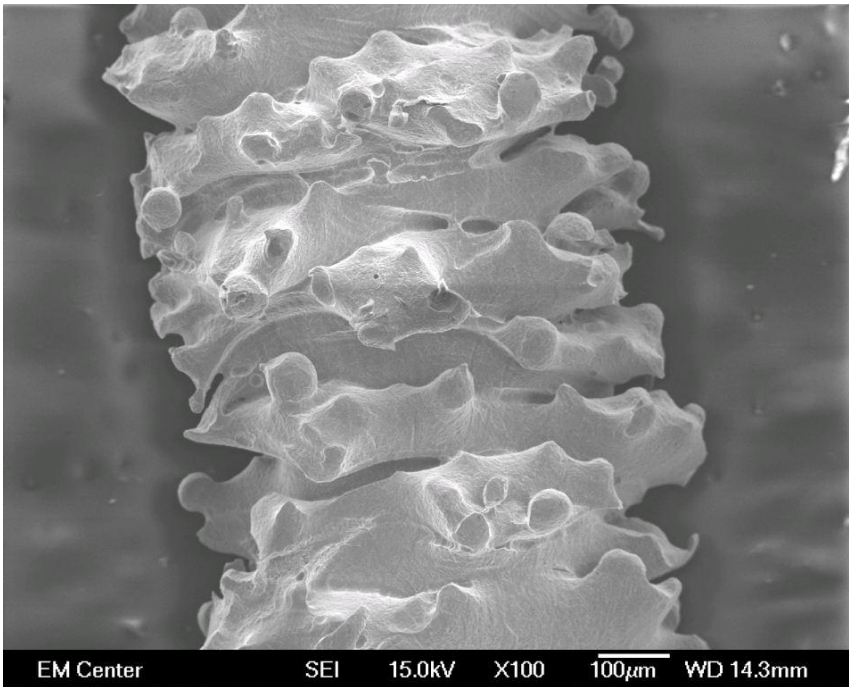


**Figure 5.43.** EBM strut after 3 minutes in HF

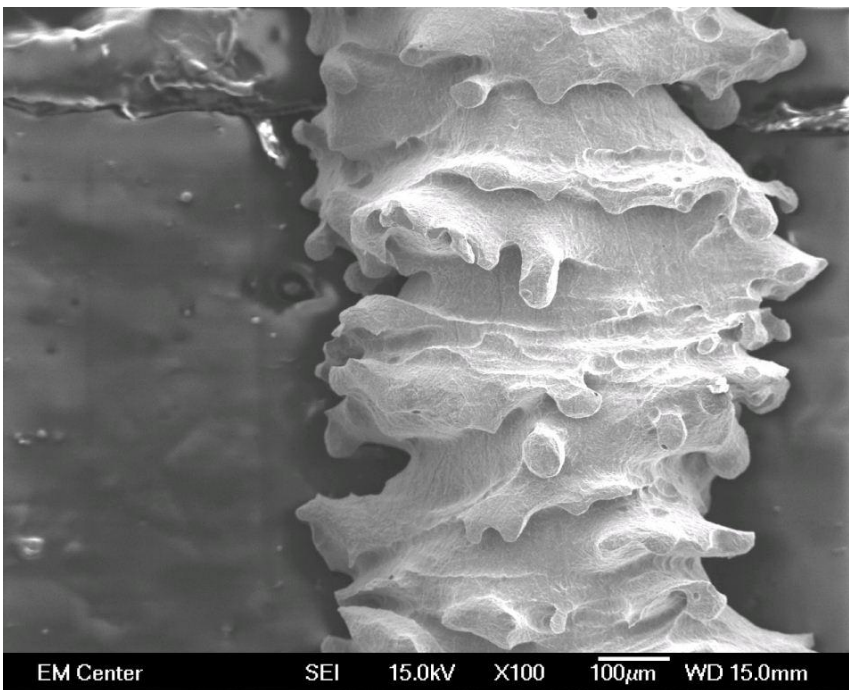


**Figure 5.44.** EBM strut after 4 minutes in HF

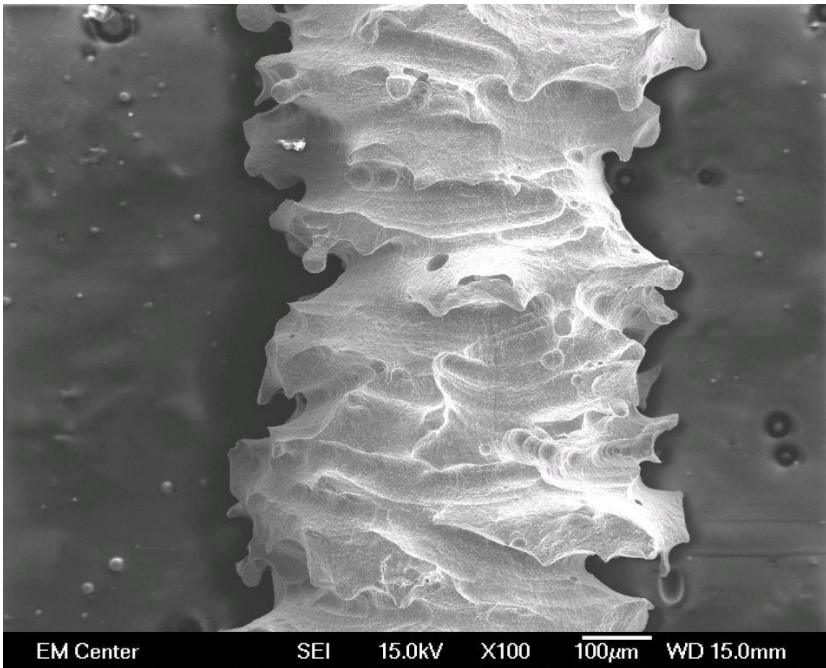


**Figure 5.45.** EBM strut after 5 minutes in HF

SWLI was used to characterize the surface roughness of the surfaces as well as to approximate the true surface area of a part, accounting for varying surface topography. This enables more accurate calculation of the surface area of a part, useful for determining more accurate e-spray time. Figures 5.46-5.50 show the micrographs captured from SWLI. Figures 5.51-5.55 show the ratio of true area to projected area and surface topography roughness from SWLI. The true area from SWLI is everywhere the light was able to reflect with the masked area ( $1\text{mm}^2$ ) so this would include all surface features. The projected area from SWLI is the area captured by the mask not accounting for any surface features.

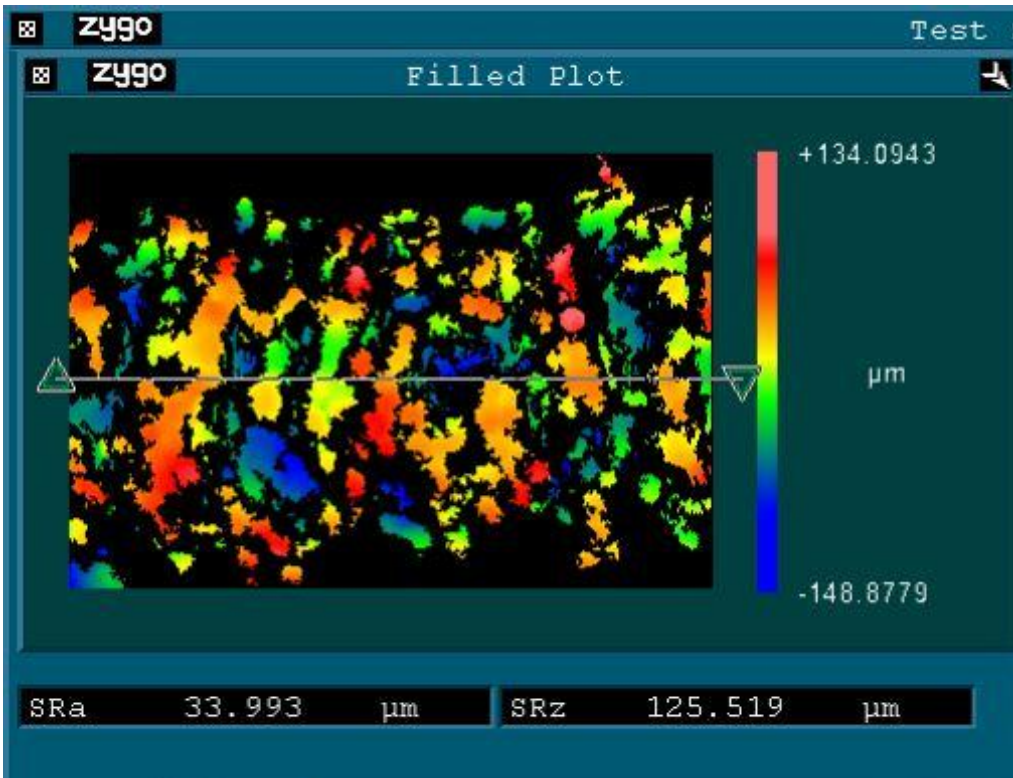


**Figure 5.46.** SWLI of as-received, un-etched EBM strut, showing area and line used to generate surface roughness values

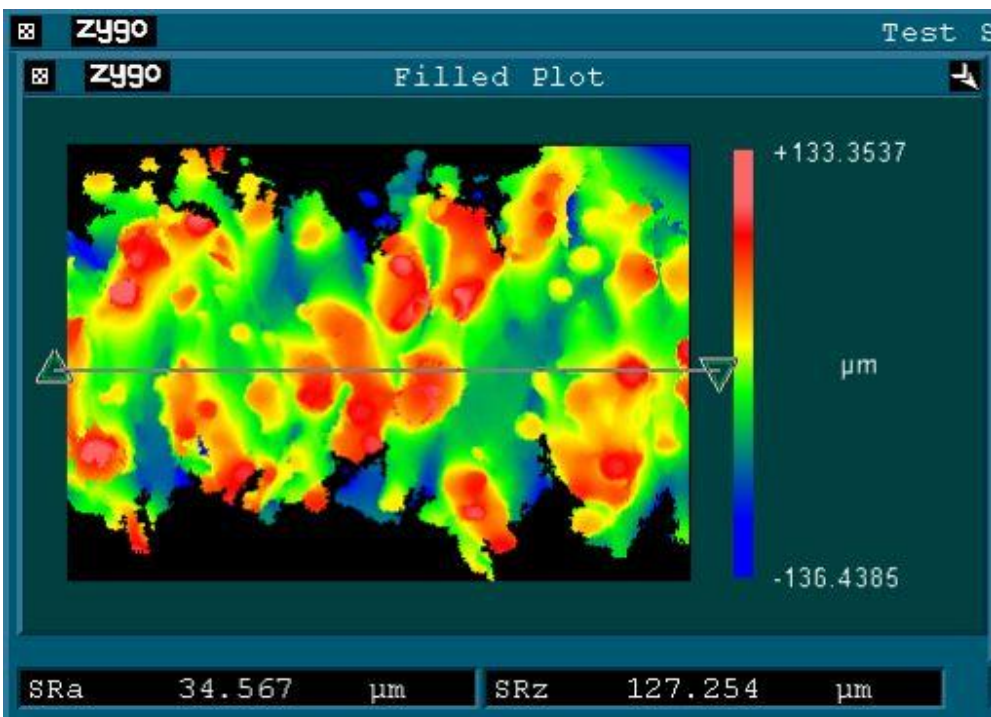


**Figure 5.47.** SWLI of strut after 2 minutes in HF, showing area and line used to generate surface roughness values

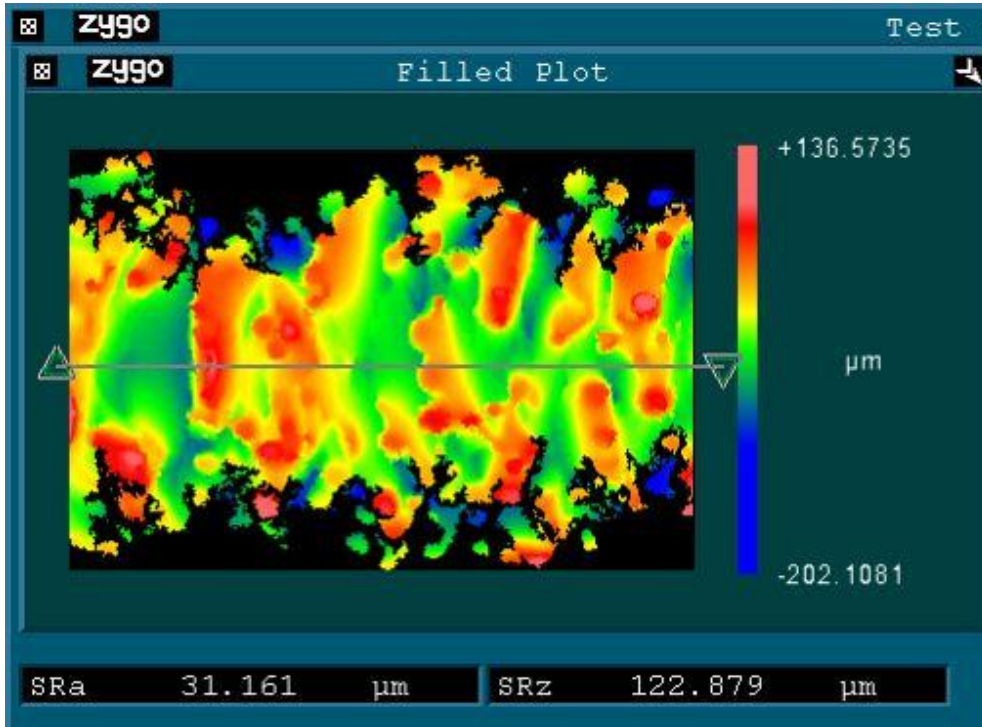


**Figure 5.48.** SWLI of EBM strut after 3 minutes in HF, showing area and line used to generate surface roughness values

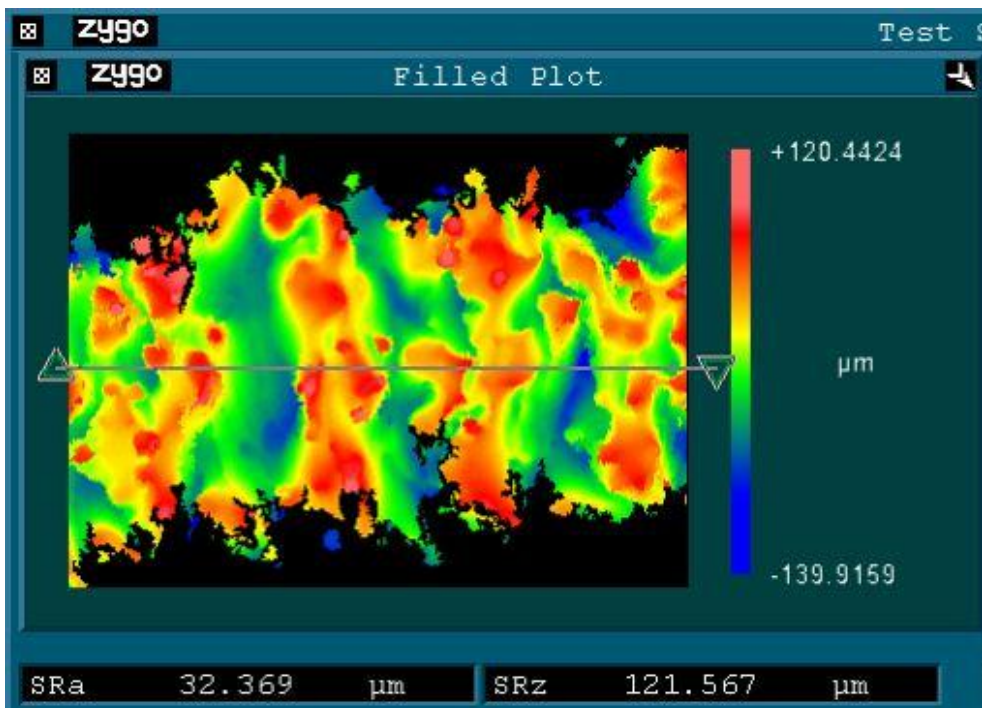


**Figure 5.49.** SWLI of EBM strut after 4 minutes in HF, showing area and line used to generate surface roughness values

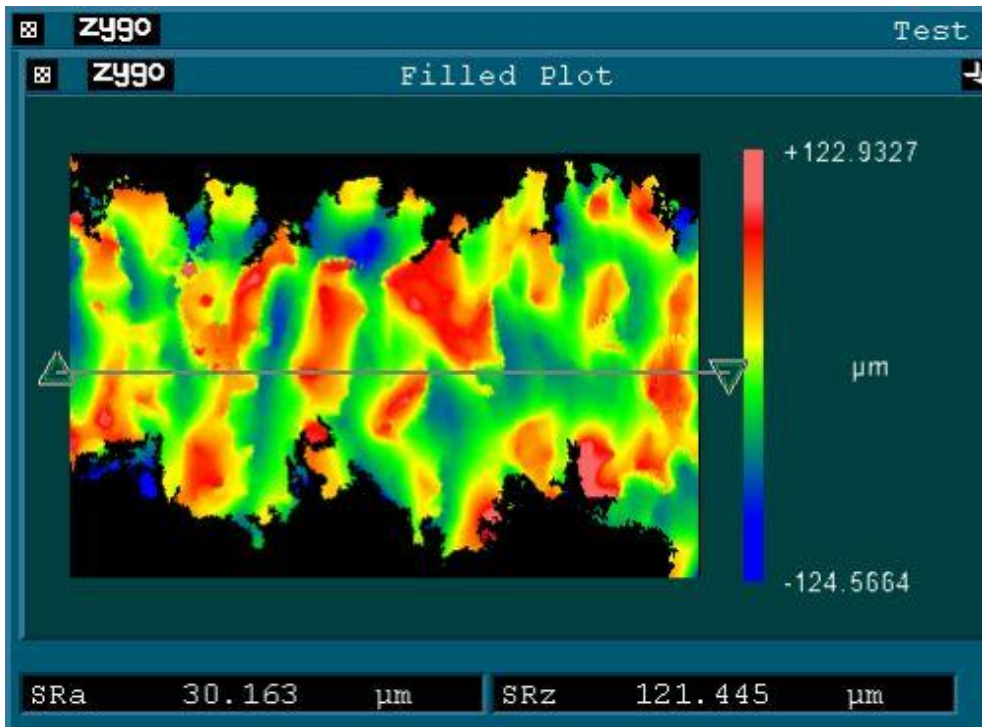


**Figure 5.50.** SWLI of EBM strut after 5 minutes in HF, showing area and line used to generate surface roughness values

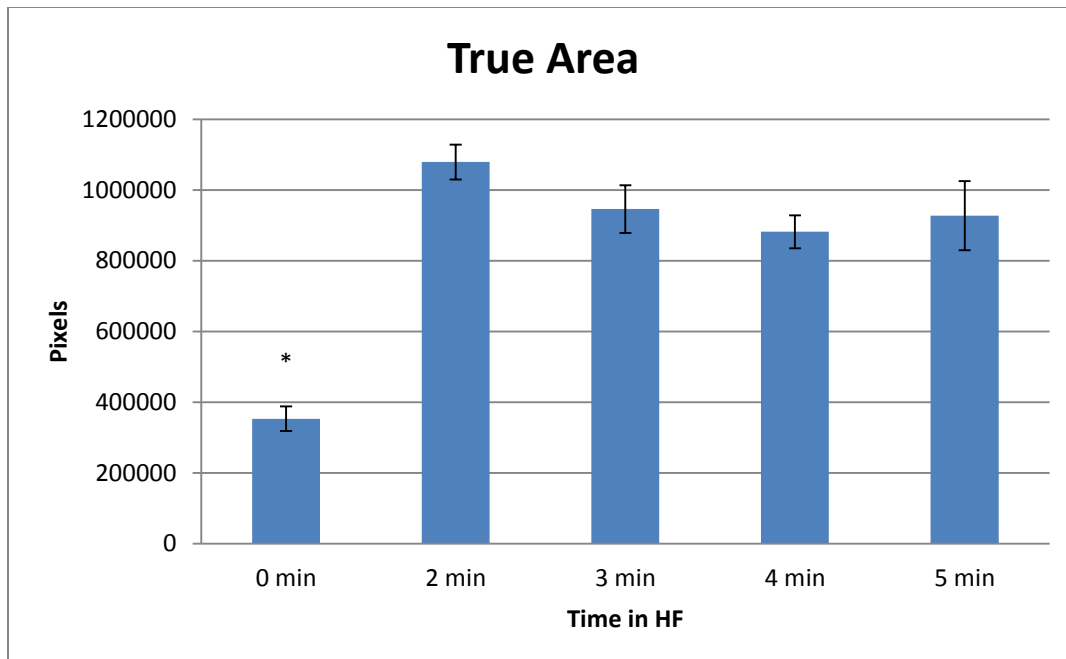


**Figure 5.51.** SWLI data for the true area of a 1 mm<sup>2</sup> mask \*indicates significant difference to all other time points

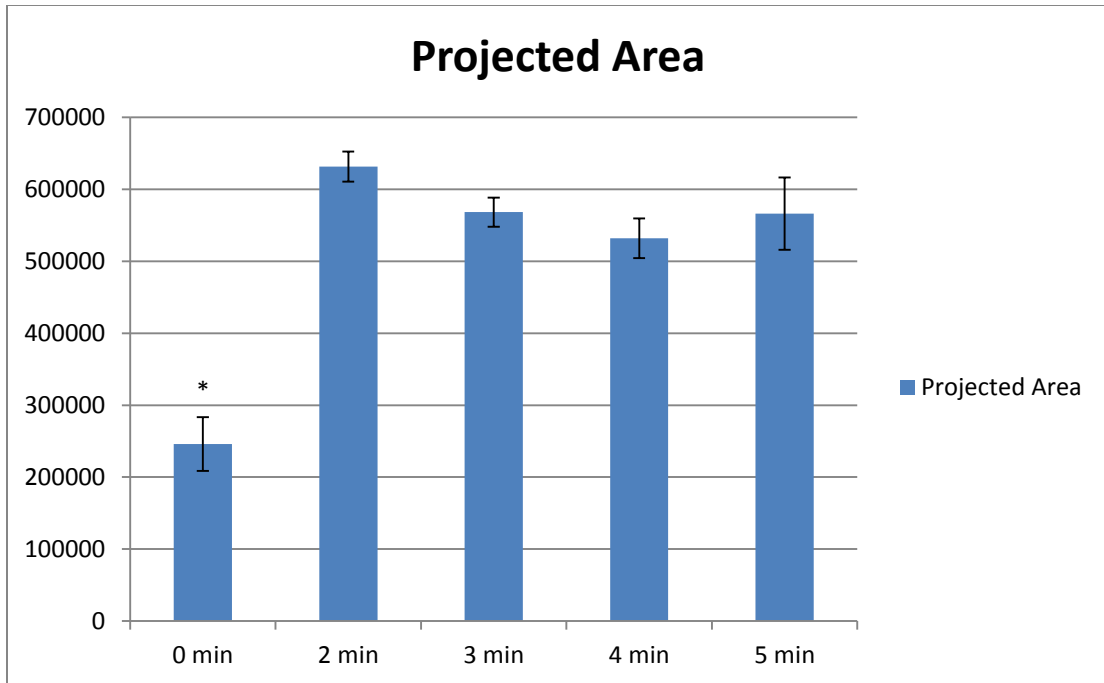


**Figure 5.52.** SWLI data for the projected area of a 1 mm<sup>2</sup> mask \*indicates significant difference to all other time points

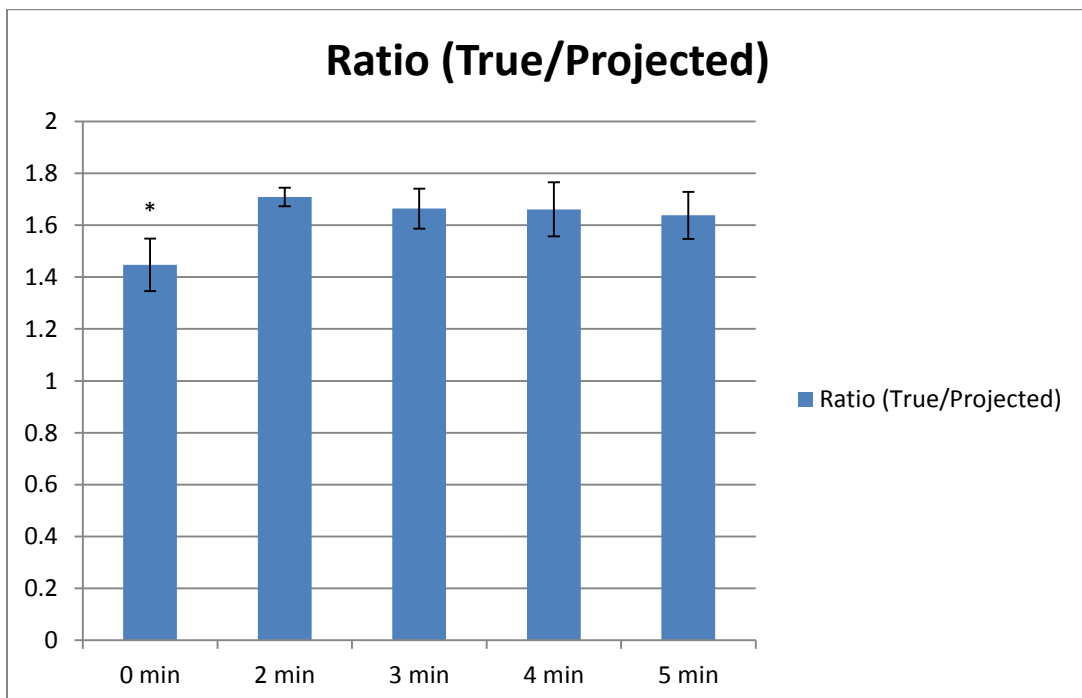


**Figure 5.53.** Ratio of true area to project area generated by SWLI. \*significantly different from all other time points

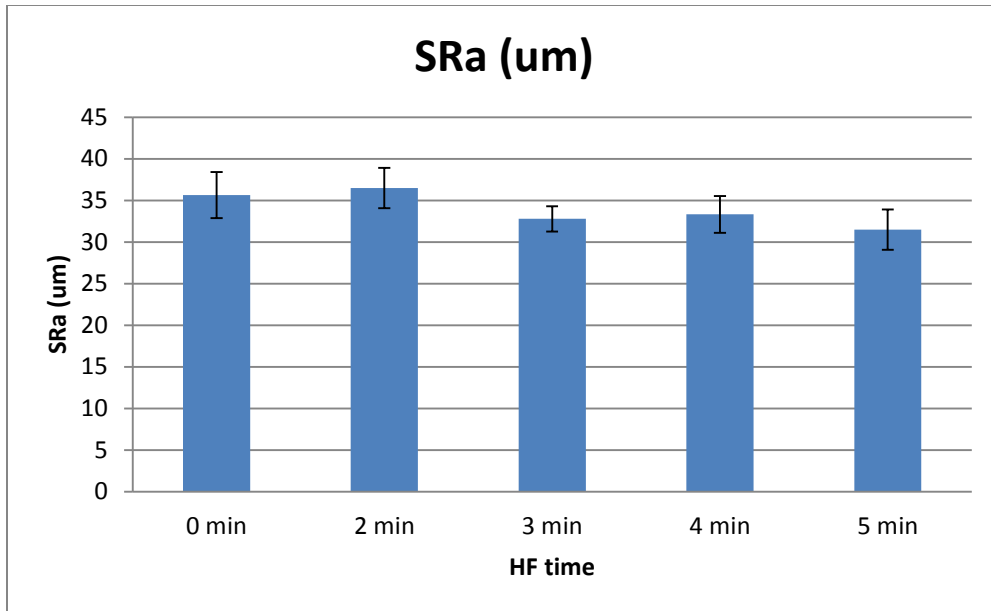


**Figure 5.54.** Surface roughness data generated by SWLI, no significant difference

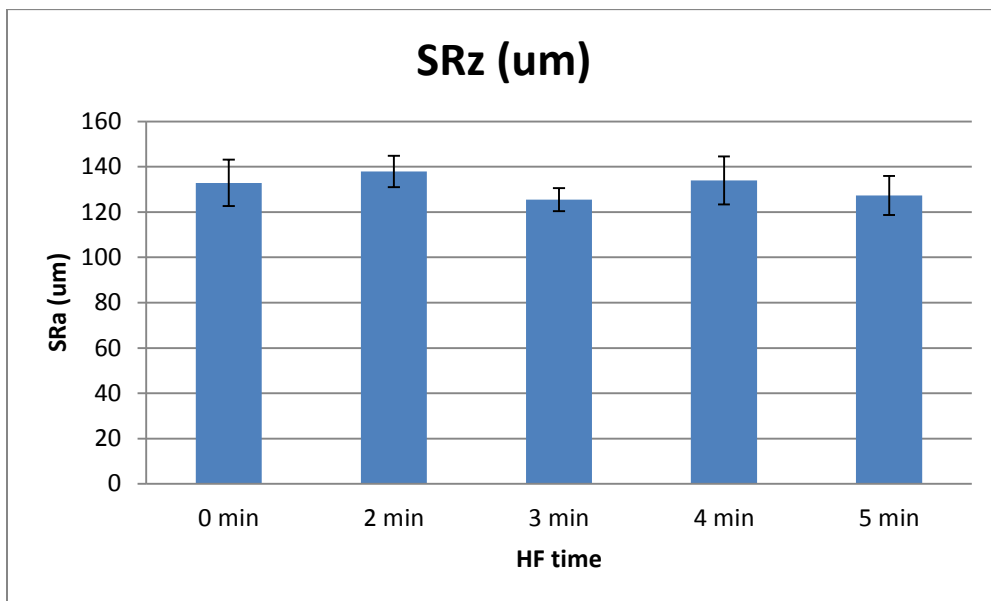


**Figure 5.55.** Surface roughness data generated by SWLI, no significant difference

In addition to using SEM and SWLI to characterize the changes in struts due to acid etching time in HF we also had people unfamiliar with the EBM struts count the number of excess Ti “particles” visible on the surface at each time point. Each set of data was normalized to itself using the number of particles counted by each person at the zero time point (un-etched strut). This provided a baseline for how each person

perceived particles. The percent difference is calculated the time point in HF subtracted from the zero number divided by the zero number, thus the higher the percent difference the less number of particles seen.

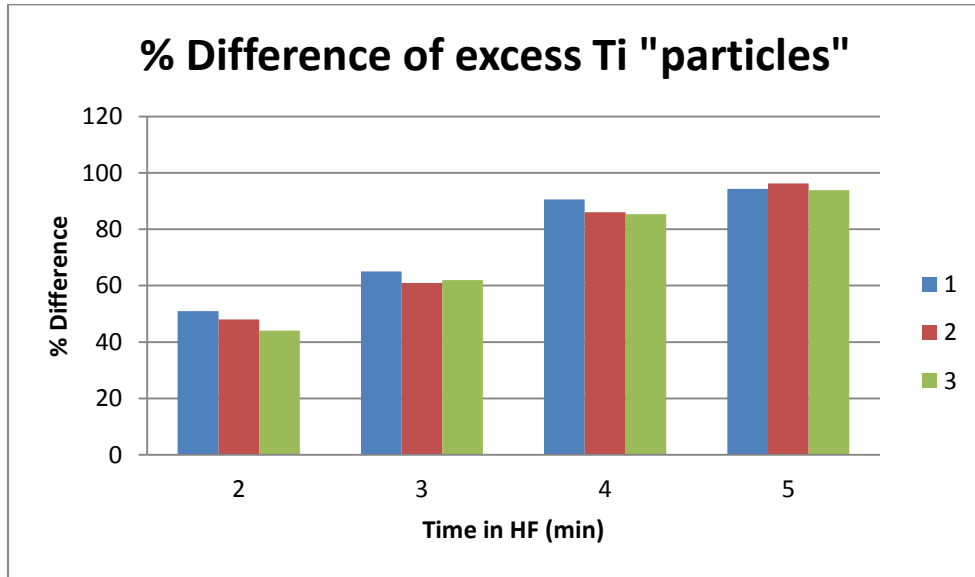


**Figure 5.56.** % difference of Ti particles counted at each time point of strut in HF

### 5.3.2.1 Discussion

It can be seen from figure 5.50 and 5.51 that the surface area of an as received EBM part is significantly lower from those that have undergone acid etching. This is due to the surface roughness as seen on a larger scale in the SWLI micrographs above. The surface roughness plays a considerable role in the surface area of a part. As the surface area is the primary determinate of the time required for e-spray being able to more accurately determine this is very useful and important especially in such complex parts where calculating the true surface area is difficult. The surface area used in determined spray time in this work was the nominal surface area multiplied by 1.5. The factor of 1.5 was used as an estimate to account for surface topography as the nominal surface area does not. The nominal surface area calculated by us is similar to the projected area

from SWLI. The ratio from SWLI indicates (figure 5.53) that the factor should have been higher closer to 1.6 or 1.7 than the 1.5 used. This would have provided a more accurate surface area estimate and thus a more accurate e-spray time. If a study were done comparing the morphologies of coatings on raw EBM material and acid etched EBM material and the e-spray time were held constant based on surface area it would likely yield similar results to those found figure 5.39 and 5.40. The results in figure 5.39 and 5.40 are from a time study in which all parameters were held constant and time was constant with increasing surface area. The e-spray was on flat Ti with no large scale topographical variance, so the relationship for surface area was 1 minute of e-spray per  $\text{cm}^2$  of surface area. The morphologies of the different time points are essentially indiscernible from one another with identical coatings on each part. This confirms the theory that if time is held constant with surface area the coating created in each case will be uniform and conformal.

From the SEM there is a very clear visual difference between the different time points of the struts after they were acid etched. The un-etched EBM strut has many excess Ti particles on it and after 5 minutes in HF the strut has almost no excess Ti particles. People were able to identify different morphologies based on excess particles counted on the struts. In figure 5.56 it is seen that the counters identified different numbers of particles based on the time spent in HF. This visual change in morphology is as important as the surface roughness values generated because this how the removal of particles can be identified.

It is important to understand that the particles can be removed before implantation because if they detached *in vivo* they could cause biocompatibility concerns and decrease *in vivo* erosion resistance. This erosion could have negative effects on the implants life span as it may interfere with BIC and allow for a fibrous encasement to form [3]. It is also possible that this erosion could also have a positive impact by making it harder for the fibrous tissue layer to form. In some *in vivo* studies of EBM parts erosion has been seen that prevented the formation of the fibrous tissue to form [60]. The source of this erosion is not identified and thus the excess particles should be considered detrimental until there is more work verifying if this is erosion of excess particles or some other sort of erosion.

The morphology (excess particles) is controllable with acid etching applied to EBM Ti structures. The results of SWLI (figures 5.54-5.55) show that there is actually no significant difference in the roughness (SRa and SRz) of the parts despite the distinct changes in morphology. It is likely that as a result that the etching, while removing the excess particles, does not change the overall height of peaks and valleys in the parts. These peaks and valleys are what results in the high surface roughness values. The SRa and SRz address um scale changes to the topology, surface roughness is usually thought of on the nana scale. We consider surface roughness on this scale because that is size of the excess particles removed, thus impacting the surface topology. It is possible that if the etching were continued long enough there would be some significant change in surface roughness but it would also likely cause structural damage to the part. As the etching time increase an increased amount of material is removed from the entire part

not just from the peaks. In the case where valleys backed up to one another on different sides of the part, if that material were etched away it would result in a very thin section that would more likely to fail. It is important not to over etch the parts and remove so much material that the part is no longer structurally sound.

This work was limited by primarily by the methods used for characterization. The SWLI is not able to capture areas with steep slope or materials that absorb light. This would lead to gaps in the data with the parts being imaged. The characterization done by people has the limitation of each person evaluating things slightly differently. Acid-etching can be used to remove a layer of material to control the oxide layer that reforms [48] though this work used it to actually alter the surface topography. When using the acid to remove so much material it is important to remember that it loses potency as it removes material.

In summary changing the surface area of the parts has no impact on surface morphology of the coating as long as the time is held constant with changing surface area. It is also possible to control the surface morphology of part through chemical etching though the Sra and SRz values do not change dramatically or significantly, the morphology of the part does.

## 6 Conclusions and Future Work

### 6.1 Conclusions from Current Work

Osseointegrative coatings are the next step in improving BIC in orthopedic implant and e-spray is a suitable method for creating these thin, adherent coatings. Orthopedic implants are a complex geometry and require a process that is capable of overcoming this and still applying a coating. Electro spraying has a good record for producing the thin, uniform, consistent coatings on flat Ti that could improve mechanical stability of an implant especially when compares with other techniques [15]. Improved mechanical stability will lengthen the lifespan of the implant and improve quality of life for the patient. This is critical because the number of joint replacements each year is already well over 500,000 and this number is only expected to rise [92]. Improving the life span of an implant from the average 12-15 years [95] is crucial as the average life span of implant recipients increases. The demand for revision surgeries will increase with increasing recipient life span so an implant that lasts longer will help diminish the number of necessary revision surgeries [96]. Coatings can help be a part of the next step to improved implant life.

In this work the electro spray process was applied to porous 3D Ti-6V-4Al lattice structures. The electro spray process is one of the best candidates for applying coatings to such complex geometries as it utilizes field lines to deposit materials. During the tenure of this research it was discovered that when these complex parts are introduced into a charged field at certain porosities they develop into Faraday cages that completely limit coating depth of the structures. While at a low enough porosity,

between 54% - 80% porosity, the effect is great enough to completely stop the process at higher porosities it affects the morphology of the coating but does not stop the process entirely. 61% porosity lattices, tested in this work, turned into Faraday cages when externally insulated. The external insulation enhances the Faraday cage effect. The Faraday cage effect essentially causes all of the field lines inside of it to cancel out. As these field lines are canceled the e-spray process loses efficacy as it relies on field lines to deposit material on the target. This work proved that Ti lattices when externally insulated turn into Faraday cages. The Faraday cage effect is commonly encountered in the powder coating industry. Powder coating is an analogous process to e-spray, the primary difference being that the working fluid is air and not liquid. There has been much work done on mitigating the Faraday cage effect in powder coating and some of this work is likely applicable to e-spray and the Faraday cage effect. Some preliminary studies were done in this work to begin to understand the relationship between the Faraday cage effect and its impact on the electro spray process and its unique and variable parameters. Understanding how and why the lattice structures turn into Faraday cages is the first big step in being able to coat them because before now it was previously unknown in the realm of electro spraying that parts could turn into Faraday cages.

In this work the relationship between the Faraday cage effect and the electro sprayed coatings was investigated. We discovered that the Faraday cage effect causes non-uniform and non-conformal coatings even on the lattices (61% and 71% porosity) that were able to be coated fully. The morphology of the coating changed

from area to area within one part as well as different parts displaying different morphologies. The buildup of field lines at the outer edges causes an overspray morphology and the coating appears thicker at the outer edges of all lattices, even those that the coating could penetrate into. In the lattices that the Faraday cage effect was too strong and penetrating coatings were not possible there were small, thin patches of coating slightly interior. This was very irregular and did not penetrate fully into the interior of the lattice. This work proved that at low enough porosities (54%) Ti lattices, when not externally insulated, exhibit the Faraday cage effect.

As the parameters of e-spray are very important in the coating created it was important to investigate the relationship of e-spray parameters to the Faraday cage effect. The e-spray parameters were varied in study using lattices that could be fully coated using electrospray. Without external insulation was the 54% porosity lattice did not coat fully but the 61% and 71% porosity lattices did though the coatings were not uniform or conformal showing mixed morphologies. The variation of parameters did not create any more or less uniform and conformal coatings. All parts continued to show mixed morphologies. With regard to the morphology of the coating, the Faraday cage effect overpowers the effect of varying any one parameter. The Faraday cage effect must first be mitigated before a uniform and conformal coating can be created. This work disproved the hypothesis that with high enough lattice porosity (when lattices can fully coat, 61% and 71%) the coating will be uniform and conformal. It did confirm that lattices not able to coat (54% porosity) would exhibit spotty, uneven coatings with

overspray at the outside of the lattice. The work disproved the hypothesis that decreasing voltage would increase coating uniformity and conformity.

Time plays a role in coating coverage, as time is increased the coating coverage increases until the entire part is coated and then it begins to create a thicker layer. The time selected to create a full coating is based on the surface area of the part. The time should be held constant based on surface area. The topographical roughness has an impact on the surface area of the part and must be considered in selecting appropriate e-spray times. SWLI is able to give an accurate relationship between the nominal surface area of a part to the true surface area. This can be used to more accurately measure surface area. Proved in this work was that increasing e-spray time increased coating coverage and depth as well that decreasing surface roughness (changing surface area) would not cause different morphologies as long as e-spray time is constant based on surface area.

Also important is controlling the surface morphology of the part before it is coated. Acid etching can be used to change the topography of the lattice structure by removing excess titanium particles that attached to the part during manufacture. Being able to remove these particles is not only useful for controlling the topology and roughness of the part but also when considered from a corrosion standpoint. The particles are not well attached and would corrode easily if on an implant *in vivo*. This corrosion could be detrimental to the implant. This work proved that surface roughness and morphology can be controlled with chemical etching though it disproved the theory that roughness will decrease with increased etching time.

## 6.2 Future Work

The most important future work to be done is to determine how to mitigate the Faraday cage effect in the process of electro spraying. If this mitigation cannot be achieved then the coating technology will remain limited in its use for coating complex, porous geometries. In the case that mitigation is not possible finding a way to adapt the e-spray process would be necessary. The mitigation of the Faraday cage effect may be possible through the use of a fluid pressurizer, such as a nozzle. If the fluid is pressurized then those forces may help to overcome the Faraday cage effect. This could be achieved in a method that would involve the integration of an aerosol spray system with the electro spray system. It would likely end up very similar to the systems used for powdercoating, most like the corona gun. Another potential method for mitigating the effects would be the introduction of a free ion collector into the system. This would serve to collect the excess ions that are created during the process. A corona discharge is created in e-spray systems and the free ions move rapidly towards the surface and change the potential of the surface which can rapidly lead to rejection of the source material. This effect exacerbates the Faraday cage effect. Also potentially useful in mitigating the Faraday cage effect would be a pulsing system, pulsing the electric field or an applied mechanical pressurizer.

Another important thing to consider is to try and actually understand what is happening inside the field at the part. What is needed is a very high sensitivity power supply, one that has highly accurate read outs for both voltage and current. The current is the an important parameter in the electric field that is generated and understanding

what is happening to the current during the spray would be useful in developing a relationship of e-spraying to the Faraday cage effect to the porosity of the structure (i.e. perhaps the current changes dramatically when the Faraday cage effect kicks in). Once the current in the system is understood being able to vary it would also provide the possibility of lowering the electric field. The lower the field the less effect a Faraday cage is going to have.

There are many important parameters in electro spraying that could potentially have an effect on the Faraday cage that have not been investigated. Creating an environment in which as many parameters can be locked and studied will be critical to the furthering of this work. Parameters need to be tightly controlled so that the way the electric field is moving through space and time can be replicated and understood that will help to generate more consistent coatings.

A final thought is actually creating a mathematical and computer model of this system. While modeling this system would be very complex it would provide useful information that could be input to help determine appropriate parameters as well as being used to predict sizes and porosity for complex shapes. Truly seeing the electric field and how it changes as the process is going on would be very valuable.

## REFERENCES

1. Carter, J.S. *Lipids: Fats, Oils, Waxes, etc.* 2012 [01/09/2012]; Available from: <http://biology.clc.uc.edu/courses/bio104/lipids.htm>.
2. Biology, D.o. *Phospholipids are Like Triglycerides with a Phosphate Group.* 2012 [01/02/2012]; Available from: [http://bioweb.wku.edu/courses/biol115/wyatt/biochem/lipid/Lipid\\_2.asp](http://bioweb.wku.edu/courses/biol115/wyatt/biochem/lipid/Lipid_2.asp).
3. Wuthier, R., *LIPID COMPOSITION OF ISOLATED EPIPHYSEAL CARTILAGE CELLS, MEMBRANES AND MATRIX VESICLES.* *Biochimica et Biophysica Acta*, 1975. **409**: p. 128-143.
4. Childs, G. *Membrane Structure and Function.* 2001; Available from: [http://www.cytochemistry.net/cell-biology/membrane\\_intro.htm](http://www.cytochemistry.net/cell-biology/membrane_intro.htm).
5. Christie, W.W. *PHOSPHATIDYLSERINE AND RELATED LIPIDS: STRUCTURE, OCCURRENCE, BIOCHEMISTRY AND ANALYSIS.* 2012 [12/05/2011]; Available from: <http://lipidlibrary.aocs.org/lipids/ps/index.htm>.
6. Eanes, E.D., *Mixed Phospholipid Liposome Calcification.* *Bone and Mineral*, 1992. **17**: p. 269-272.
7. Camolezi, F.L., et al., *Construction of an alkaline phosphatase–liposome system: a tool for biomineralization study.* *The International Journal of Biochemistry & Cell Biology*, 2002. **34**: p. 1091-1101.
8. Letellier, S.R., et al., *Oriented growth of calcium oxalate monohydrate crystals beneath phospholipid monolayers.* *Biochimica et Biophysica Acta*, 1998. **1380**: p. 31-45.
9. Eanes, E.D., *Biophysical Aspects of Lipid Interaction With Mineral: Liposome Model Studies.* *The Anatomical Record*, 1989. **224**: p. 220-225.
10. Johnson K and e. al., *Linked deficiencies in extracellular inorganic pyrophosphate (PPi) and osteopontin expression mediate pathologic ossification in PC-1 null mice.* *J. Bone Min. Res*, 2003. **18**: p. 1994-1004.
11. CHRISTOFFERSEN, J. and W.J. LANDIS, *A Contribution With Review to the Description of Mineralization of Bone and Other Calcified Tissues In Vivo.* *The Anatomical Record*, 1991. **230**: p. 435-450.
12. Bosetti, M., et al., *Effects of phosphatidylserine coatings on titanium on inflammatory cells and cell-induced mineralisation in vitro.* *Biomaterials*, 2005. **26**: p. 7572-7578.
13. Sela, J., et al., *PRIMARY MINERALIZATION AT THE SURFACES OF IMPLANTS.* *Critical Reviews in Oral Biology & Medicine*, 2000. **11**(4): p. 423-436.
14. Raggio, C.L., B.D. Boyan, and A.L. Boskey, *In Vivo Hydroxyapatite Formation Induced by Lipids.* *Journal of Bone and Mineral Research*, 1986. **1**(5): p. 409-415.
15. Merolli, A., et al., *In vivo assessment of the osteointegrative potential of phosphatidylserine-based coatings.* *Journal of Material Science*, 2006. **17**: p. 789-794.
16. Abrahamsson, *Early bone formation adjacent to rough and turned endosseous implant surfaces - an experimental study in the dog.* *Clinical Oral Implants Research*, 2004. **15**(4): p. 381-392.
17. Thelen, S., F. Barthelat, and C. Brinson, *Mechanics considerations for microporous titanium as an orthopedic implant material.* *Journal of Biomedical Materials Research Part A*, 2004. **69a**(4): p. 601-610.
18. HALLAB, N.J., et al., *Evaluation of Metallic and Polymeric Biomaterial Surface Energy and Surface Roughness Characteristics for Directed Cell Adhesion.* *Tissue Engineering*, 2001. **7**(1): p. 55-71.

19. Pressl, D., et al., *Characterization of Phospholipid Bilayers on Ti-6Al-4V and Ti-6Al-7Nb*. *Advanced Engineering Materials*, 2008. **10**(10).
20. Navarro, M., et al., *Biomaterials in orthopaedics*. *Journal of the Royal Society Interface*, 2008. **5**: p. 1137-1158.
21. Manivasagam, G., D. Dhinasekaran, and A. Rajamanickam, *Biomedical Implants: Corrosion and its Prevention - A Review*. *Recent Patents on Corrosion Science*, 2010. **2**: p. 40-54.
22. Kim, B.-H., et al., *Hydroxyapatite layers prepared by sol-gel assisted electrostatic spray deposition*. *Ceramics International*, 2007. **33**: p. 119-122.
23. Knabe, C., et al., *The effect of different titanium and hydroxyapatite-coated dental implant surfaces on phenotypic expression of human bone-derived cells*. 2004.
24. Yoshinari, M., et al., *Influence of surface modifications to titanium on antibacterial activity in vitro*. *Biomaterials*, 2001. **22**: p. 2043-2048.
25. SUNDGREN, J.-E., P. BODO, and I. LUNDSTROM, *Auger Electron Spectroscopic Studies of the Interface between Human Tissue and Implants of Titanium and Stainless Steel*. *Journal of Colloid and Interface Science*, 1985. **110**(1): p. 9-20.
26. Lausmaa, J., *Surface spectroscopic characterization of titanium implant materials*. *Journal of Electron Spectroscopy and Related Phenomena*, 1995. **81**: p. 343-361.
27. Khan, M.A., R.L. Williams, and D.F. Williams, *In-vitro corrosion and wear of titanium alloys in the biological environment*. *Biomaterials*, 1996. **17**: p. 2117-2126.
28. Thomas, K.A. and S.D. Cook, *An evaluation of variables influencing implant fixation by direct bone apposition*. *Journal of Biomedical Materials Research*, 1985. **19**: p. 875-901.
29. Bower, K.T., et al., *Optimization of surface micromorphology for enhanced osteoblast responses in vitro*. *Int. Journal of Oral Maxillofacial Implants*, 1992. **7**: p. 302-310.
30. Schwartz, Z., et al., *Effect of titanium surface roughness on chondrocyte proliferation, matrix production, and differentiation depends on the state of cell maturation*. *Journal of Biomedical Materials Research*, 1996. **30**: p. 145-155.
31. Garvey, B.T. and R. Bizios, *A transmission electron microscopy examination of the interface between osteoblasts and metal biomaterials*. *Journal of Biomedical Materials Research*, 1995. **29**: p. 987-992.
32. Lincks, J., et al., *Response of MG63 osteoblast-like cells to titanium and titanium alloy is dependent on surface roughness and composition*. *Biomaterials*, 1998. **19**: p. 2219-2232.
33. Buser, D., et al., *Influence of surface characteristics on bone integration of titanium implants. A histomorphometric study in miniature pigs*. *Journal of Biomedical Materials Research*, 1991. **25**: p. 889-902.
34. Piattelli, A.L., et al., *Histologic and histomorphometric analysis of the bone response to machined and sandblasted titanium implants: An experimental study in rabbits*. *Int. Journal of Oral Maxillofacial Implants*, 1998. **13**(6): p. 805-810.
35. Martin, J.Y., et al., *Effect of titanium surface roughness on proliferation, differentiation, and protein synthesis of human osteoblast-like cells (MG63)*. *Journal of Biomedical Materials Research*, 1995. **29**: p. 389-401.
36. Anselme, K., *Osteoblast adhesion on biomaterials*. *Biomaterials*, 1999. **21**: p. 667-681.
37. Larsson, C., et al., *Bone response to surface-modified titanium implants: studies on the early tissue response to machined and electropolished implants with different oxide thicknesses*. *Biomaterials*, 1996. **17**: p. 605-616.
38. Bigi, A., et al., *In vitro culture of mesenchymal cells onto nanocrystalline hydroxyapatite-coated Ti13Nb13Zr alloy*. 2006.

39. Branemark, P., et al., *A 15-year study of osseointegrated implants in the treatment of the edentulous jaw*. International Journal of Oral Surgery, 1981: p. 387-416.
40. Carlsson, L., T. Rostlund, and B. Albrektsson, *Osseointegration of Titanium Implants*. Acta Orthopaedica Scandinavica, 1986. **57**(4): p. 285-289.
41. Frenkel, S.R., et al., *Osseointegration on Metallic Implant Surfaces: Effects of Microgeometry and Growth Factor Treatment*.
42. Puleo, D.A. and A. Nanci, *Understanding and controlling the bone/implant interface*. Biomaterials, 1999. **20**: p. 2311-2321.
43. Kasemo, B., *Biocompatibility of titanium implants: A Surface science aspects*. The Journal of Prosthetic Dentistry, 1983. **49**(6): p. 832-837.
44. Frosch, K.H., et al., *Migration, Matrix Production and Lamellar Bone Formation of Human Osteoblast-Like Cells in Porous Titanium Implants*. Cell Tissue Organs, 2002. **170**: p. 214-227.
45. Kenny, S.M. and M. Buggy, *Bone Cements and Fillers: A Review*. Journal of Material Science, 2003. **14**: p. 923-938.
46. Harper, E.J., *Bioactive bone cements*. Proc Instn Mech Engrs 1998. **212 Part H**: p. 113-120.
47. Pilliar, R.M., *Cementless implant fixation--toward improved reliability*. Orthopedic Clinical North America, 2005. **36**(1): p. 113-119.
48. Prawel, D., *A DRUG ELUTING, OSSEOINTEGRATIVE PHOSPHOLIPID COATING FOR ORTHOPEDIC IMPLANTS*, in *Biomedical Engineering 2011*, Colorado State University. p. 265.
49. Joshi, M.G., et al., *Analysis of a femoral hip prosthesis designed to reduce stress shielding*. Journal of Biomechanics, 2000. **33**(12): p. 1655-1662.
50. Black, J., *Biological Performance of Materials: Fundamentals of Biocompatibility*. 3rd ed. 1999: CRC Press.
51. Karageorgiou, V. and D. Kaplan, *Porosity of 3D biomaterial scaffolds and osteogenesis*. Biomaterials, 2005. **27**: p. 5474-5491.
52. St-Pierre, J.-P., et al., *Three-dimensional growth of differentiating MC3T3-E1 pre-osteoblasts on porous titanium scaffolds*. Biomaterials, 2005. **26**: p. 7319-7328.
53. Boby, J.D., et al., *The optimum pore size for the fixation of porous-surfaced metal implants by the ingrowth of bone*. Journal of Clinical Orthopedics and Related Research, 1980. **150**: p. 263-270.
54. Ryan, G.E., A.S. Pandit, and D.P. Apatsidis, *Porous titanium scaffolds fabricated using a rapid prototyping and powder metallurgy technique*. Biomaterials, 2008. **29**: p. 3625-36335.
55. Cansizoglu, O., et al., *Properties of Ti-6Al-4V non-stochastic lattice structures fabricated via electron beam melting*. Materials Science and Engineering A, 2008. **492**: p. 468-474.
56. Gibson, I., et al., *The use of rapid prototyping to assist medical applications*. Rapid Prototyping Journal, 2006. **12**(1): p. 53-58.
57. Li, X., et al., *Fabrication and characterization of porous Ti6Al4V parts for biomedical applications using electron beam melting process*. Materials Letters, 2009. **63**: p. 403-405.
58. Kowalczyk, P., *Orthotropic properties of cancellous bone modelled as parameterized cellular material*. Computer Methods in Biomechanics and Biomedical Engineering, 2006. **9**(3): p. 135-147.

59. Thomsen, P., et al., *Electron Beam-Melted, Free-Form-Fabrication Titanium Alloy Implants: Material Surface Characterization and Early Bone Response in Rabbits*. Journal of Biomedical Materials Research Part B: Applied Biomaterials, 2008.
60. Ponader, S., et al., *In vivo performance of selective electron beam-melted Ti-6Al-4V structures*.
61. Palmquist, A., et al., *Long-term biocompatibility and osseointegration of electron beam melted, free-form-fabricated solid and porous titanium alloy: Experimental studies in sheep*. Journal of Biomaterials Applications, 2011.
62. Viceconti, M., A. Toni, and A. Giunti, *Effects of some technological aspects on the fatigue strength of a cementless hip stem*. Journal of Biomedical Materials Research, 1995. **29**: p. 875-881.
63. Delecrin, J., et al., *Specific Resorbable Calcium Phosphate Coating to Enhance Osteoconduction*. Cells and Materials, 1994. **4**(1): p. 51-62.
64. Heimann, R.B., *Materials Science of Crystalline Bioceramics: A Review of Basic Properties and Applications*. CMU Journal, 2002. **1**(1): p. 23-47.
65. Zhao, S.F., et al., *Effects of magnesium-substituted nanohydroxyapatite coating on implant osseointegration*. Clinical Oral Implants Research, 2011: p. 1-8.
66. Kim, S., et al., *Aerosol deposition of hydroxyapatite and 4-hexylresorcinol coatings on titanium alloys for dental implants*. Journal of Oral Maxillofacial Surgery, 2011. **69**(11): p. 354-363.
67. Tranquilli Leali, P. and e. al., *Evaluation of different preparations of plasma-spray hydroxyapatite coating on titanium alloy and duplex stainless steel in the rabbit*. JOURNAL OF MATERIALS SCIENCE: MATERIALS IN MEDICINE, 1994. **5**(6): p. 345-349.
68. Santin, M., et al., *Calcium-binding phospholipids as a coating material for implant osteointegration*. Journal of the Royal Society Interface, 2006. **3**(7): p. 277-281.
69. Bosetti, M., et al., *Cell behaviour on phospholipids-coated surfaces*. Journal of Material Science Materials in Medicine, 2007. **18**(4): p. 611-617.
70. Shen M. and H. T.A., *The effects of surface chemistry and adsorbed proteins on monocyte/macrophage adhesion to chemically modified polystyrene surfaces*. Journal of Biomaterial Resources, 2001. **57**(3): p. 336-345.
71. Satsangi, A., et al., *Osteoblast response to phospholipid modified titanium surface*. Biomaterials, 2003. **24**(25): p. 4585-4589.
72. Satsangi, N., et al., *Osteoblast response and calcium deposition on phospholipid modified surfaces*. JOURNAL OF MATERIALS SCIENCE: MATERIALS IN MEDICINE, 2004. **15**: p. 693-697.
73. Parker, L.C., et al., *A phosphatidylserine species inhibits a range of TLR, but not IL-16, induced inflammatory responses by disruption of membrane microdomains*. Journal of Immunology, 2008. **181**(8): p. 5606-5617.
74. GRACE, J.M. and J.C.M. MARIJNISSEN, *A REVIEW OF LIQUID ATOMIZATION BY ELECTRICAL MEANS*. Journal of Aerosol Science, 1994. **25**(6): p. 1005-1019.
75. Jayasinghe, S.N. and A. Townsend-Nicholson, *Bio-electrosprays: The next generation of electrified jets*. Journal of Biotechnology, 2006. **1**: p. 1018-1022.
76. Kumbar, S.G., et al., *A Preliminary Report on a Novel Electrospray Technique for Nanoparticle Based Biomedical Implants Coating: Precision Electrospraying*. Journal of Biomedical Resources and Applied Biomaterials, 2007. **81**(1): p. 91-103.
77. Huang, Z.-M., et al., *A review on polymer nanofibers by electrospinning and their applications in nanocomposites*. Journal of Composites and Science Technology, 2003. **63**: p. 2223-2253.

78. Chen, C.H., E.M. Kelder, and J. Schoonman, *Electrostatic sol-spray deposition (ESSD) and characterisation of nanostructured TiO<sub>2</sub> thin films*. Thin Solid Films, 1999. **342**: p. 35-41.
79. CLOUPEAU, M. and B. PRUNET-FOCH, *ELECTROSTATIC SPRAYING OF LIQUIDS IN CONE-JET MODE*. Journal of Electrostatics, 1989. **22**: p. 135-159.
80. Shin, Y.M., et al., *Experimental characterization of electrospinning: the electrically forced jet and instabilities*. Polymer, 2001. **42**(25): p. 09955-09967.
81. Hartman, R.P.A., et al., *ELECTROHYDRODYNAMIC ATOMIZATION IN THE CONE JET MODE PHYSICAL MODELING OF THE LIQUID CONE AND JET*. Journal of Aerosol Science, 1999. **30**(7): p. 82-849.
82. Uematsu, I., et al., *Surface morphology and biological activity of protein thin films produced by electrospray deposition*. Journal of Colloid and Interface Science 2004. **269**: p. 336-340.
83. Chung, D., *Composite Materials: Functional Materials for Modern Technology*, ed. B. Derby. 2002, Great Britain: Springer - Verlag.
84. Forsey, M. *Protection against the effects of lightning*. in *IEE Colloquium on Integration of Earthing Practices*. 1997. London.
85. Biris, A.S., et al. *Parametric study of the Faraday cage effect of charged particles and its implications in the powder coating process*. in *Industry Applications Conference, 2002. 37th IAS Annual Meeting. Conference Record of the 2002*.
86. Kyrk, C. and B. Olseth, *Powder Coating*, in *Industrial Paint and Powder*.
87. Guskov, S. *Application of Powder Coatings: Old Problems, New Findings, New Developments*. in *Powder Coating*. 1996. Indiana.
88. Utech, B., *A guide to high-performance powder coating*. 2002, Michigan: SME.
89. Kim, H.-H., A. Ogata, and J.-H. Kim. *High Speed Camera Observation of Electro spray*. in *Electrostatics Joint Conference*. 2009. Boston.
90. Jaworek, A. and A. Krupa, *Classification of the modes of EHD spraying*. Journal of Aerosol Science, 1999. **30**: p. 873-893.
91. Popat, K., et al., *Decreased Staphylococcus epidermis adhesion and increased osteoblast functionality on antibiotic-loaded titania nanotubes*. Biomaterials, 2007. **28**: p. 4880-4888.
92. AAOS. *Total Knee Replacement*. 2011 12/2011 [cited 2012 01/12/2012]; Available from: <http://orthoinfo.aaos.org/topic.cfm?topic=A00389>.
93. Soundrapandian, C., S. Datta, and B. Sal, *Drug-Eluting Implants for Osteomyelitis*. Therapeutic Drug Carrier Systems, 2007. **24**(6): p. 493-495.
94. Aberdeen, U.o. *Bone*. [cited 2012 01/03/2012]; Available from: [http://www.abdn.ac.uk/orthopaedics/res\\_bone.shtml](http://www.abdn.ac.uk/orthopaedics/res_bone.shtml).
95. Hospital, H. *Knee Replacement (Total and Partial)*. 2007 01/04/2012]; Available from: <http://www.urmc.rochester.edu/hh/quality-of-care/knee-replacement/index.cfm>.
96. Ong, K.L., et al., *Economic Burden of Revision Hip and Knee Arthroplasty in Medicare Enrollees*. Clinical Orthopedics and Related Research, 2006. **446**: p. 22-28.
97. Cune, J., et al., *A Superficial Swab Culture is Useful for Microbiologic Diagnosis in Acute Prosthetic Joint Infections*. Clinical Orthopedics and Related Research, 2009. **467**: p. 531-535.
98. Kummoona, R., *Posttraumatic Missile Injuries of the Orofacial Region*. THE JOURNAL OF CRANIOFACIAL SURGERY, 2008. **19**(2): p. 300-305.
99. Grimer, R.J., *Two-stage revision for infected endoprostheses used in tumor surgery*. Clinical Orthopaedics and Related Research, 2002. **395**: p. 193-203.

100. Price, J.S., *Controlled release of antibiotics from coated orthopedic implants*. Journal of Biomedical Materials Research Part B: Applied Biomaterials, 1996. **30**(3): p. 281-286.
101. Rajaratnam, S.S., et al., *Long-term results of a hydroxyapatite-coated femoral component in total hip replacement*. The Journal Of Bone and Joint Surgery, 2008. **90-B**(1): p. 27-30.
102. Steflik, D.E., et al., *Ultrastructural analyses of the attachment (bonding) zone between bone and implanted biomaterials*. 1997.
103. Coating, P. *Powder Coating FAQ*. 2011 [cited 2012 03/21/12]; Available from: [http://www.powdercoating.org/frequently\\_asked\\_questions.php](http://www.powdercoating.org/frequently_asked_questions.php).

## APPENDICES

### Appendix A: E-spray Protocol

Hudson September 2011

#### Materials and Supplies

- 1010 Gastight Glass Syringe and plunger
- Pipetter Gun and 5mL graduated pipette
- 50mL beaker , 100mL beaker, small vials with Teflon tabbed lids
- Titanium lattices
- Kim wipes
- Sufficient chloroform and phospholipid
- well plate(s) to store samples
- Small copper alligator clip
- Electro spraying apparatus and needle

#### Methods

*\*Always wear gloves*

##### Chemical Set Up

1. Set up clean work space in hood with Kimwipes
2. Clean all glass wear (syringe, beakers, pipette, vials) thoroughly with chloroform before beginning to avoid any possible contamination
3. Rinse needle with chloroform to make sure to remove any remaining solution from previous use, and ensure needle works properly –air dry
4. Weigh and label all titanium samples.
5. Clean inside of chamber. Make sure the chamber is free of any old phospholipid and all tape is in place covering any leads you will not be using.
6. Connected needle tube to syringe.
7. Prepare the DOPS/Chloroform solution as required. Keep container closed as much as possible to avoid (rapid) evaporation of the mixture.
8. Carefully transfer the solution to the syringe. Get prepared in advance and work quickly – the solution evaporates very quickly. Attach tube and needle to syringe. Push syringe plunger completely in. Open vial containing chloroform mixture. Draw all solution into Syringe. Minimize air intake.

##### Electro-Spray Apparatus Set up

1. Check the pump rate on pump (\*every third or fourth use you will want to check the pump rate and ensure calibration)
2. Put syringe in place on pump and clamp needle into holder in apparatus
3. Rubber band both halves of sample together and ensure that no large gap is created.
4. Attach small copper alligator clip to sample
5. Clamp sample mounting board in place

- a. Align needle such that it points at the center of the sample
- b. Adjust distance from needle tip to back of sample
- c. Recheck alignment, and then distance again.
6. Attach ground wire to small copper alligator clip
7. Attach positive pole to needle tip
8. Check that Voltage on power supply is set as required
9. Double check sample (make sure alligator clip is touching both halves)
10. Double check all connections: that sample is grounded and needle is powered
11. Push pump activator manually until you see fluid start to move again in tube, this is to make sure the pump activator is in contact with the syringe plunger
12. Turn on power supply
13. Turn on pump
14. Watch for a spray cone, once you see the spray cone, start the timer and close the door to the apparatus
15. When the prescribed time has run out, turn off the pump and turn off the power supply
16. Remove ground and power wires, and remove sample
17. Reweigh samples
18. Clean inside of chamber

#### Clean Up

1. Push a few mls of chloroform through the syringe, into a waste beaker
2. Clean all glass wear (beakers, pipette, vials) and needle with chloroform
3. Very carefully clean syringe
4. Store needle with E-spraying apparatus
5. Rinse glass wear with lab soap and then rinse in DI water
6. Dry carefully and store
7. Double check that E-spray apparatus is clean and clean up area in hood
8. Do one last check of lab and make sure you have stored everything properly – leave the lab in better shape than you found it

## Appendix B: Titanium Cleaning and Surface Preparation Protocol

Prawel July 2010

Allocate about 2 hours, plus possible overnight rinse, for complete procedure.

### Solvent Cleaning

Purpose:

In this procedure, Ti samples are sonicated in solvents and de-ionized water to remove organic debris and oils.

Notes:

Use glassware on solvents.

Need:

Sonicator  
Acetone

Procedure

1. Sonicate 30 minutes in 100 ml Acetone (stirring vigorously every 5 minutes)
2. Rinse in tap water
3. Sonicate 15 minutes in 100 ml 2% Liquinox (stirring vigorously every 5 minutes)
4. Rinse in DI water until no evidence of soap
5. Sonicate 15 minutes in 100 ml DI water (stirring vigorously every 5 minutes)
6. Rinse once in acetone
7. Air dry and store in dessicator.

### Surface Preparation

Need:

Hydrofluoric Acid  
Nitric Acid

**Polypropylene**, HDPE or PTFE lab equipment (for handling HF):

Tweezers or forceps  
Beaker (>150 ml)  
Chloroprene gauntlet gloves (or double nitrile)  
Graduated cylinder (10 ml)  
Storage bottle for waste solution

Calcium gluconate gel (in case of skin contact with HF)

Note:

In the nitric-hydrofluoric pickling solution, the ratio of nitric acid to hydrofluoric acid is more important than the concentration of either of these two acids. When this ratio is maintained at 10 to 1, hydrogen absorption during pickling is minimized. (from ASTM B600)

Avoid pouring water in acid. It's best to always pour acid into water.

Procedure

Summary: Samples are bathed in 3.5% HF for 30 seconds to remove the existing Ti oxide layer and then soaked in 35% HNO<sub>3</sub> for 30 minutes to regenerate a new oxide coating.

1. Slowly add 50 ml of 54% HNO<sub>3</sub> to 50 ml de-ionized water and warm to 50°C, stirring at 150 RPM.
2. In a **polypropylene beaker**, slowly add 7.3 ml of 48% HF (measured in a **polypropylene** graduated cylinder) to 71.7 ml de-ionized water, at room temperature.
3. Gently bath no more than 50 Ti samples at once in the HF solution for 30 seconds.
4. Pour off the HF solution into another **polypropylene** beaker, and carefully transfer samples to the HNO<sub>3</sub> solution, stirring at 150 RPM, at 50°C. Stir for 30 minutes, manually mixing samples every few minutes to prevent samples from stacking on each other for more than a few minutes.
5. Then, samples are then rinsed briefly in de-ionized water and either soaked in DIH<sub>2</sub>O water at 37°C for 24 hrs or boiled in DIH<sub>2</sub>O water for 1 h.
6. Following this chemical treatment, samples are rinsed with de-ionized water, vacuum dried, and placed in desiccator for relatively immediate (few days) use, or vacuum packed in Nitrogen, and stored at room temperature for future use.

## Appendix C: Lattice Surface Area Calculation Protocol

Hudson August 2011

Materials:

- Calipers
- Calculator
- Sample

$$V = \frac{1}{4}\pi d^2 L \quad (1)$$

$$m = \rho V \quad (2)$$

$$SA = \pi dL \quad (3)$$

$$F = \frac{ms}{m} \quad (4)$$

$$SAs = F \cdot SA$$

Procedure:

1. Using calipers measure the strut diameter and length in three different places
2. Average these diameters and lengths
3. Weigh and record sample weight
4. Calculate the volume of strut using equation 1, the volume of a cylinder using diameter (d), and length (L) to find volume (V)
5. Calculate the mass of the strut using equation 2, where the density of titanium is 0.0043 g/mm<sup>3</sup>, use density ( $\rho$ ) and volume (V) to calculate mass (m)
6. Calculate the surface area of the strut using equation 3, the surface area of a cylinder, calculate surface area (SA) using diameter (d) and length (L)
7. Create a ratio (F) of theoretical strut weight (m) to measured sample weight (ms) using equation 4
8. Use the ratio to calculate the surface area of the entire sample using equation 5, the sample surface area (SAs) is found by multiplying the ratio (F) by the theoretical strut surface area (SA)

## Appendix D: Mixing PL Protocol

Prawel March 2009

Note, actual amount of PL/chloroform mixture created is always greater than necessary in this protocol, due to loss of small amount of PL on weighing dish, and desire to keep the concentration of PL as desired.

All at room temperature ...

M = desired total mls of PL/chloroform mixture in solution

[PL] = desired concentration (weight %) of PL/chloroform solution

$G_{PL}$  = grams of PL to get desired [PL]

Algorithm...

For M grams (mls) of PL/chloroform mixture,

$$M \times [PL] = G_{PL}$$

$M - G_{PL}$  = grams of chloroform / 1.48 g/ml = ml chloroform to get M ml of solution

$$G_{PL} = [PL] \times (1.48 \times M) / (1 - [PL]) = 0.0526 \times (1.48 \times M)$$

Weigh out PL using Teflon weighing dishes

(grounding hands and weighing dish whenever possible – PL is very electrostatic)

Place PL in small beaker (~50 ml)

Weigh empty weighing dish

Calculate W, the actual weight of PL in beaker (weight with PL – weight without PL)

Calculate amount of chloroform actually needed to get desired [PL]

$$W = 0.0526 \times (1.48 \times M), \text{ solve for } M = 0.0779 \times M$$

So,  $M = W / 0.0779$  in mls

Example:

Desire 2.7 mls of 5% PL/CHCl<sub>3</sub>

$$0.0526 \times (1.48 \times 2.7) = 0.21 \text{ g PL}$$

Weigh out 0.2172 g PL. Weighing dish weighs 0.0112, so actual weight of PL is 0.2060

$$0.206 / 0.0779 = 2.64 \text{ ml CHCl}_3$$

Measure out this much chloroform and pour into beaker with PL.

Mix with spatula until no PL is visible (few minutes).

Pour mixture into small vial with Teflon-lined lid and close lid (it evaporates quickly).

Draw mixture as need, quickly opening and closing lid on vial.

Store any remaining mixture at -20° C.